早稲田大学大学院 環境・エネルギー研究科

博士学位論文

A New Hierarchical Fault Diagnosis Method for Power Distribution Networks with PV Systems

---Equivalent-Input-Disturbance-Based Approach---

太陽光発電システムを含む配電ネットワークに関する新しい階層的故障診断手法

― 等価入力外乱手法によるアプローチ ―

2013 年 02 月

胡　　波

Hu　　Bo

ABSTRACT

Modern power system is huge and complex. State monitoring and fault diagnosis are necessary to guarantee its stability and safety. The traditional fault diagnosis methods for distribution network are mainly based on a large amount of sensor information and a complete model of distribution network. These methods have solved the fault diagnosis problems in a certain degree, but still remains some shortcomings, such as high dependency of sensor information and enormous size of fault diagnosis model. Moreover, with the penetration of grid-connected PV generation, the conventional fault diagnosis method encounter an increasing number of bottlenecks, such as fluctuation of PV output and malfunctions of protective relays caused by PV power injection.

The doctoral dissertation concerns the above problems and presents a new hierarchical fault diagnosis (HFD) method for power distribution network that is based on a hierarchical model and the equivalent-input-disturbance (EID) approach.

Due to the complexity of power distribution, a complete model of an entire distribution is extremely complicated. Therefore, a hierarchical technology is applied to build a hierarchical model of distribution network for fault diagnosis. Fault diagnosis is carried out from the top down through the layers to gradually locate a fault and to identify its type.

While faults occur, the faults will cause large disturbances to the system from the standpoint of power supply. Based on this concept, the EID approach, which can estimate the magnitude of system disturbances, is used to diagnose the faults. To eliminate the influence of PV for the fault diagnosis, the fault signal is abstracted by removing the PV output fluctuation from EID.

Unlike conventional methods, the proposed method uses the hierarchical model for fault diagnosis, which reduces the complexity involved in modeling, shortens the computation time and does not need a large amount of sensor information. Furthermore, our fault diagnosis method shows a good performance in the case of PV generation embedded in the feeder. The simulations on IEEE 37 nodes radial distribution test feeder model demonstrate the validity and superiority of the HFD method.

ACKNOWLEDGMENTS

I would like to express my acknowledgements to all the persons who helped me during the writing of this thesis.

My deepest gratitude goes first and foremost to my supervisor, Professor R. Yokoyama, for his support, patience, and consistent encouragement throughout the course of my Ph.D study. His technical advice was essential to the successful completion of this dissertation. I also would like to acknowledge my co-advisor Professor J. She of Tokyo University of Technology. During my three-year doctoral study, he provided me many invaluable guidance for my research and helped me to revise the papers strictly.

Moreover, I want to thank the other members of my review committees, Professor M. Katsuta, and Professor S. Tomonari for their helpful comments during the grueling thesis review process. I am also grateful to Dr. Y. Zhou of the Fujitsu Limited Company, Professor M. Wu of Central South University. They provided me with selfless help and guidance whatever in my study or in my life.

To my family and friends, I dedicate my heartfelt thanks and gratitude for the support and encouragement that they provided me through my entire life. None of my achievements would have been possible achieved without them in these years.

In addition, it is also a pleasure to thank my colleagues from Yokoyama laboratory for their support and help. I must acknowledge Dr. H. Magori, Dr. T. Nimura and Dr. K. Koyanagi for teaching me many basic skills and background knowledge on power system. I also give my thanks to the doctoral students D. Yamasida, Y. Hida, J. Zhang, and M. Ding for all of their computer and technical assistance in my study, and special thanks to our administrative staff Mrs Y. Inaba and Mrs H. Kano for their guidance of the doctoral review procedures.

Financial support from the “National Construction High level University Government-sponsored Graduate Student Project” provided by the China Scholarship Council is also gratefully acknowledged.

Bo Hu

Jan. 2013

Contents

List of Figures

List of Tables

Abbreviations

HFD: hierarchical fault diagnosis

EID: equivalent-input-disturbance

PV: photovoltaic

EMS: energy management system

SCDA: supervisory control and data acquisition

BFS: backward and forward sweep

LC: load cluster

SISO: single-input single-output

MPPT: maximum power point tracking

PWM: pulse-width modulation

SNR: signal-noise ratio

PVNSM: *PV-specified* node sensitivity matrix

Chapter 1
Background and Research Outline

1.1 Chapter Introduction

The electrical power system represents not only one of the most complex artificial systems in the world, but also one of the most significant ones in modern society. Power system are key elements of modern society, providing clean and convenient energy to drive motors, light houses and streets, run manufacturing plants and business, and power our communications and computer systems. With the development of human society, the demand of electrical power is ever-increasing. In a word, the power system is the basic of modern human life, which plays a vital and important role in maintaining the society operation.

The stable and security operation is the most important issue for power system. When the fault occurs, location and type of the fault should be identified exactly and rapidly to lessen the loss or influence of fault. The traditional fault diagnosis methods for power distribution are mainly based on the fusion of sensor information from protection system. Although, these methods solved the problems in a certain degree, there are still many limitations.

In recent years, the renewable energy power such as solar energy, wind energy and etc. have experienced a remarkably rapid growth because they are pollution-free power sources. Photovoltaic (PV) system, as a kind of renewable energy, has been widely installed in the distribution feeders. With these distributed PV generators embedded, many new problems are also brought to relay protection system, which did not consider this situation when it was built. Furthermore, the conventional fault diagnosis methods based on the relay protection system are suffered from this situation.

This dissertation mainly investigates the new challenges of fault diagnosis for distribution network when the large-scale of PV generators embedded, and wants to design a novel fault diagnosis method for distribution feeders, which can overcome the limitations of conventional methods.

In this chapter, the background and the research outline of this doctoral thesis are presented. The definition and categories of faults in power system distribution network are given out. In addition, the overview of conventional fault diagnosis methods, which includes monitoring information-based and model-based fault diagnosis methods are presented. Furthermore, the influence of grid-connected PV system to the distribution network is analyzed. Finally, the objective and the structure of this thesis will be presented briefly.

1.2 Faults in Electrical Power System

The operation of a power system involves a complex transfer of electrical energy form one station to another, thus faults occur frequently. This section will give out the definition of faults in power system and classify them.

1.2.1 Electrical Power System

In general, the electrical power system consists of power generators, power transmission and distribution, power control, power conversion and power measurement and monitoring. The block diagram of an electrical power system is shown in Fig.1-1. The electrical powers are produced by generators, delivered by power transmission and distribution to the power consumers and the electricity supply and the electricity consumption need to keep the balance. The Supervisory Control and Data Acquisition (SCDA) system is necessary to monitor the operation state of entire power system. The information for fault diagnosis usually comes from the data collected by the SCDA system.

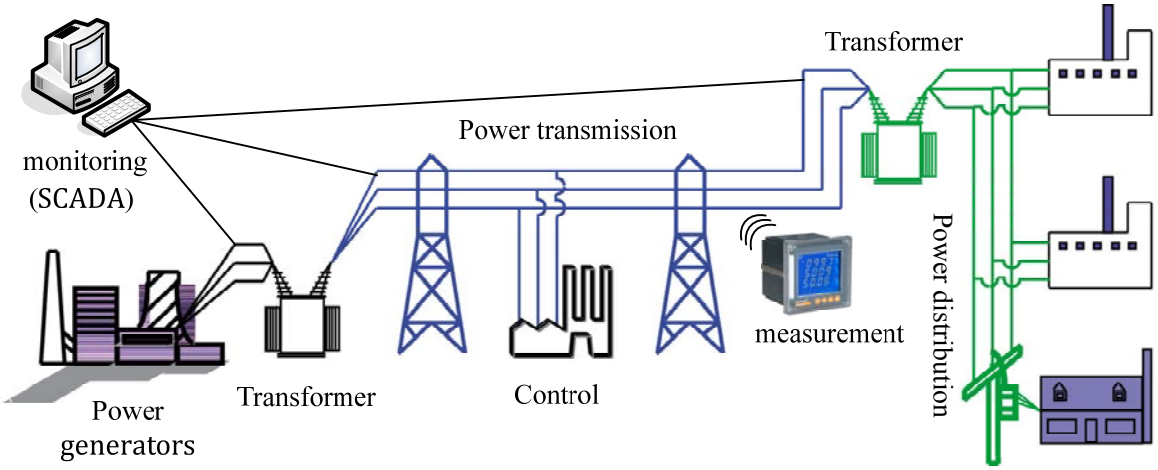

Fig. 1-1 Block diagram of an electrical power system.

1.2.2 Faults Definition and Classification

Nowadays, severe consequences have been coursed by large-scale blackouts of power system, such as blackouts in the USA (1965) and Europe (2006). In July 2012, the blackout in India affected over 700 million people, about of 9% of the world population, more than 2 days. The blackouts cause the immeasurable financial losses for human society. Moreover, blackouts not only lead to financial losses, but also lead to potential dangers to society and humanity. So it is necessary to pay attention to fault diagnosis of power system, to detect and remove it timely. Faults can be broadly classified into two main areas which have been designated Active Faults

and Passive Faults.

a) *Active Faults*

The Active Faults are when actual current flows from one phase conductor to another (phase-to-phase) or alternatively from one phase conductor to earth (phase-to-earth). This type of fault can also be further classified into two areas, namely the "solid" fault and the "incipient" fault.

The solid fault occurs as a result of an immediate complete breakdown of insulation as would happen if, say, a pick struck an underground cable, bridging conductors etc. or the cable was dug up by a bulldozer or rock fall. In these circumstances the fault current would be very high, resulting in an electrical explosion. This type of fault must be cleared as quickly as possible, otherwise there will be bring dangerous to electrical equipments and operating personnel.

The incipient fault, on the other hand, is a fault that starts from very small beginnings. For example, some partial discharge in a void in the insulation, increasing and developing over an extended period, until such time as it burns away adjacent insulation, eventually running away and developing into a solid fault.

Other causes can typically be a high-resistance joint or contact, alternatively pollution of insulators causing tracking across their surface. Once tracking occurs, any surrounding air will ionize which then behaves like a solid conductor consequently creating a solid fault.

b) *Passive Faults*

Passive faults are not real faults in the true sense of the word but are rather conditions that are stressing the system beyond its design capacity, so that ultimately active faults will occur. Typical examples are:

- Overloading: Leading to overheating of insulation (deteriorating quality, reduced life and ultimate failure).
- Over-voltage: Stressing the insulation beyond its limits.
- Under frequency: Causing plant to behave incorrectly.
- Power swings: Generators going out-of-step or synchronism with each other.

1.2.3 Fault Types in the Three-Phase Network

The types of faults that can occur on a three phase alternating current system are as shown in Fig. 1-2. It will be noted that for a phase-to-phase fault, the currents will be high, because the fault current is only limited by the inherent series impedance of the power system up to the

point of faulty.

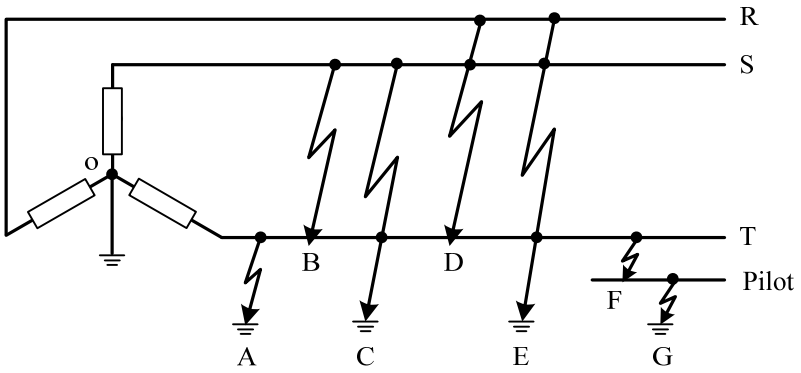

Fig. 1-2 Type of faults on a Three Phase System. (A): Phase-to-earth fault; (B) Phase-to-phase fault; (C) Phase-to-phase-to-earth fault; (D)Three phase fault; (E) Three phase-to-earth fault; (F)Phase-to-pilot fault; (G)Pilot-to-earth fault.

By design, this inherent series impedance in a power system is purposely chosen to be as low as possible in order to get maximum power transfer to the consumer and limit unnecessary loss in the network itself in the interests of efficiency. On the other hand, the magnitude of earth faults currents will be determined by the manner in which the system neutral is earthed. Solid neutral earthing means high earth fault currents as this is only limited by the inherent earth fault impedance of the system. Meanwhile, it is worth noting at this juncture that the power factors of bus nearby the fault site will descend.

1.3 Conventional Fault Diagnosis Methods

When a fault occurs in power system, it is imperative to limit the impact of outages to the minimum and to restore the faulted facilities as quickly as possible. This requires that the location and type of the fault first be identified. This identification function is referred to as "fault diagnosis of power system". This fault diagnosis function is then the most basic fault handling function of power system supervisory and control system such as Energy Management System (EMS) and SCADA systems. The configuration of a fault diagnosis system is shown in Fig. 1-3.

Fault diagnosis can be divided into local fault diagnosis and centralized fault diagnosis. Local fault diagnosis takes place at power plant and substation facilities and aims to diagnose these facilities. Centralized fault diagnosis takes place at control centers equipped with EMS and SCADA systems using transmitted fault information. This dissertation is primarily concerned with centralized fault diagnosis.

The objects of fault diagnosis in power system contain power generators, transmission line,

distribution network, electrical equipments and so on. In this thesis, we focus on the fault diagnosis in distribution network (distribution feeder).

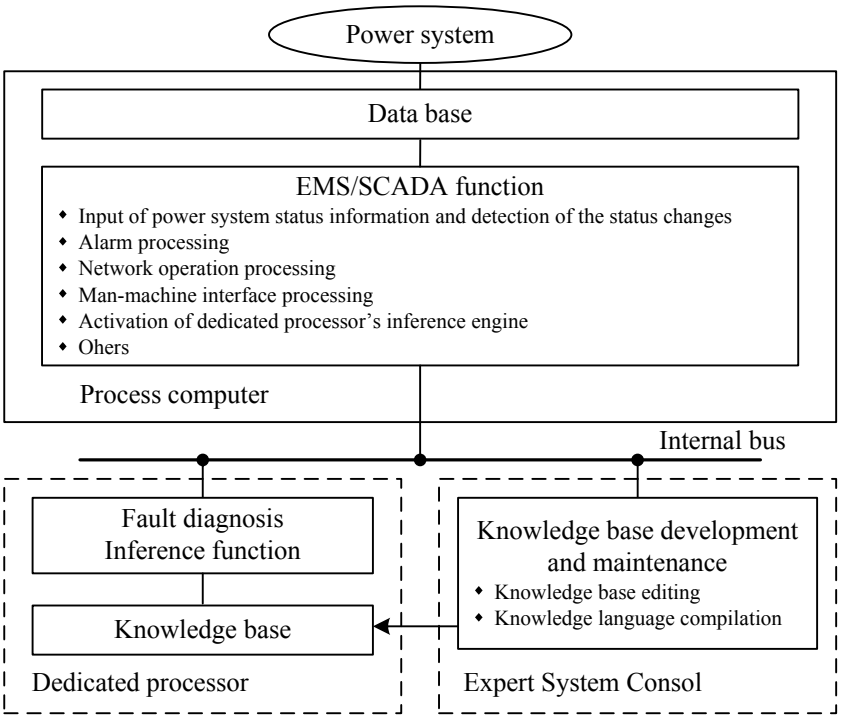

Fig. 1-3 Configuration of a fault diagnosis system with function distributed.

In conventional systems, fault diagnosis is performed using a table of possible faults that contains information concerning operating protective relays, tripped circuit breakers, fault location, and fault type that is prepared in advance. When a fault occurs in the power system, this table is referred to in order to identify the location and type of fault. This approach correctly diagnoses the case of a simple fault like a single fault with correct operation of protective relays and circuit breakers. However, in the case of a single fault complicated by unwanted operation of protective relays and circuit breakers or simultaneous multiple faults as often occur in the case of lightning strokes, the processing becomes excessively complex and the diagnosis is not always correct.

The fault diagnosis method can be classified into two approaches.

a) The first approach consists of organizing monitoring information from operating relays and tripped circuit breakers during a fault and its relationship to fault conditions into a tree structure or in tabular form. This is referred to as the monitoring information-based approach.

b) In the other approach, the structure and functions of the protective relaying system are modeled, the fault conditions are simulated and diagnosis is made comparing the simulation results with the actual monitoring information. This is referred to as the protective structure

model based approach.

An overview of each approach and their characteristics are presented in the following sections.

1.3.1 Monitoring Information-Based Approach

In the early systems such as [1-1], the knowledge base was closely tied to a particular network configuration and was thus fixed. In actual operation this proved problematic since the systems could not adequately cope with changes in the network configuration. Several systems including [1-2]-[1-12], [1-5] were subsequently developed to resolve this problem. The algorithms that are used in these systems can largely be divided into three types.

a) In the first type, a method used in early systems that did not apply a knowledge-based system was employed. The fault is diagnosed from the cases where all operating relays and circuit breakers operate properly, to the cases of incorrect maloperation and then unwanted operation [1-6].

b) In the second type, the knowledge-based systems were applied to improve the efficiency of detection of incorrect maloperation and unwanted operating relays and circuit breakers using experience rules [1-3]. Based on the information provided by relays and breaks, Fukui and Kawakami constructed a database of expert knowledge to carry out on-line fault diagnosis using expert inference [1-1]. In addition, systems that perform verification by using the results of the first method as the input to a protective relay system simulator were developed [1-6], [1-7], [1-11].

c) In the third type, the fault location is diagnosed by judging the incorrect maloperation and unwanted operation of relays and circuit breakers using the intersection set of the protection zones of operating relays. If there is only one element in the intersection set, it is judged that element is faulted. If there are two or more elements in the intersection set, the fault is located at element, but it is impossible to make further identification. If the intersection results in an empty set, the operating relays are divided into two groups and the intersection is repeated in order to allow for a multiple fault. Finally, fault diagnosis using knowledge in the form of experience rules to deal with unusual fault cases such as blind faults that involve relay characteristics is performed.

In order to obtain a high-speed algorithm in the monitoring information-based approach, not all of the relaying system's complex functions are taken into consideration. One example of this simplification is setting the protection zone of the protective relay equal to the set of protected equipment. All of the systems [1-3]-[1-5], [1-8]-[1-l0] at the field testing stage utilize

this approach. It has been indicated that this approach allows configuration of a practical system for the preparation of fault restoration guidelines.

1.3.2 Model-Based Fault Diagnosis Approach

In the model-based approach, a number of proposals have been made that differ in the manner of expressing the model. One effort has been directed at expressing the protective relaying system configuration and functions as an AND-OR logic circuit, and using logic circuit diagnostics to perform fault diagnosis [1-13], [1-15]. However, not all of the protective relaying system's functions can be converted into AND-OR logic circuits. Since it is necessary to completely express the operating logic of the protective relaying system in logical format, some technique must be developed to simplify the representation for application to large-scale power systems.

Several systems have been proposed that utilize simulators of the protective relaying system as the model [1-16]. The basic approach to utilizing a simulator for fault diagnosis is proposed in [1-17]. Several other simulators of protective relaying systems have since been proposed.

In fault diagnosis utilizing simulation, a hypothesis as to the fault conditions is prepared from the monitoring information and the hypothesis is then verified via simulation [1-18]. If the results of simulation match the monitoring information, the hypothesis is then judged as the solution of fault diagnosis. If the simulation results do not match the monitoring information, a new hypothesis with revised fault conditions is generated. Fault diagnosis is completed when all hypotheses have been simulated.

With the development of artificial intelligence, many new methods were applied. A fault diagnosis model based on PN to simulate the relationship between the protective relaying systems and the faults was established [1-20, 1-21]. Meanwhile, this method can handle different topological structural models. Moreover, Wen and Han built a mathematical model to detect faults based on the information of protective relays, and they converted the fault-detecting problem into a 0-1 integer programming problem [1-22].

In this method it is necessary to prepare knowledge for generation and revisions of fault condition hypotheses in addition to the simulation. In order to perform correct fault diagnosis, there must be a good correspondence between the level of simulator functions and the knowledge used to perform generation and revisions of the fault condition hypotheses. Obtaining this correspondence involves implementing complex functions in the simulator in order to increase the accuracy of fault diagnosis, which is expected to be fairly problematic. For

this reason, a method of using general-purpose procedures to process the model, instead of knowledge contained in the object system to generate and revise fault condition hypotheses, has been proposed [1-23]-[1-24], [1-25]. According to [1-25], since the fault diagnosis system can be implemented just by creating a model, the validity of fault diagnosis results resides solely in the model. As a result, one benefit of the system is that the performance of the system can be easily evaluated by verifying the accuracy of the model.

1.4 Influence of PV Installation

PV systems, which can convert sunlight energy into electricity, have gained much attention as a measure for reducing CO2 emissions against global warming. The grid-connected PV systems can convert sunlight into alternating current electricity for power consumers and also can inject the surplus electrical power into the distribution directly. The main purpose of it is to reduce the electrical energy imported from the electric utility. Meanwhile, grid-connected PV systems are usually installed to enhance the performance of the electric network by reducing the power losses and improving the voltage profile of the network [1-26]-[1-28]. Therefore, the penetration level of PV system is rapid growth in recent years. In Japan, the installation target of PV grid-connected system is set at 28GW by 2020, and 53GW by 2030 [1-29]. Furthermore, because of the event of Japanese nuclear leak in Fukushima nuclear power station, the government will revise the country's energy policy that decrease the nuclear power and increase the renewable energy. On such a background, it is estimated that a large-scale PV Grid-connected system will be installed in electrical power networks in the near future.

However, as a coin has two sides, grid-connected PV systems also impose several negative impacts on the network, especially if their penetration level is high. Such negative impacts include power and voltage fluctuation problems, harmonic distortion, malfunctioning of protective devices and overloading and under loading of feeders. These problems and effects also bring many new difficult and challenges to the fault diagnosis for power system.

The structure of traditional power distribution network is shown as Fig. 1-4 (a). The power flow of distribution is unidirectional, from the generator to load consumers. However, with the larger-scale PV embedded into the distribution, the reverser power may be occurred, as shown in Fig. 1-4 (b). This situation was not taken into account in the former fault diagnosis method. Therefore, the relationship between faults and operation information of protection relays and circuit breakers may changed a lot, which will destroy the fault diagnosis system has been established based on knowledge.

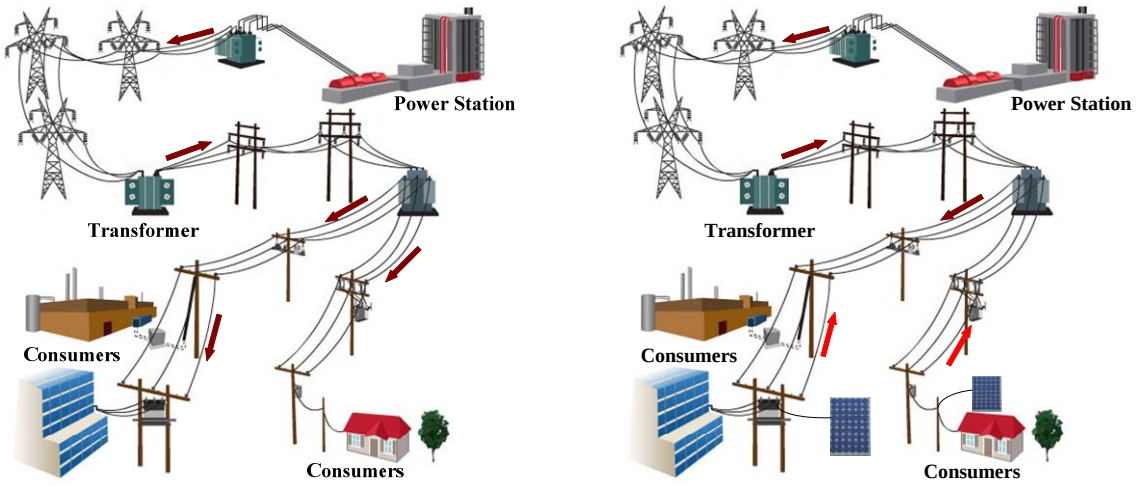

(a) (b)

Fig. 1-4 Power flow of network: (a) Power flow of network without PV connected; (b) Power flow of network with PV connected.

1.5 Research Outline

The doctoral dissertation concerns the above problems and presents a new hierarchical fault diagnosis (HFD) method for power distribution that is based on a hierarchical model and the equivalent-input-disturbance (EID) approach.

1) Construction method of the HFD Model is proposed.

For a local distribution network, the amount of load nodes is varied from the dozens to thousands and the numbers of sensors are numerous. Due to the complexity of it, a complete mathematical model of an entire distribution system is extremely complicated and contains a huge number of parameters. Since the use of such a model for fault diagnosis involves a time-consuming deduction process, a high-performance microprocessor is needed for real-time diagnosis. Therefore, a hierarchical modeling technology is applied to the power system. In the each layer of HFD model, the distribution network can be divided into several Load clusters, which of them contains a number of load nodes. Fault diagnosis is carried out from the top down through the layers of the HFD model to locate the faults.

2) The EID approach [1-30] [1-31] is applied to the fault diagnosis method for the Load Cluster.

The parameter fluctuation, measurement noise and the external disturbance always exist in the actual system, beside the power system. For a stable operation system, if the disturbances caused by these factors are under an allowable range, the system will undergo a little oscillation and come back to the steady state in a short time. However, if the disturbances are too large and

exceed the tolerance range, even resulting in running failure of the system, we regards that a fault occurs in the system. Therefore, faults can be defined as: the disturbances exceed the allowable range and break the stability of system. The fault diagnosis method proposed in this thesis is based on this viewpoint.

The power system is a larger-scale system, with ten of thousands of electrical equipments. In order to maintain the safe and stable operation of power system, the most important issue is keep the balance between the power supply and power consumption. As we know, the power consumptions are unpredictable and change with the time lapse. From the perspective of power supply, the variation of power consumption is a kind of disturbance to power supply, and we regard it as a normal disturbance, not a fault. When a fault occurs in power system, the consequence is current increasing and/or voltage dropping in a short time, which can be regarded as an abnormal disturbance or fault disturbance. The abnormal disturbance has different characteristics with the normal disturbance, for example the magnitude and differential of them. Therefore, if we can obtain the normal disturbances and fault disturbance of system and distinguish them, the fault diagnosis would be carried out.

Based on this concept, the EID approach, which can estimate the system disturbances, is applied to diagnose the faults.

3) To eliminate the influence of PV to the fault diagnosis, the fault signal is abstracted by removing the PV fluctuation from the EID.

The fluctuation of the output power of PV systems due to the variations in the solar irradiance caused by the movement of clouds is the main factor impacting on the distribution feeders and brings the large distribution to the utility power supply. By measuring the PV generation output variation and estimating the EID of PV to the Load Cluster, the PV's influence could be eliminated in the fault diagnosis.

The structure of this doctoral thesis is planned as follows:

Chapter 1. The background of the research is presented. Then the definition and categories of faults in electrical power system are introduced briefly. Moreover, the overview of conventional fault diagnosis methods is expounded. In addition, the influence of grid-connected PV generation to the fault diagnosis is analyzed.

Chapter 2. The HFD Model based on Backward and Forward Sweep (BFS) power flow calculation algorithm [1-32] is set up. Considering the PV system has two different operation types, thus we improve the BFS algorithm to adapt them.

Moreover, the IEEE 13 nodes radial distribution feeder [1-33] is used as an example to illustrate the hierarchical modeling process.

Chapter 3. The fault diagnosis method for distribution network based on EID approach is proposed. The theory basis and design method of EID approach are described in detail at the standpoint of control theory. Furthermore, the simulation results on a case study are presented to illustrate the effective of the method.

Chapter 4. The fault diagnosis method for distribution feeder with PV generation embedded is presented. The influence of PV generation to fault diagnosis is analyzed in depth. Additionally, the approach for separation of PV's impact on the fault diagnosis is designed. A case study testifies the validity of our method.

Chapter 5. In order to make the procedure of Hierarchical Fault Diagnosis Method easy to understand, the IEEE 37 nodes test feeder model is used as an example.

Chapter 6. The conclusions and the possible future works are presented in this chapter.

Chapter References

[1-1] **C. Fukui and J. Kawakami.** *An expert system for fault section estimation using information from protective relays and circuit breakers.* IEEE Trans. Power Del., vol. 1, no. 4, pp. 83-90, Nov. 1986.

[1-2] **N. Koike, T. Maeshiro, T. Gotoh, M. Kunugi, T. Hirokawa, and N. Wada.** *A real-time expert system for power system fault diagnosis*. in Proc. JASTED Power High-Tech '86, Bozeman, MT, pp. 376-380, 1986.

[1-3] **T. Minakawa, Y. Ichikawa, M. Kunugi and K. Shimada.** *Development and implementation of a power system fault diagnosis expert system.* IEEE Trans. Power Syst., vol. 10, no. 2, pp. 932-940, May 1995.

[1-4] **M. Vazquez, E. Chacon M., O. L. Altuve F. and H. J.** *An On-line Expert System For Fault Section Diagnosis In Power Systems.* IEEE Trans. Power Syst., vol. 12, no. 1, pp. 357-362, Feb. 1997.

[1-5] **K. Kimura, S. Nishimatsu, Y. Ueki and Y. Fukuyama.** *An on-line expert system for estimating fault section in control center.* in Proc. 3rd Symp. on Expert Systems Application to Power Systems, Tokyo, Kobe, pp. 95401, Apr. 1991.

[1-6] **M. S. Choi, S. J. Lee and D. S. Lee.** *A new fault location algorithm using direct circuit analysis for distribution systems.* IEEE Transactions on Power Delivery, vol. 19, no. 1, pp. 35-41, 2004.

[1-7] **O. A. S. Youssef.** *Combined fuzzy-logic wavelet-based fault classification technique for power system relaying.* IEEE Transactions on Power Delivery, vol. 19, no. 2, pp. 582-589, 2004.

[1-8] **R. Szczesny, P. Kurzynski, H. Piqueb and K. Hwan.** *Knowledge-base system approach to power electronic systems fault diagnosis.* in Proc. IEEE International Symposium, 1996, pp. 1005-1010.

[1-9] **H. Yang, W. Chang and C. Huang.** *Power System Distributed Online Fault Section Estimation Using Decision Tree Based Neural Nets Approach.* IEEE Trans. Power Del., vol. 10, no. 1, pp. 540-546, Jan. 1995.

[1-10] **E. M. Davidson, S. McArthur and J. R. McDonald.** *Applying multiagent system technology in practice: automated management and analysis of SCADA and digital fault recorder data.* IEEE Trans. Power Syst., vol. 21, no. 2, pp. 559-567, May 2006.

[1-11] **L. Xu and M. Y. Chow**. *A Classification Approach for Power Distribution Systems Fault Cause Identification.* IEEE Trans. Power Syst., vol. 21, no. 1, pp. 53-60, Feb. 2006.

[1-12] **C. L. Hor., P. A. Crossley and S. J. Watson.** *Building Knowledge for Substation-Based Decision Support Using Rough Sets.* IEEE Trans. Power Del., vol. 22, no. 3, pp. 1372-1379, Jul. 2007.

[1-13] **A. Wake and T. Sakaguchi.** *Method to determine the fault components of power system based on description of structure and function of relay system.* Trans. IEE Japan, vol. 104-B, no. 10, Oct. 1984.

[1-14] **K. Matsumoto, T. Sakaguchi, and T. Wake.** *Fault diagnosis of a power system based on a description of the structure and function of the relay system.* Expert systems, vol. 2, no. 3, pp. 134-138, July 1985.

[1-15] **E. M. Davidson, S. D. J. McArthur and J. R.** *McDonald. A Toolset for Applying Model-Based Reasoning Techniques to Diagnostics for Power Systems Protection.* IEEE Trans. Power Syst., vol. 18, no. 2, pp. 680-687 May 2003.

[1-16] **K. Komai, K. Matsumoto, and T. Sakaguchi.** Network fault diagnosis based on event simulation of protective relay systems. Trans. IEE Japan, vol. 108-B, no. 6, pp. 245-252, June 1988.

[1-17] **X. Luo and M. Kezunovic.** *A Novel Digital Relay Model Based on SIMULINK and Its Validation Based on Expert System.* Transmission and Distribution Conference and Exhibition: Asia and Pacific, IEEE/PES, 2005

[1-18] **M.S. Serwan, N. Hamzah and Z. Zakaria.** *Hypothesis Testing for Fault Analysis and The Propagation of Faulted Voltage through Transformer Connections.* IEEE Research and Development (SCOReD), Dec. 2011

[1-19] **C. Wu, F. Jiang, Q. Wang and J. Liu.** *Bayesian network methods for Fault Diagnosis of Power Systems.* Electrical and Control Engineering (ICECE), 2011.

[1-20] **L. Jenkins and H. P. Khincha**. *Deterministic and stochastic Petri net models of protection schemes.* IEEE Transactions on Power Delivery, vol. 7, no. 1, pp. 84-90, Jan. 1992.

[1-21] **V. Calderaro, C. N. Hadjicostis, A. Piccolo and P. Siano.** *Failure Identification in Smart Grids Based on Petri Net Modeling.* IEEE Trans. Ind. Electron., vol. 58, no. 10, pp. 4613-4623, Oct. 2011.

[1-22] **F. S. Wen and Z. X. Han.** *Fault section estimation in power systems using simulated evolution.* Transaction of China Electrotechnical Society, vol. 9, pp. 57-63, Feb. 1994.

[1-23] **W.H. Chen, S.H. Tsai and H.I. Lin.** *Fault Section Estimation for Power Networks Using Logic Cause-Effect Models.* IEEE Trans. Power Del., vol. 26, no. 2, Apr. 2011.

[1-24] **W. Wang, X. Bai, W. Zhao, J. Ding and Z. Fang.** *Hybrid Power System Model and the Method for Fault Diagnosis.* IEEE/PES Asia and Pacific Transmission and Distribution Conference and Exhibition, 2005

[1-25] **K. S. Swarup and H. S. Chandrasekharaiah.** *Model-based fault diagnosis of power systems.* in Proc. 3rd Symp. on Expert Systems Application to Power Systems, Tokyo, Kobe, pp. 223-227, Apr. 1991.

[1-26] **X. Dong, E. Gorashi, T. Elmirghani and J. M. H..** *Renewable energy for low carbon emission IP over WDM networks.* International Conference on Optical Network Design and Modeling (ONDM),Feb. 2011

[1-27] **C. Xuansan.** *Renewable Energies, Present & Future. Advanced Technology of Electrical Engineering and Energy,* vol. 24, no. 1, pp. 69-75, Jan. 2005.

[1-28] **Y. Liu, J. Bebic, and W. Ren.** *Distribution System Voltage Performance Analysis for High-Penetration PV***.** IEEE Energy 2030 Conference, 2008.

[1-29] **J. Yoshinaga, T. Hirai, and Y. Kowada.** *Development of Central Voltage Control Method for Distribution Systems.* In Proc. of the Fifteenth Annual Conference of Power & Energy Society. IEE Japan, no. 30, 2004.

[1-30] **S. X. Ding.** *Model-based Fault Diagnosis Techniques. Design Schemes*, *Algorithms, and Tools.* Springer, Duisburg Germany, 2008, pp. 11-23.

[1-31] **J. She, M. Fang, Y. Ohyama, H. Hashimoto and M. Wu.** *Improving Disturbance Rejection Performance Based on an Equivalent-Input-Disturbance Approach.* IEEE Trans. Ind. Electron., vol. 55, no, 1, pp. 380-389, Jan. 2008.

[1-32] **C. S. Cheng and D. Shirmohammadi.** *A three-phase power flow method for real-time distribution system analysis.* IEEE Trans. Power Syst., vol. 10, no. 2, pp. 671-679, May 1995.

[1-33] **W. H. Kersting.** *Radial distribution test feeders.* IEEE Trans. Power Syst., vol. 6, no. 3, pp. 975-985, Oct. 2002.

Chapter 2
Hierarchical Fault Diagnosis Model of Power Distribution Networks

2.1 Chapter Introduction

Modern power systems are enormous and complex. In a distribution network, the amount of consumers is varied from the dozens to thousands and the numbers of sensors are numerous. Due to the complexity of the systems, a complete mathematical model of an entire distribution system is extremely complicated and contains a huge number of parameters. Since the use of the complete model for fault diagnosis involves a time-consuming deduction process, a high-performance microprocessor is needed for real-time diagnosis.

In order to reduce the complexity of system model, the hierarchical modeling technology is widely applied in many fields. In the spacecraft health monitoring and fault diagnosis, A. Barua *et al*, [2-1] and [2-2], develop a systematic and transparent fault-diagnosis methodology within the hierarchical fault-diagnosis concepts and framework. A hierarchical model for the assessment of high level quality attributes in object-oriented was designed in [2-3]. Similarly, in this thesis, we attempt to introduce the hierarchical modeling technology into the power distribution network fault diagnosis. By the hierarchical model, Fault diagnosis can be carried out form the top down through the layers to gradually locate a fault accurately.

The structure of this chapter is planned as follows:

Section 2.2: The framework of Hierarchical Fault Diagnosis model for distribution network is proposed. The Tokyo-23-districts distribution network is used as an example to illustrate the construction method of the HFD model. The procedures of HFD method are also presented in this section.

Section 2.3: The model parameters, which are used to construct the HFD model, are calculated by the Backward and Forward Sweep algorithm. In the power flow calculation, the PV system can be classified into *PV-specified* node and *PQ-specified* node, therefore, the BFS algorithm is improved to accommodate the different operation type of PV systems.

Section 2.4: The definition of Load Cluster is given out in this section. The load cluster is the basic unit of the distribution network in hierarchical model. And the dynamic model of the load cluster is given out.

Section 2.5: The IEEE 13 nodes radial distribution feeder is used as an example to illustrate the modeling process for the HFD model.

2.2 HFD Model Construction

For the proposed fault diagnosis method, not the complete model of network, but the hierarchical model is used to diagnose the fault instead. In this section, the framework of HFD model is given out and the procedures HFD algorithm is also proposed.

2.2.1 Framework of HFD Model

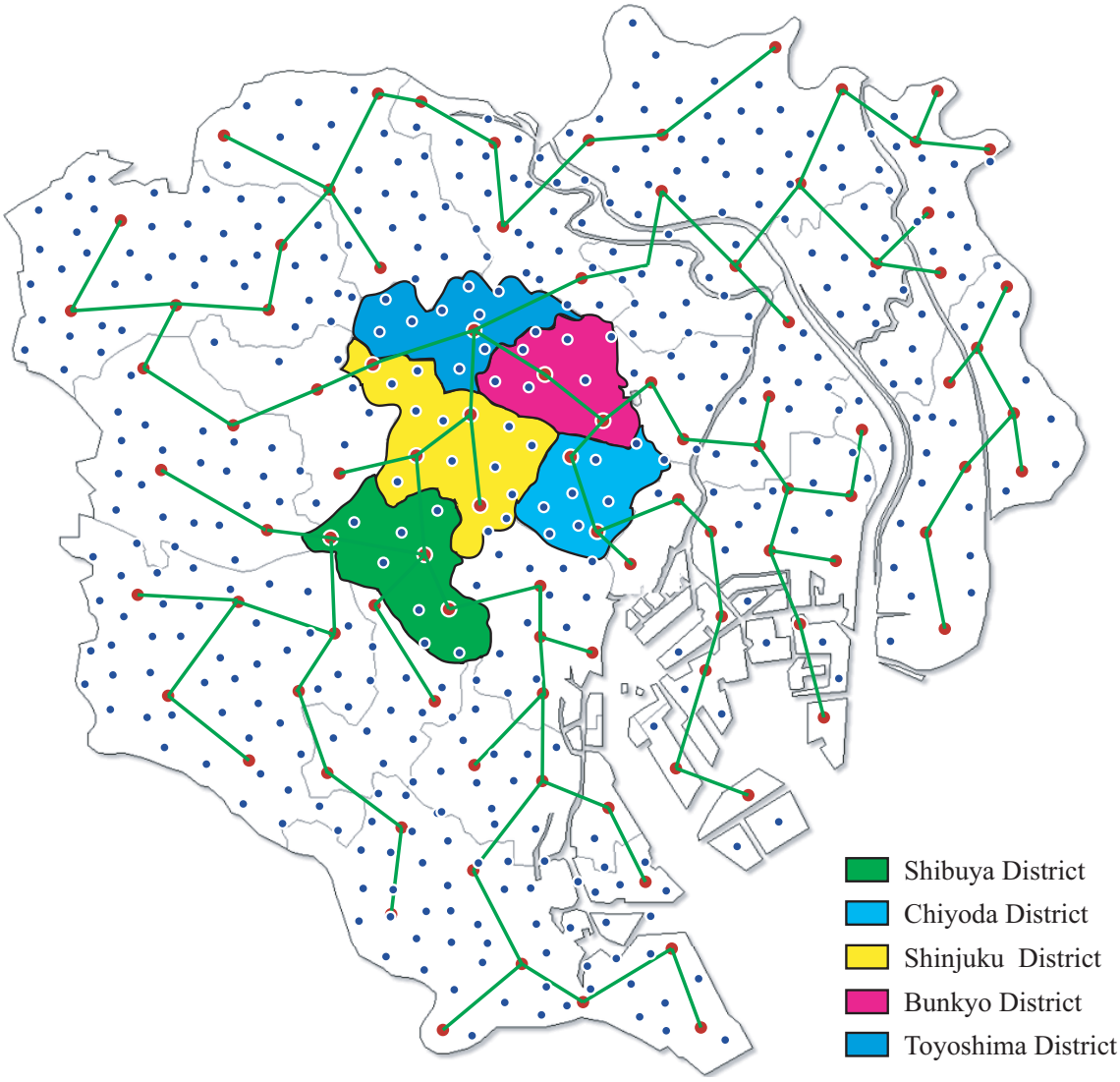

Fig. 2-1 Schematic Diagram of Tokyo 23 districts distribution networks.

The distribution network is constituted by many load nodes. A hierarchical model of a distribution network is built by first dividing it into multiple clusters based on the locality and/or logical topology. Then, the clusters are subdivided successively into smaller clusters. This produces both a multilayer structure and a hierarchical model of the system. Fault diagnosis is carried out from the top down through the layers to gradually locate a fault and to identify its type.

Take the Tokyo 23 districts as an example. Fig. 2-1 is the overview diagram of Tokyo 23-districts distribution networks. According to the administrative divisions, Tokyo city can be divided into 23 clusters at first, including the Shibuya, Shinjuku, Chiyoda, Bunkyo, Toyoshima and other districts. If we treat the entire Tokyo as the Layer 0 of the HFD model, the 23 districts construct the Layer 1 of the HFD model and each district is a component at Layer 1. In addition, each of the districts can be subdivided again, according to the community structure or the logical topology of the distribution networks. Takes the Shinjuku district as an example, Waseda Campus and Nishi-Waseda Campus are the components of the Shinjuku district and both of them contain a number of load nodes. Meanwhile, the Shinjuku district also contains other clusters just like the Waseda Campus and Nishi-Waseda Campus, and all of clusters construct the Layer 3 of the HFD model. Furthermore, the Nishi-Waseda Campus can be subdivided at Layer 4. The building of the campus is the components at this layer, for example, 55-building, 53-building, 63 building and so on.

Fig. 2-2 is hierarchical framework of Tokyo 23-districts distribution networks. In the framework of the Tokyo 23-districts distribution network, the entire network is divided into *n* layers. With the deeper of layer, the cluster is smaller. At the last layer, the cluster can not be subdivided any more. In each layer of the model, there are several clusters. Each of them contains a number of load nodes. In this thesis, this kind of cluster, which contains many load nodes, is called Load Cluster. The load cluster is the basic unit for the hierarchical fault diagnosis model.

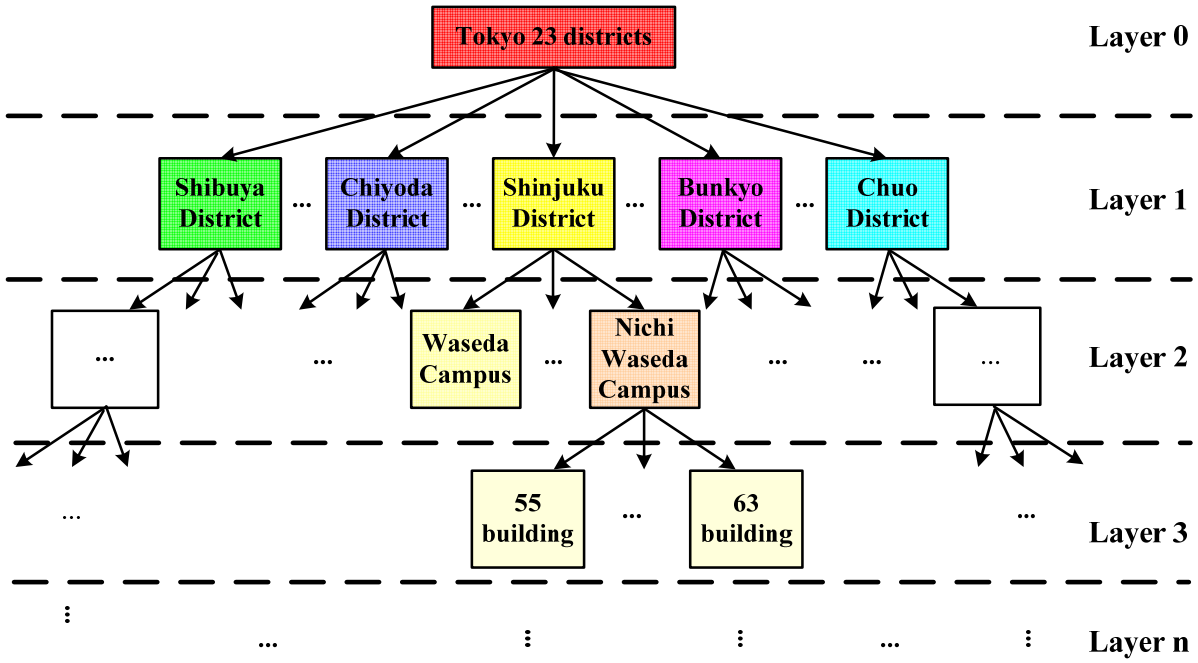

Fig. 2-2 Hierarchical framework of Tokyo 23 districts distribution networks.

The equation (2.1) is the complex power calculation approach for the Load Cluster *n* in Layer *k*, $\mathcal{C}_n^{(k)}$:

$$S_n^{(k)} = \sum_{i \in \Phi_n^{(k)}} S_i . \tag{2.1}$$

Where, the $\Phi_n^{(k)}$ is the set of all the nodes in Load Cluster $\mathcal{C}_n^{(k)}$, S_i is the complex power of the Node *i* and the $S_n^{(k)}$ is the total complex powers of Load Cluster $\mathcal{C}_n^{(k)}$ in layer *k*.

In the HFD model, fault diagnosis can be carried out from the top down through the layers to gradually locate the fault. For example, we assume that a fault occurs at load cluster "63 building" of the Fig. 2.2. Firstly, the fault can be detected at Layer 1 and located at Load Cluster "Shinjuku District" of Layer 1. And then, diagnose the child load clusters belong to the load cluster "Shinjuku District" at the Layer 2 and the fault can be further located at load cluster "Nishi-Waseda Campus". Finally, diagnose the child load cluster belong to the "Nishi-Waseda Campus" at Layer 3 and the fault can be located at "63 building".

The HFD model is applied to diagnose the faults have two advantages.

1) The faults location is gradually located from the top of the hierarchical structure downward through the layers. It is simple and computationally inexpensive.

The entire distribution networks contain thousands of nodes. When a fault occurs at a certain node, it is hard to locate the fault node from all the nodes in one time. For the HFD model, we can locate the fault layer by layer from the top to down. In each layer, there are only several or dozens of Load Clusters. Compared to the entire model, the HFD model is simpler and the computation time is faster.

2) Whatever the effect of the fault is small or large, the hierarchical model is always able to locate the fault in final.

In the standpoint of entire Tokyo 23 districts dispatching center, faults can be classified into 3 levels.

a) The fault occurs at the household electricity equipment, we call it tiny level;

b) The fault occurs at the community electricity equipment, we call it middle level;

c) The fault occurs at the district electricity equipment, we call it large level.

The different level of faults, have the different influence range to the dispatching center of Tokyo. If a fault occurs at the electrical equipment of the district and leads to blackout in a large-scale area, the effect of the fault is large and it is easy to be identified by the dispatching center of Tokyo. However, if the fault is the tiny fault, due to the little influence of it, the dispatch

center is hard to detect it.

However, in our model, by monitoring the different layer of model, whatever the fault is large or small, the fault can be detected layer by layer. For example, we can monitor the Layer 1 or lower Layer (Layer 2) to monitor the fault may be occurred at Layer 3. In this way, the fault can be identified earlier and removed it timely, avoiding the worse impact on the network.

2.2.2 Procedures of HFD Algorithm

As mentioned above, the fault diagnosis start from the top to down and locate the fault position gradually. There are many reasons for performing a fault diagnosis. For example, a supervisor might want to know if it is safe for one of the power plants in a large system to supply power to the loads it services. In this case, diagnosis should start at the layer containing that plant. On the other hand, for maintenance, a supervisor might need to check if there is a fault in a particular area. In that case, the diagnosis should start at the relevant layer. Hierarchical fault diagnosis provides the flexibility needed to handle a variety of diagnostic needs.

Extracting the key points from the above discussion gives us the following HFD algorithm. If Layer k is to be checked, fault diagnosis starts from that layer.

Step 1) Construct a hierarchical model of the network and calculate the dynamic model of each load cluster.

Step 2) Monitor the Layer k of the hierarchical model in a real-time fashion. If a fault occurs at load cluster C_k, then go to the next step.

Step 3) Go to Layer k+1 and check the child load clusters of C_k in this layer to determine which cluster contains the fault (C_{k+1} for example). If the cluster containing the fault has only one node, go to Step N.

Step 4) Go to Layer k+2 and examine the child clusters of C_{k+1} in this layer to determine which cluster contains the fault. If the cluster containing the fault has only one node, go to Step N.

…

Step N) Determine the type of fault by analyzing the amplitude and phase of the estimated state of the smallest cluster containing the fault, which was produced by the dynamic model.

Note that, if a cluster containing a fault has only one node, then the location of the fault is determined in that step and the type is determined in the next step; there is no need to always descend to the lowest layer. Furthermore, the fault diagnosis does no need to scan all the load

clusters and only diagnose the clusters and their child clusters that might have a fault. This can reduce the computation complexity and save much computation time.

2.3 Model Parameters Calculation Algorithm

In the section 2.2, the construction method of HFD model is expounded. Before constructing the model, the model parameters including nodal voltages and transmission lines current, need to be calculated at first. In this section, the BFS algorithm is used to calculate the model parameters of the distribution feeders. With the PV system embedded to the feeders, the BFS algorithm need to be improved to accommodate the different of PV system operation model.

2.3.1 Basis of BFS Algorithm

The algorithm for the BFS power flow simulation for three-phase unbalance radial distribution system was formulated by D. Shirmohammadi and C. S. Cheng [2-4]. The algorithm is quite simple since it was only based from the two basic laws in electrical engineering, the kirchhoff's current and voltage laws. Since specially formulated for the power flow of a distribution system, which is usually, radial to up to weakly meshed in the configuration, it is fast and a very effective tool for a simulation where speed is a factor, like the power flow of a large scale system.

The primary feeders of the distribution system consist of mostly three-phase overhead or underground line sections (branches), and occasionally double-phase or single-phase line sections near the end of the feeder laterals. In the three-phase power flow algorithm, we number each node or line section in the network by a single index, regardless of the number of phases of this node or line section. The series impedance of a line section, *l*, is represented by a 3×3 matrix:

$$Z_l = \begin{bmatrix} z_{aa,l} & z_{ab,l} & z_{ac,l} \\ z_{ab,l} & z_{bb,l} & z_{bc,l} \\ z_{ac,l} & z_{bc,l} & z_{cc,l} \end{bmatrix}. \tag{2.2}$$

If any phase of the line section does not exist, the corresponding row and column in this matrix contain all zero entries. Fig. 2-3 shows line section *l* between nodes *i* and j with shunt admittances and loads attached to each node.

To apply the single-phase power flow algorithm described in [2-5] to three-phase we first convert the primary distribution network to a radial system by breaking all the loops. Line sections in the radial network are ordered by layers away from the root node (substation bus),

and the Fig. 2-4 is reprinted below as an example.

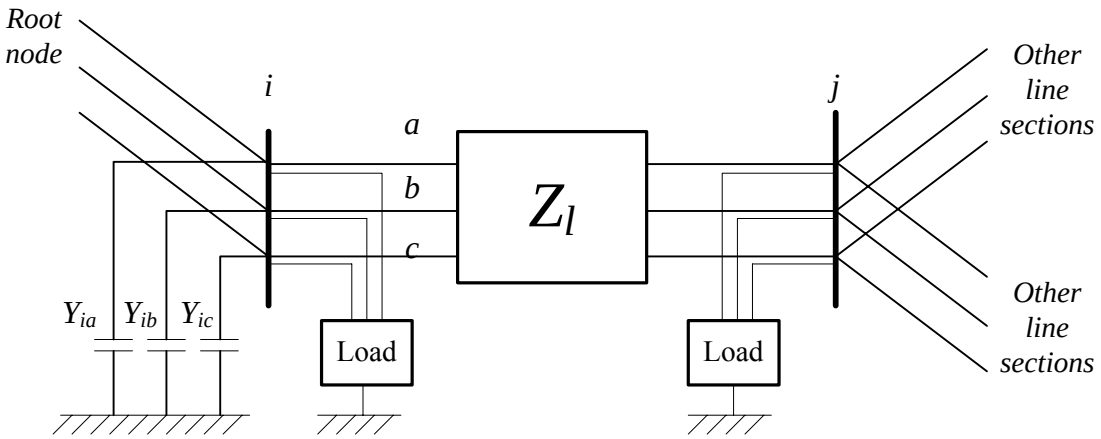

Fig. 2-3 A three-phase line section.

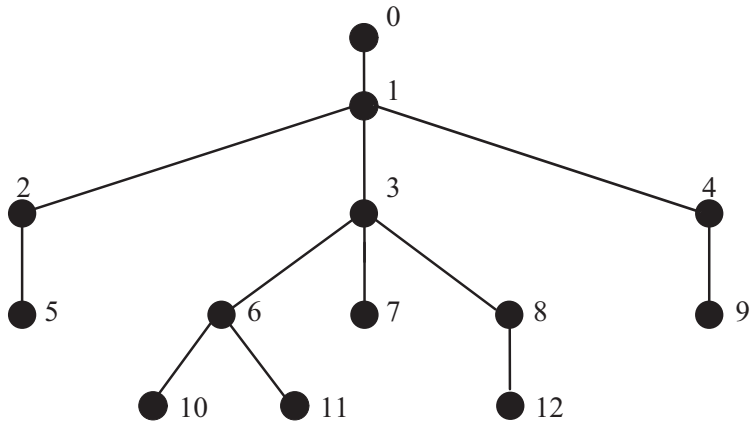

Fig. 2-4 Branch numbering scheme for radial distribution network.

Let the root node be the slack node with known voltage magnitude and angle, and let the initial voltage for all other nodes be equal to the root node voltage. The iterative algorithm for solving the radial system consists of three steps. At iteration k:

Step 1) Current injection calculation for each node:

$$\begin{bmatrix} I_{ia} \\ I_{ib} \\ I_{ic} \end{bmatrix}^{(k)} = \begin{bmatrix} \left(S_{ia} / V_{ia}^{(k-1)} \right)^* \\ \left(S_{ib} / V_{ib}^{(k-1)} \right)^* \\ \left(S_{ic} / V_{ic}^{(k-1)} \right)^* \end{bmatrix} - \begin{bmatrix} Y_{ia}^* & & \\ & Y_{ib}^* & \\ & & Y_{ic}^* \end{bmatrix} \begin{bmatrix} V_{ia} \\ V_{ib} \\ V_{ic} \end{bmatrix}^{(k-1)} . \tag{2.3}$$

Where $I_{ia,}\, I_{ib,}\, I_{ic,}$ are current injection at node i correspoding to constant power load and shunt elements S_{ia}, S_{ib}, S_{ic} are scheduled power injections at node i; V_{ia}, V_{ib}, V_{ic} are voltage at node i; Y_{ia}, Y_{ib}, Y_{ic} are admittances of all shunt elements at node i.

Step 2) Backward sweep to sum up line section current: starting from the line section in the last layer and moving towards the root node, the current in line section *l* is:

$$\begin{bmatrix} J_{la} \\ J_{lb} \\ J_{lc} \end{bmatrix}^{(k)} = -\begin{bmatrix} I_{ja} \\ I_{jb} \\ I_{jc} \end{bmatrix}^{(k)} + \sum_{m \in M} \begin{bmatrix} J_{ma} \\ J_{mb} \\ J_{mc} \end{bmatrix}^{(k)} . \tag{2.4}$$

Where J_{la}, J_{lb}, J_{lc} the current flows on line section *l*; *M* is the set of line sections connected to node *j*. Note that the negative sign in (2.4) is to keep consistent with current injection as calculated in (2.3).

Step 3) Forward sweep to update nodal voltage: starting from the first layer and moving towards the last layer, the voltage at node *j* is:

$$\begin{bmatrix} V_{ja} \\ V_{jb} \\ V_{jc} \end{bmatrix}^{(k)} = \begin{bmatrix} V_{ia} \\ V_{ib} \\ V_{ic} \end{bmatrix}^{(k)} - \begin{bmatrix} Z_{aa,l} & Z_{ab,l} & Z_{ac,l} \\ Z_{ab,l} & Z_{bb,l} & Z_{bcl} \\ Z_{ac,l} & Z_{bc,l} & Z_{cc,l} \end{bmatrix} \begin{bmatrix} J_{la} \\ J_{lb} \\ J_{lc} \end{bmatrix}^{(k)} . \tag{2.5}$$

After these three steps are executed in an iteration, the power mismatches at each node for all phase are calculated:

$$\begin{cases} \Delta S_{ia}^{(k)} = V_{ia}^{(k)} (I_{ia}^{(k)})^* - Y_{ia}^* \left| V_{ia} \right|^2 - S_{ia} \\ \Delta S_{ib}^{(k)} = V_{ib}^{(k)} (I_{ib}^{(k)})^* - Y_{ib}^* \left| V_{ib} \right|^2 - S_{ib} \\ \Delta S_{ic}^{(k)} = V_{ic}^{(k)} (I_{ic}^{(k)})^* - Y_{ic}^* \left| V_{ic} \right|^2 - S_{ic} \end{cases} . \tag{2.6}$$

If the real or imaginary part (real or reactive power) of any of these power mismatches is greater than a convergence criterion, steps 1, 2 and 3 are repeated until convergence is achieved. The Fig. 2-5 is the flow chart of the BFS algorithm.

Equations (2.3)-(2.6) provide the solution for a three-phase radial network. In a meshed system, it is necessary to simulate loops by injecting currents at both ends of all breakpoints. Currents at breakpoints are calculated using the compensation technique and a breakpoint impedance matrix. This procedure is based on the same principle as described in [2-6] and [2-7]. In this thesis, we do not discuss the fault diagnosis in the meshed distribution network. Therefore, we do not describe it in detail.

2.3.2 Improved BFS Algorithm

In the power flow calculation problem, the variables are nodal complex voltages and complex powers: *V*, *θ*, *P*, *Q*. Usually, two variables at each node are assumed known before the calculation. According to the original data, the nodes in power system can be classified into

three types.

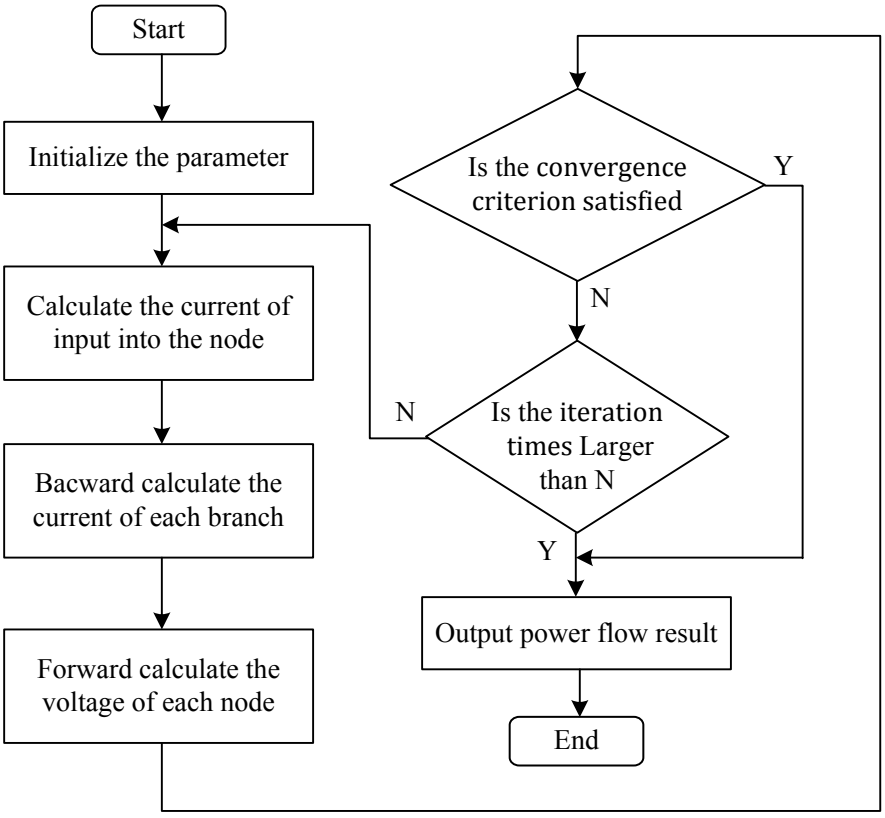

Fig. 2-5 Flow chart of BFS algorithm.

a) *PQ*-specified Nodes: For *PQ-specified* nodes, the active and reactive power (P, Q) are specified as known parameters, and the complex voltage (V, θ) is to be resolved. In the feeders, most nodes belong to *PQ-specified* nodes, because the load is the known.

b) *PV-specified* Nodes: For *PV-specified* nodes, active power and voltage magnitude (P, V) are specified as known variables, while the reactive power Q and voltage angle θ are to be resolved. Usually, *PV-specified* nodes should have some controllable and large enough reactive power resources and can thus maintain node voltage magnitude at a desirable value. Generally speaking, the nodes of power plant can be taken as *PV-specified* nodes, because voltages at these nodes can be controlled with reactive power capacity of their generators. Some substations and embedded generators can also be considered as *PV-specified* nodes when they have enough reactive power compensation devices to control the voltage.

c) Slack Nodes: For Slack nodes, the voltage magnitude V and phase θ are given as known variables, while the active power P and reactive power Q are variables to be solved. Usually, in the large feeders, usually there should be one and only one slack node specified. For the Fig. 2-4, the node 0 (root node) is the slack node of the feeder.

The PV system connected to the nodes by the inverters, which can control the output active

power P_{pv}, reactive power Q_{pv} and/or voltage V_{pv} to the consumers. Therefore, the PV systems can be regarded as two kinds of node in power flow calculation.

1) *PV-specified* node. As a *PV-specified* node,, the active power and voltage magnitude (P, V) of PV systems are specified.

2) *PQ-specified* node. As a *PQ-specified* node, the active power and reactive power (P, Q) of PV system are specified.

For different demands, the consumers can choose the different PV system. If the consumer is strict with the voltage, the *PV-specified* node type PV system can be installed. If not, *PQ-specified* node type PV system can be used.

In former section, the BFS algorithm is described how to solve the power flow. And all the load nodes of the feeder are assumed to be *PQ-specified node*s in calculation. The complex power of node S is known in advance, in the equation (2.3). With the different PV systems connected to the load node, the BFS algorithm should be improved to accommodate the two kinds of PV system.

If the PV system is regarded as *PQ-specified* node, the output complex power $S_{pv}=P_{pv}+jQ_{pv}$ is known. In this situation, the PV system and the node where it installs are considered to be a new node, and the complex power of new node need to be updated (2.7) before starting the iteration of BFS algorithm. Specifically, in the Step 1) of the BFS algorithm, the complex power S_{ia}, S_{ib}, S_{ic} are replaced by the new complex power $S_{ia}^{'}$, $S_{ib}^{'}$, $S_{ic}^{'}$.

$$S_{ia}^{'} = S_{ia} + S_{pva}, S_{ib}^{'} = S_{ib} + S_{pvb}, S_{ic}^{'} = S_{ic} + S_{pvc}. \tag{2.7}$$

If the PV system regards as *PV-specified* node, the output reactive power of PV system Q_{pv} is unknown and in order to keep the voltage of the node stable, the reactive power Q_{pv} should be changed. Therefore, special procedures must be performed to maintain its voltage magnitude after the each iteration of BFS algorithm, as well as to monitor its reactive power capability.

In the thesis, we have applied a compensation method using a *PV-specified* node sensitivity matrix to eliminate the voltage magnitude mismatch for all *PV-specified* nodes. The basic idea of this method can be explained as follows. Suppose a power flow calculation has converged, and the magnitude of voltage at *PV-specified* nodes is not equal to the scheduled values. In order to obtain the scheduled voltage magnitude at a *PV-specified*, we need to determine the correct amount of reactive power or reactive current injection generated by the unit. Therefore, the problem of compensating *PV-specified* node voltage magnitude becomes: Find the reactive current injection, I_q for each *PV-specified* node so that the voltage magnitude, $|V|$, of this node is

equal to the scheduled value. Since the relation between I_q and $|V|$ is nonlinear, I_q can only be determined iteratively. A *PV-specified* node sensitivity matrix is introduced to approximate the nonlinear relation between $|V|$ and I_q and is used to evaluate I_q iteratively as described below.

1) *PV-specified Node Sensitivity Matrix*

A *PV-specified* node is modeled in a similar manner as in [2-8]-[2-11], i.e., the constants for a PV system are the three-phase real power output and the magnitude of the positive sequence voltage. The use of positive sequence representation for voltage magnitude regulation makes it possible to properly represent the automatic voltage regulation mechanism of a generating unit, where in most cases, the average of voltage magnitude of all three phases is the voltage magnitude that is regulated.

The incremental relation between the magnitude of positive sequence, voltage and the magnitude of the positive sequence reactive current injection is expressed as

$$\left[Z_v\right]\left[I_q\right]^{(\gamma)} = \left[\Delta V\right]^{(\gamma)}. \tag{2.8}$$

Where, $[Z_v]$ is a constant real matrix, referred to as the *PV-specified* node sensitivity matrix. The dimension of $[Z_v]$ is equal to the number of *PV-specified* nodes. Column j of $[Z_v]$ may be determined by applying $I_j = \{0,1\}$ to *PV-specified* node j with all loads and sources removed, and solving a positive sequence network with one back and forward sweep for the change of voltage magnitudes at all *PV-specified* nodes.

Equivalently, $[Z_v]$ can be formed by observing the following numerical properties of its entries. The diagonal entry, z_{ii}, in $[Z_v]$ is equal to the modulus of the sum positive sequence impedance of all line sections between *PV-specified* node i and the root node (substation bus). If two *PV-specified* nodes, i and j, have completely different path to the root node, then the off-diagonal entry z_{ij} is zero. If i and j share a piece of common path to the root node, then z_{ij} is equal to the modulus of the sum positive sequence impedance of all line sections on this common path. Based on these, $[Z_v]$ can be formed by identifying the path between *PV-specified* nodes and the root node. When forming $[Z_v]$ for a group of feeders connected to different substations, the impedance paths will be between the *PV-specified* node on a feeder and the substation bus (root node) to which the feeder is connected.

In our power flow algorithm, $[Z_v]$ is formed for all initial *PV-specified* nodes and factorized into LU before any power flow iteration is performed. Depending on whether there are PV to *PQ-specified* node conversions, $[Z_v]$ and its factors may have to be updated.

2) *Iterative Process for Voltage Magnitude Correction*

Suppose there are *n PV-specified* nodes in a system. The reactive current injections at these *PV-specified* nodes are determined through an iteration loop outside the breakpoint current compensation. Each time after the breakpoint voltage mismatches are reduced below a threshold (2.6), the following steps are performed to correct the voltage magnitude at all *PV-specified* nodes. At iteration γ:

Step a) Calculate positive sequence voltage magnitude mismatch for all *PV-specified* nodes

$$\Delta V_i^{(\gamma)} = \left|V_i^s\right| - \left|V_i^{(\gamma)}\right|, \qquad i = 1, 2, ..., n. \tag{2.9}$$

Where V_i^s is the scheduled voltage magnitude for node *i*. If any of these mismatches is greater than a threshold, then perform the next step.

Step b) Solve for *PV-specified* node reactive current injection using (2.8). The solution provides a linear approximation of the reactive current injection needed to eliminate the voltage magnitude mismatch in this iteration. If the reactive power generations were unlimited, we would inject I_{iqa}, I_{iqb}, I_{iqc}, at 90 degrees leading the corresponding voltage, V_{ia}, V_{ib}, V_{ic}, at each *PV-specified* node, *i*:

$$\begin{cases} I_{iqa}^{(\gamma)} = \left|I_{iq}\right|^{(\gamma)} e^{j(90° + \delta_{Via}^{(r)})} \\ I_{iqb}^{(\gamma)} = \left|I_{iq}\right|^{(\gamma)} e^{j(90° + \delta_{Vib}^{(r)})} \\ I_{iqc}^{(\gamma)} = \left|I_{iq}\right|^{(\gamma)} e^{j(90° + \delta_{Vic}^{(r)})} \end{cases}. \tag{2.10}$$

Where, δ_{Via}, δ_{Vib}, δ_{Vic} are voltage angles of the three phase of the *PV-specified* node. Since in reality the reactive power capability of a generator is always limited, the reactive power limits must be checked first to determine whether the required current injections are available, as in the next step:

Step c) Calculate the required reactive power generation Q_{ig} for all *PV-specified* nodes:

$$Q_{ig}^{(\gamma)} = Q^{'(\gamma)} + Q_{id}, \quad i = 1, 2, \ldots, n. \tag{2.11}$$

Where $Q_i^{'}$ is the new reactive power injection at node i. It is calculated using the *PV-specified* node voltage and the new current injection:

$$Q_i^{'(\gamma)} = \mathrm{Im}\left[V_{ia} I_{ia}^{'*}\right]^{(\gamma)} + \mathrm{Im}\left[V_{ib} I_{ib}^{'*}\right]^{(\gamma)} + \mathrm{Im}\left[V_{ic} I_{ic}^{'*}\right]^{(\gamma)}. \tag{2.12}$$

The new current injection at *PV-specified* node *i* is a combination of the desired reactive current injection and load current injection:

$$\begin{cases} I_{ia}^{'(\gamma)} = I_{iqa}^{(\gamma)} + I_{ia}^{(\gamma)} \\ I_{ib}^{'(\gamma)} = I_{iqb}^{(\gamma)} + I_{ib}^{(\gamma)} \\ I_{ic}^{'(\gamma)} = I_{iqc}^{(\gamma)} + I_{ic}^{(\gamma)} \end{cases}. \tag{2.13}$$

Q_{id} in (11) is the scheduled reactive load at *PV-specified* node *i*.

Step d) Q_{ig} then is compared with the reactive power generation limits. If Q_{ig} is within the limits, i.e.,

$$Q_{ig}^{\min} < Q_{ig}^{(\gamma)} < Q_{ig}^{\max} \tag{2.14}$$

then the corresponding reactive current, I_{iqa}, I_{iqb}, I_{iqc}, are injected to *PV-specified* node *i* according to (2.10). In subsequent iterations, these currents will be combined with other nodal current injections. Otherwise, if Q_{ig} violates any reactive power generation limit, it will be set to that limit, divided by three for three phases and combined with the reactive load of each phase at this node. Subsequently, the row and column in the *PV-specified* node sensitivity matrix, $[Z_v]$, corresponding to this node are removed and the LU factors of $[Z_v]$ are updated.

The iteration described in steps a)-d) will continue until the voltage magnitude mismatches for all *PV-specified* nodes as calculated in (2.14) become less than a threshold.

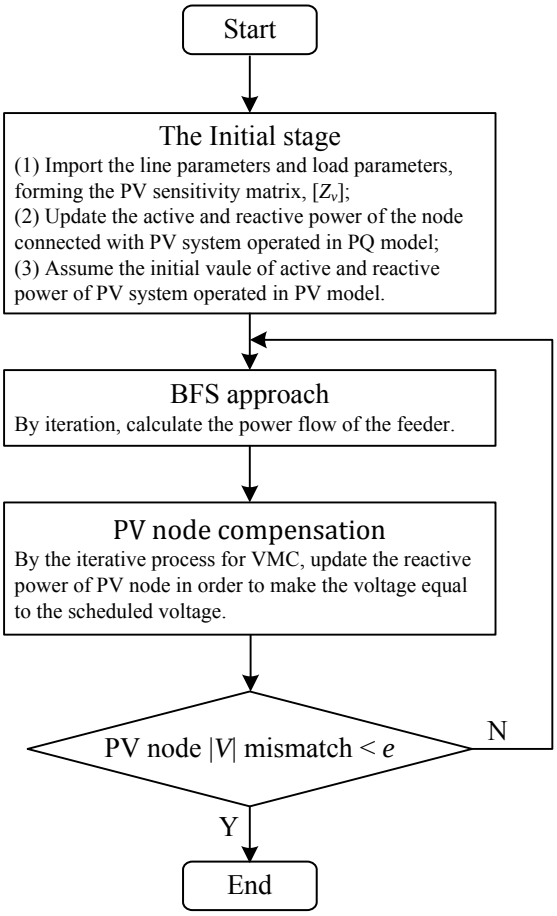

Fig. 2-6 Flow chart of the power flow algorithm with PV-specified *node compensation*.

The flow chart of overall power flow algorithm is shown in Fig. 2-6. It is seen that the algorithm consists of two nested iteration loops for radial power flow and *PV-specified* node voltage magnitude compensation, respectively. The termination of each iteration loop is controlled by a threshold. Our experience shows that once the *PV-specified* node compensation starts after the initial iterative radial power flow, subsequent radial power flows always converge in one or-two iterations under the same threshold for power mismatches.

2.4 Dynamic Model for Load Cluster

Applying the BFS algorithm, the system parameters are obtained. It gives the voltage of each node and the current of each transmission line. The procedure for building a dynamic model of load cluster is explained below. For simplicity, only faults on the load side are considered.

The hierarchical model of distribution network should be constructed according to the locality and/or logical topology primary, which has been described in detail at section 2.2.

Let the set of all nodes in the load cluster be:

$$\Phi = \{Node\,1, Node\,2, \cdots, Node\,N\}. \tag{2.15}$$

The main parameters of the distribution feeder are:

- Input voltage of the cluster, $v_0(t)$;
- Line impedance between nodes, Z_{ij} ($i, j \in \Phi$); and
- Complex power of each node, S_i ($i \in \Phi$).

We assume that the load cluster $\mathcal{C}_1^{(1)}$ at layer 1 contains all the nodes of the feeder but the root node. The input of the $\mathcal{C}_1^{(1)}$ is donated as $u_1^{(1)}(t)$, which is the voltage of the load cluster $v_1^{(1)}(t)$.

The complex power of Cluster $\mathcal{C}_1^{(1)}$ is:

$$S_1^{(1)} = \sum\nolimits_{j \in \Phi \setminus \{Node\,0\}} S_j. \tag{2.16}$$

The equivalent impedance of the cluster is:

$$Z_1^{(1)} = \frac{U_1^{(1)} \bar{U}_1^{(1)}}{\bar{S}_1^{(1)}}. \tag{2.17}$$

Note that $U_1^{(1)}$ is the phasor of the variable $u_1^{(1)}(t)$, and $\bar{U}_1^{(1)}$ is the complex conjugate of

$U_1^{(1)}$.

The impedance of the load cluster, $Z_1^{(1)}$, can be represented by a resistance $R_1^{(1)}$ and a reactance $X_1^{(1)}$ connected in series (Fig. 2-7),

$$Z_1^{(1)} = R_1^{(1)} + jX_1^{(1)}. \tag{2.18}$$

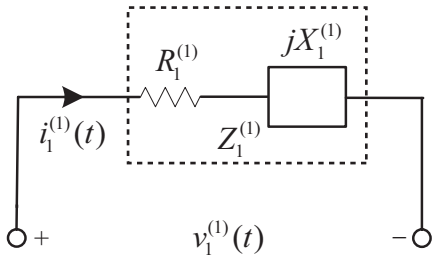

Fig. 2-7 Equivalent impedance of load cluster.

1) The impedance $Z_1^{(1)}$ is an inductive load when $X_1^{(1)} > 0$ and $X_1^{(1)}$ is given by:

$$X_1^{(1)} = \omega L = 2\pi fL \ (\Omega). \tag{2.19}$$

2) The impedance $Z_1^{(1)}$ is a capacitive load when $X_1^{(1)} < 0$ and $X_1^{(1)}$ is given by:

$$X_1^{(1)} = -\frac{1}{\omega C} = -\frac{1}{2\pi fC} \ (\Omega). \tag{2.20}$$

Actual power systems are usually inductive, which means that X>0 in most cases [2-12].

The dynamics of the equivalent circuit of Layer 1 (Fig. 2-8) are given by

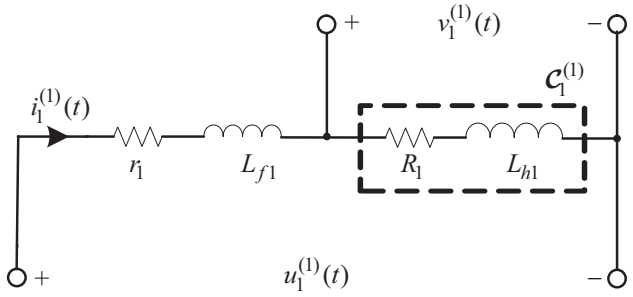

Fig. 2-8 Equivalent circuit of Cluster $\mathcal{C}_1^{(1)}$ in Layer 1.

$$\begin{cases} \dot{x}_1^{(1)}(t) = A_1^{(1)} x_1^{(1)}(t) + B_1^{(1)} u_1^{(1)}(t) \\ y_1^{(1)}(t) = C_1^{(1)} x_1^{(1)}(t) + D_1^{(1)} u_1^{(1)}(t) \end{cases}. \tag{2.21}$$

Where

$$u_1^{(1)}(t) = v_0(t),\ x_1^{(1)}(t) = i_1^{(1)}(t),\ y_1^{(1)}(t) = v_1^{(1)}(t). \tag{2.22}$$

$i_1^{(1)}(t)$ is the current flowing into $\mathcal{C}_1^{(1)}$; $v_1^{(1)}(t)$ is the voltage of $\mathcal{C}_1^{(1)}$; and

$$A_1^{(1)} = -\frac{r_1 + R_1}{L_1 + L_{h1}},\ B_1^{(1)} = \frac{1}{L_1 + L_{h1}},\ C_1^{(1)} = R_1 - \frac{L_{h1}(r_1 + R_1)}{L_{f1} + L_{h1}},\ D_1^{(1)} = \frac{L_{h1}}{L_{f1} + L_{h1}}. \tag{2.23}$$

Where r_1 and L_{f1} are the equivalent resistance and reactance, respectively, of the line from the substation to load cluster; and R_1 and L_{h1} are the equivalent resistance and reactance, respectively, of $\mathcal{C}_1^{(1)}$.

The dynamics of Cluster $n-m$ in Layer *k*, $\mathcal{C}_{n-m}^{(k)}$, is derived in the same manner:

$$\begin{cases} \dot{x}_{n-m}^{(k)}(t) = A_{n-m}^{(k)} x_{n-m}^{(k)}(t) + B_{n-m}^{(k)} u_{n-m}^{(k)}(t) \\ y_{n-m}^{(k)}(t) = C_{n-m}^{(k)} x_{n-m}^{(k)}(t) + D_{n-m}^{(k)} u_{n-m}^{(k)}(t) \end{cases} \tag{2.24}$$

where $u_{n-m}^{(k)}(t)$ is the output voltage of $\mathcal{C}_n^{(k-1)}$; $x_{n-m}^{(k)}(t)$ is the current flowing into the cluster; $y_{n-m}^{(k)}(t)$ is the output voltage of the cluster; and $A_{n-m}^{(k)}, B_{n-m}^{(k)}, C_{n-m}^{(k)}, D_{n-m}^{(k)} \in \Re$.

2.5 Application to IEEE-13 Feeder Model

The hierarchical modeling method is now applied to a small power distribution feeder, IEEE 13 nodes radial distribution feeder, "IEEE-13 feeder" for shorter. The aim is to illustrate the hierarchical procedures and testify the effective of BFS power flow calculation approach.

This chapter uses the IEEE-13 feeder model [2-13], or IEEE-13 feeder for short, as an example to illustrate how to construct a hierarchical model. The IEEE-13 bus feeder was developed by Institute of Electrical and Electronics Engineers (IEEE) as a standard simulation platform for power system analysis.

The model of IEEE-13 feeder (Fig. 2-9) has 13 nodes. Node 650 is the power substation, and the other nodes are loads. A step-down transformer connects the substation to each load, and another transformer is used between Nodes 634 and 633.

2.5.1 Data of IEEE-13 Feeder Model

The topology of the feeder was shown in Fig. 2-9. The rated output voltage of the power substation was 115 kV. All the nodes connect with substation by a transformer. Node 634 is also connected with parent node 633 by the transformer XFM-1. The parameters of transformers are shown in Table 2-1. T he transformer ratio of substation is $\gamma_{650} = 115/4.16$, and the ratio of the XFM-1 is $\gamma_{XFM-1} = 4.16/0.48$.

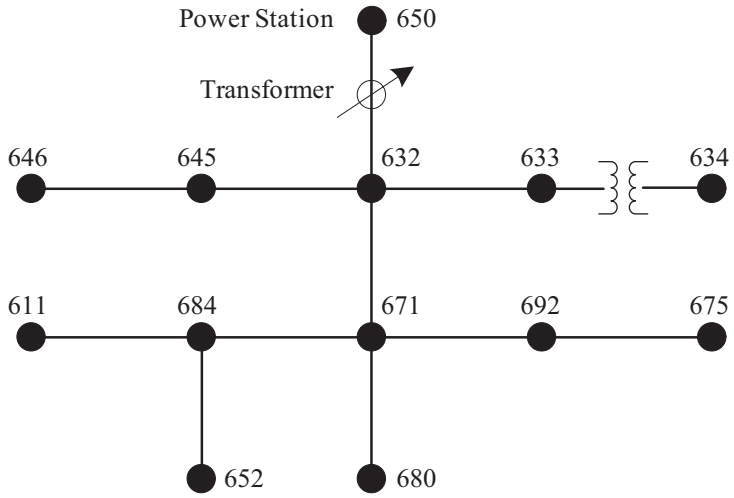

Fig. 2-9 IEEE 13 nodes radial distribution feeder (*IEEE-13 feeder*).

TABLE 2-1 TRANSFORMER DATA OF IEEE-13 FEEDER

	kVA	kV-high	kV-low	R - %	X - %
Substation:	5,000	115 - D	4.16 Gr. Y	1	8
XFM -1	500	4.16 - Gr.W	0.48 - Gr.W	1.1	2

Table 2-2 shows the line section data of feeders. The data consist of the node terminations of each line section (Starting node number and end node number) and the length of each line section. In this case, we just consider the material of line is the same, thus the line impedance was

$$Z_{\text{line}} = 0.3 + j0.6\Omega / \text{km}. \tag{2.25}$$

TABLE 2-2 LENGTHS OF LINES FOR IEEE-13 FEEDER

Line No.	Starting node No.	End node No.	Length [ft]
1	650	632	700
2	632	645	500
3	645	671	300
4	632	633	500
5	633	646	300
6	632	684	2000
7	684	680	300
8	680	692	800
9	680	634	300
10	684	611	1000
11	684	652	300
12	652	675	500

For the case study, we only consider the single-phase of load for simplify. The data of node

load is in Table 2-3, including the active power and reactive power.

TABLE 2-3 NODAL ACTIVE AND REACTIVE POWER OF IEEE-13 FEEDER

Node No.	P [kW]	Q [kVAR]
632	66.6	38.2
645	170.5	95.1
671	383.7	220
633	121.5	62.6
646	230.2	132
684	70.2	36.3
680	160.3	87.7
692	170.5	51.4
634	42.6	20.2
611	271.2	80.7
652	127.9	70.8
675	281.4	154

2.5.2 Hierarchical Framework of IEEE-13 Feeder

As mentioned in Section 2.2, the IEEE-13 feeder should be divided into several load clusters at the first layer. In order to make the structure clearer, the Fig. 2-9 can be redrew as a tree structure as Fig. 2-10.

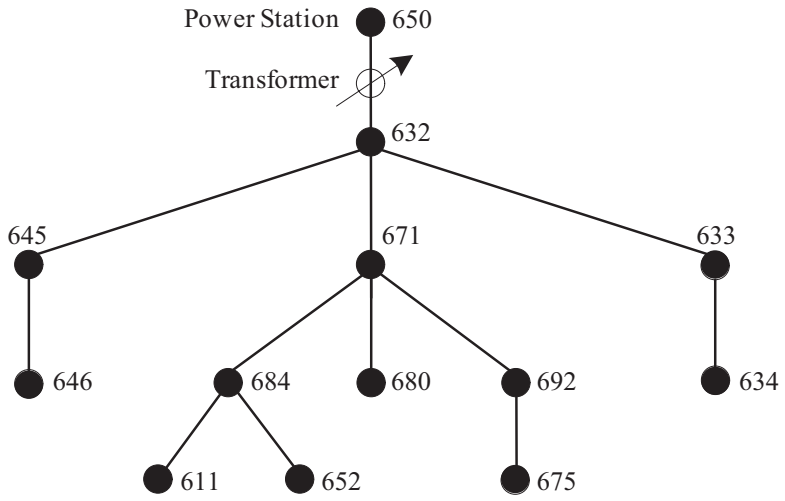

Fig. 2-10 Tree structure of Fig. 2-9.

According to the logical topology of IEEE-13 feeder, the hierarchical model of the IEEE-13 feeder is divided into 5 layers. The numbering is zero-based, and the superscript of a load cluster indicates the layer number. Clusters containing multiple nodes are broken down in successive layers, as explained in Table 2-4.

TABLE 2-4 HIERARCHICAL STRUCTURE OF IEEE-13 FEEDER

Layer 0			
$\mathcal{C}^{(0)}$	$\Rightarrow$	Whole network	Node i, $i \in \Phi$, $\Phi = \{(650),(632),(645,671,633),(646,684,680,692,634),(611,652,675)\}$.
Layer 1			
$\mathcal{C}^{(0)}$	$\Rightarrow$	$\mathcal{C}_s^{(1)}$:	Root node (Node 650, which is the substation).
		$\mathcal{C}_1^{(1)}$:	Load nodes
Layer 2			
$\mathcal{C}_1^{(1)}$	$\Rightarrow$	$\mathcal{C}_{1-1}^{(2)}$:	Node 632 (Parent node).
		$\mathcal{C}_{1-2}^{(2)}$:	Nodes 645 and 646.
		$\mathcal{C}_{1-3}^{(2)}$:	Nodes 671, 684, 680, 692, 611, 652, and 675.
		$\mathcal{C}_{1-4}^{(2)}$:	Nodes 633 and 634.
Layer 3			
$\mathcal{C}_{1-2}^{(2)}$	$\Rightarrow$	$\mathcal{C}_{1-2-1}^{(3)}$:	Node 645.
		$\mathcal{C}_{1-2-2}^{(3)}$:	Node 646.
$\mathcal{C}_{1-3}^{(2)}$	$\Rightarrow$	$\mathcal{C}_{1-3-1}^{(3)}$:	Node 671.
		$\mathcal{C}_{1-3-2}^{(3)}$:	Nodes 611, 652, 684.
		$\mathcal{C}_{1-3-3}^{(3)}$:	Node 680.
		$\mathcal{C}_{1-3-4}^{(3)}$:	Nodes 675 and 692.
$\mathcal{C}_{1-4}^{(2)}$	$\Rightarrow$	$\mathcal{C}_{1-4-1}^{(3)}$:	Node 633.
		$\mathcal{C}_{1-4-2}^{(3)}$:	Node 634.
Layer 4			
$\mathcal{C}_{1-3-2}^{(3)}$	$\Rightarrow$	$\mathcal{C}_{1-3-2-1}^{(4)}$:	Node 611.
		$\mathcal{C}_{1-3-2-2}^{(4)}$:	Node 684.
		$\mathcal{C}_{1-3-2-3}^{(4)}$:	Node 652.
$\mathcal{C}_{1-3-4}^{(3)}$	$\Rightarrow$	$\mathcal{C}_{1-3-4-1}^{(4)}$:	Node 692.
		$\mathcal{C}_{1-3-4-2}^{(4)}$:	Node 675.

From the Table 2-4, framework of the hierarchical model for the IEEE-13 feeder is divided into 5 layers.

1) Layer 0 contains one cluster, $\mathcal{C}^{(0)}$, representing the whole network.

2) In Layer 1, the network is divided into 2 clusters, $\mathcal{C}_s^{(1)}$ and $\mathcal{C}_1^{(1)}$. $\mathcal{C}_s^{(1)}$ contains only the root node, which is the substation, Node 650; and $\mathcal{C}_1^{(1)}$ contains all the load nodes.

3) In Layer 2, Cluster $\mathcal{C}_1^{(1)}$ of Layer 1 is divided into 4 clusters: $\mathcal{C}_{1-1}^{(2)}$, $\mathcal{C}_{1-2}^{(2)}$, $\mathcal{C}_{1-3}^{(2)}$, and $\mathcal{C}_{1-4}^{(2)}$. $\mathcal{C}_{1-1}^{(2)}$ contain only the parent node (Node 632), and the other clusters contain the child nodes.

More specifically, $\mathcal{C}_{1-2}^{(2)}$ contains Nodes 645 and 646; $\mathcal{C}_{1-3}^{(2)}$ contains Nodes 671, 684, 680, 692, 611, 652, and 675; and $\mathcal{C}_{1-4}^{(2)}$ contains Nodes 633 and 634.

4) In Layer 3, $\mathcal{C}_{1-2}^{(2)}$ is divided into 2 clusters ($\mathcal{C}_{1-2-1}^{(3)}$, $\mathcal{C}_{1-2-2}^{(3)}$) $\mathcal{C}_{1-3}^{(2)}$ into 4 clusters ($\mathcal{C}_{1-3-1}^{(3)}$, $\mathcal{C}_{1-3-2}^{(3)}$, $\mathcal{C}_{1-3-3}^{(3)}$, $\mathcal{C}_{1-3-4}^{(3)}$), and $\mathcal{C}_{1-4}^{(2)}$ into 2 clusters ($\mathcal{C}_{1-4-1}^{(3)}$, $\mathcal{C}_{1-4-2}^{(3)}$). $\mathcal{C}_{1-2-1}^{(3)}$ (Node 645), $\mathcal{C}_{1-2-2}^{(3)}$ (Node 646), $\mathcal{C}_{1-3-1}^{(3)}$ (Node 671), $\mathcal{C}_{1-3-3}^{(3)}$ (Node 680), $\mathcal{C}_{1-4-1}^{(3)}$ (Node 633), and $\mathcal{C}_{1-4-2}^{(3)}$ (Node 634) contain only one node; $\mathcal{C}_{1-3-2}^{(3)}$ contains Nodes 611, 684, and 652; and $\mathcal{C}_{1-3-4}^{(3)}$ contains Nodes 692 and 675.

5) In Layer 4, $\mathcal{C}_{1-3-2}^{(3)}$ is divided into 3 clusters [$\mathcal{C}_{1-3-2-1}^{(4)}$ (Node 611), $\mathcal{C}_{1-3-2-2}^{(4)}$ (Node 684), $\mathcal{C}_{1-3-2-3}^{(4)}$ (Node 652)], and $\mathcal{C}_{1-3-4}^{(3)}$ into 2 clusters [$\mathcal{C}_{1-3-4-1}^{(4)}$ (Node 692), $\mathcal{C}_{1-3-4-2}^{(4)}$ (Node 675)].

Fig. 2-11 is the hierarchical model of IEEE-13 feeder. In the Fig. 2-11, there are two type of load cluster: square and circle. Squares type indicate single-node clusters and circles type indicate multi-node clusters, which are subdivided in the next layer. The fault diagnosis will be located at the square type load cluster finally.

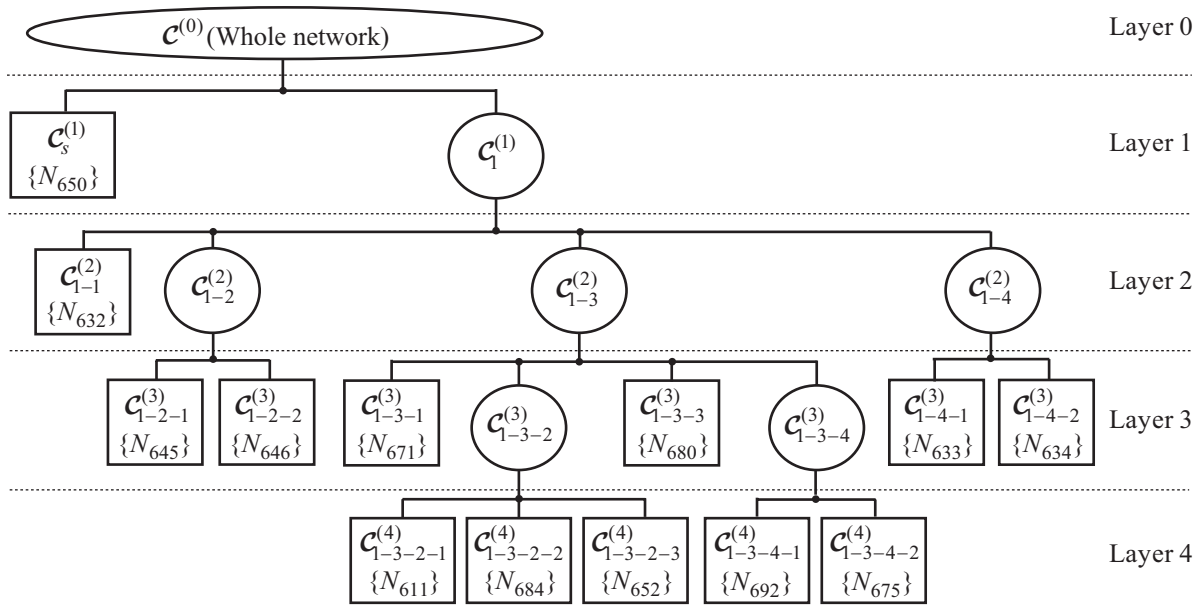

Fig. 2-11 Hierarchical structure of IEEE-13 feeder.

2.5.3 Model Parameters Calculation Results

Apply the BFS algorithm to calculate the power flow of IEEE-13 feeder, which are used to construct the system matrixes of fault diagnosis dynamic model. In order to simplify the programming for BFS algorithm, we renumber the nodes from 0 to 12. Table 2-5 is the details.

TABLE 2-5 NEW NUMBER OF NODE

Original Number of node	New number of nodes	Original Number of node	New number of nodes
650	0	680	7
632	1	692	8
645	2	634	9
671	3	611	10
633	4	652	11
646	5	675	12
684	6		

Fig. 2-12 shows the simulation result of nodeal voltage without PV embedded. V_1 is assumed to be the sending voltage and V_{12} is assumed to be terminal voltage. To regulate V_{12} which is the lowest within the proper range, sending voltage is controlled.

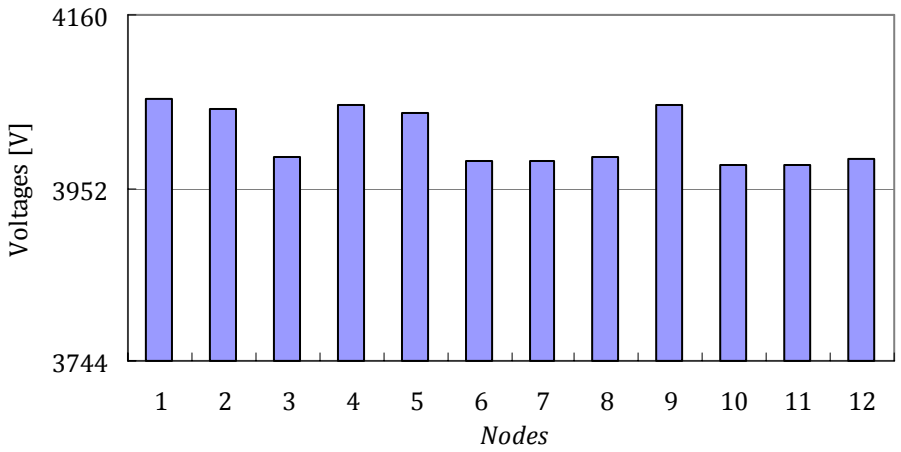

Fig. 2-12 Nodal voltages of IEEE-13 feeder without PV embedded.

With PV systems embedded into the feeders, the power flow of feeder will changed. AS mentioned in section 2.3.2, the PV systems can be regarded as two kinds of nodes: *PQ-specified* Nodes and *PV-specified* Nodes in power flow calculation. We assume the PV systems install in terminal node 646 (5), 611 (10), 652 (11), 680 (7), 675 (12), 634 (9) and the capacity of PV is equal to the 50% of the load of the node where PV installed, as shown in Fig. 2-13.

1) PV system regards as a *PQ-specified* node.

In this case, we assume the PV active power is the 50% of the active power in the node where PV embedded and the reactive power is equal to zero. The information of PV system is shown in Table 2-6.

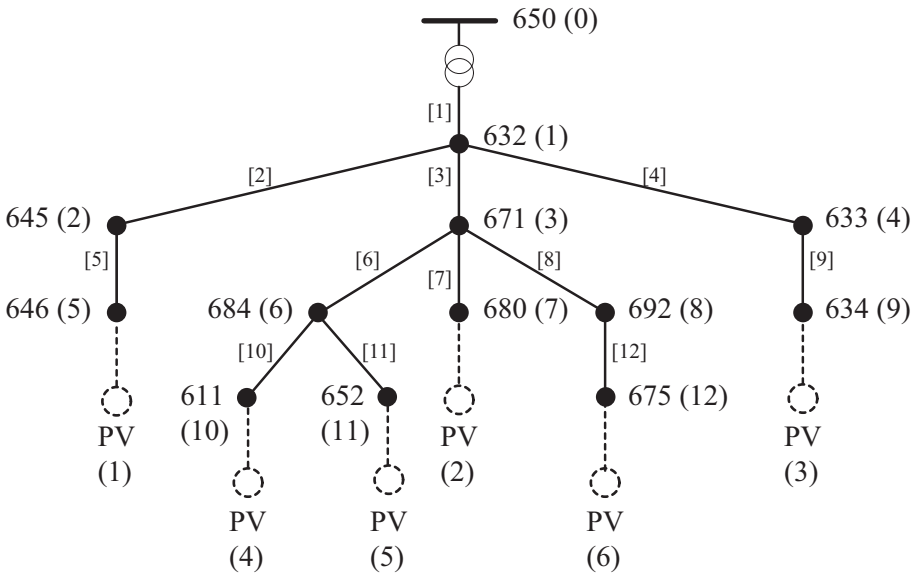

Fig. 2-13 IEEE-13 feeder with PV installation.

TABLE 2-6 DATA OF PV GENERATIONS WHICH ARE REGARDED AS PQ-SPECIFIED NODE

PV number	Location node	New numbers of node in BFS	Load of the nodes [kW] + *j* [kVAR]	PV capacities, [kW]+ *j* [kVAR]
PV 1	646	5	230.2+ *j* 132	115.1+*j*0
PV 2	680	7	160.3+ *j* 87.7	80.2+*j*0
PV 3	634	9	42.6+ *j* 20.2	21.3+*j*0
PV 4	611	10	271.2+ *j* 80.7	135.6+*j*0
PV 5	652	11	127.9+ *j* 70.8	64.0+*j*0
PV 6	675	12	281.4+ *j* 154	140.7+*j*0

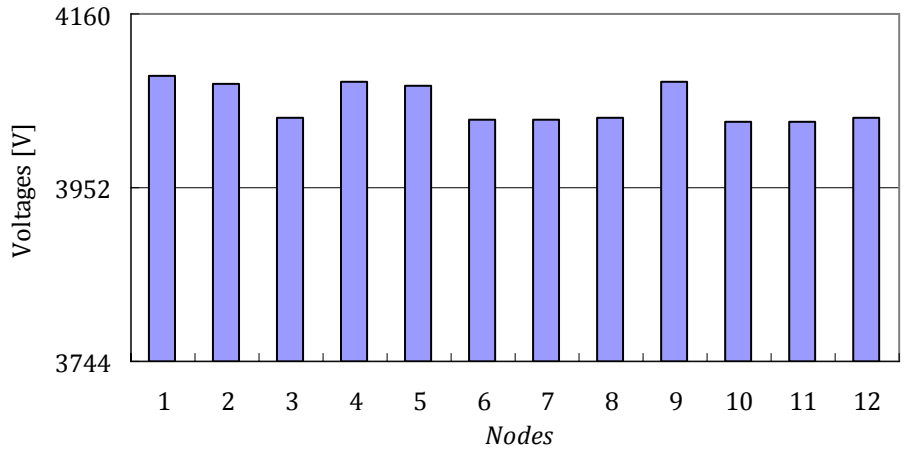

Fig. 2-14 Nodal voltages of IEEE-13 feeder with PVs, which are PQ-specified nodes.

Apply the Backward and Forward approach to the feeder, the results of node voltages are shown in Fig. 2-14. The voltages increased in the feeders, not only the nodes embedded with the

PV system, but also the other nodes. The PV generator can produce the electrical power to the nodes. It can reduce the current come from the substation and reduce the voltage loss in the transmission lines. Therefore, the voltage of all the nodes increased.

2) PV system regards as a *PV-specified* node.

In this case, we assume the PV active power and the voltage magnitude. The information of PV system is shown in Table 2-7.

TABLE 2-7 DATA OF PV GENERATIONS WHICH ARE REGARDED AS PV-SPECIFIED NODE

PV number	Location node	New numbers of node in BFS	PV capacities, [kW]+ *j* [kVAR]	Voltage magnitude
PV 1	646	5	115.1+*j*0	0.980 *p.u.*
PV 2	680	7	80.2+*j*0	0.980 *p.u.*
PV 3	634	9	21.3+*j*0	0.980 *p.u.*
PV 4	611	10	135.6+*j*0	0.975 *p.u.*
PV 5	652	11	64.0+*j*0	0.975 *p.u.*
PV 6	675	12	140.7+*j*0	0.975 *p.u.*

For the *PV-specified* node, the *PV-specified* Node Sensitivity Matrix of the feeder should be constructed at first. According the construction principle of the matrix, the *PV-specified* Node Sensitivity Matrix *Z* of Fig. 2-13 is

$$Z_{\mathrm{PVNSM}} = \begin{bmatrix} Z_{11} & Z_{12} & Z_{13} & Z_{14} & Z_{15} & Z_{16} \\ Z_{21} & Z_{22} & Z_{23} & Z_{24} & Z_{25} & Z_{26} \\ Z_{31} & Z_{32} & Z_{33} & Z_{34} & Z_{35} & Z_{36} \\ Z_{41} & Z_{42} & Z_{43} & Z_{44} & Z_{45} & Z_{46} \\ Z_{51} & Z_{52} & Z_{53} & Z_{54} & Z_{55} & Z_{56} \\ Z_{61} & Z_{62} & Z_{63} & Z_{64} & Z_{55} & Z_{66} \end{bmatrix}. \tag{2.26}$$

Where, the elements of Z_{PVNSM}, Z_{ij} (i, j = 1, 2, … , 6), is the impedance of PV systems and i, j is the number of PV systems. The diagonal elements of Z: z_{11}, z_{22}, z_{33}, z_{44}, z_{55}, z_{66}, are the self-impedances of the PV systems respectively and other elements of Z_{PVNSM} are mutual impedances among the PV systems.

$$\begin{cases} Z_{11} = z_1 + z_2 + z_5 \\ Z_{12} = z_1 \\ Z_{13} = z_1 \\ Z_{14} = z_1 \\ Z_{15} = z_1 \\ Z_{16} = z_1 \end{cases} \quad \begin{cases} Z_{21} = z_1 \\ Z_{22} = z_1 + z_3 + z_7 \\ Z_{23} = z_1 \\ Z_{24} = z_1 + z_3 \\ Z_{25} = z_1 + z_3 \\ Z_{26} = z_1 + z_3 \end{cases} \quad \begin{cases} Z_{31} = z_1 \\ Z_{32} = z_1 \\ Z_{33} = z_1 + z_4 + z_9 \\ Z_{34} = z_1 \\ Z_{35} = z_1 \\ Z_{36} = z_1 \end{cases}$$

$$\begin{cases} Z_{41} = z_1 \\ Z_{42} = z_1 + z_3 \\ Z_{43} = z_1 \\ Z_{44} = z_1 + z_3 + z_6 + z_{10} \\ Z_{45} = z_1 + z_3 + z_6 \\ Z_{46} = z_1 + z_3 \end{cases} \quad \begin{cases} Z_{51} = z_1 \\ Z_{52} = z_1 + z_3 \\ Z_{53} = z_1 \\ Z_{54} = z_1 + z_3 + z_6 \\ Z_{55} = z_1 + z_3 + z_6 + z_{11} \\ Z_{56} = z_1 + z_3 \end{cases} \quad \begin{cases} Z_{61} = z_1 \\ Z_{62} = z_1 + z_3 \\ Z_{63} = z_1 \\ Z_{64} = z_1 + z_3 \\ Z_{65} = z_1 + z_3 \\ Z_{66} = z_1 + z_3 + z_8 + z_{12} \end{cases} . \quad (2.27)$$

Where, the z_k (k=1, 2, … , 12) is the impedance of transmission line as shown in Table 2-2, which can be calculated before the iteration of BFS algorithm according to the parameters of feeder. Substituting the line impedance to the (2.27), yields the *PV-specified* node sensitivity matrix Z_{PVNSM}:

$$\begin{bmatrix} 0.195+j0.362 & 0.064+j0.248 & 0.064+j0.248 & 0.064+j0.248 & 0.064+j0.248 & 0.064+j0.248 \\ 0.064+j0.248 & 0.175+j0.620 & 0.064+j0.248 & 0.138+j0.496 & 0.138+j0.496 & 0.138+j0.496 \\ 0.064+j0.248 & 0.064+j0.248 & 0.194+j0.321 & 0.064+j0.248 & 0.064+j0.248 & 0.064+j0.248 \\ 0.064+j0.248 & 0.138+j0.496 & 0.064+j0.248 & 0.242+j0.565 & 0.164+j0.521 & 0.138+j0.496 \\ 0.064+j0.248 & 0.138+j0.496 & 0.064+j0.248 & 0.164+j0.521 & 0.294+j0.635 & 0.138+j0.496 \\ 0.064+j0.248 & 0.138+j0.496 & 0.064+j0.248 & 0.138+j0.496 & 0.138+j0.496 & 0.165+j0.501 \end{bmatrix}.$$

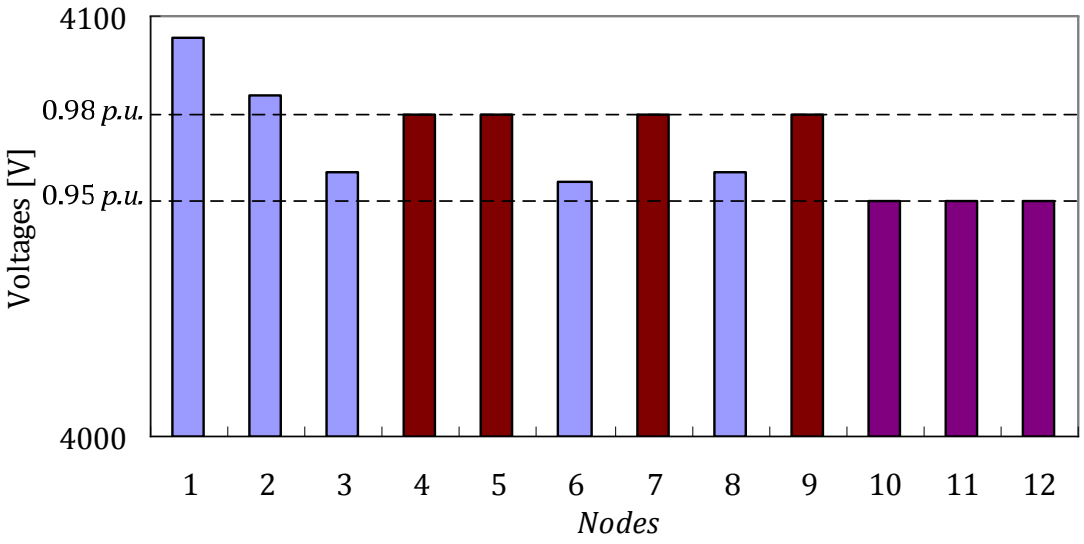

Fig. 2-15 Nodal voltages of IEEE-13 feeder with PVs, which are PV-specified nodes.

Fig. 2-15 is the results of node voltages when PV systems are regard as the *PV-specified* nodes. The voltage of nodes 4, 5, 7, 9 are reaches scheduled values 0.98 *p.u.* and the voltages of nodes 10, 11, 12 are reaches scheduled value 0.95 *p.u.*. The output reactive powers compensation of PV systems are also calculated in Table 2-8.

TABLE 2-8 REACTIVE POWER OF PV GENERATION

PV number	Location node	New numbers of node in BFS	Reactive powers compensation of PV [kVAR]
PV 1	646	5	103
PV 2	680	7	61
PV 3	634	9	21
PV 4	611	10	122
PV 5	652	11	53
PV 6	675	12	119

2.5.4 Dynamic of Load Clusters

In the former calculation, the power flow of the test feeder, including the nodal voltage and line currents, have been obtained. Then, apply the equation (2.16) - (2.20) to obtain the dynamics of all the load clusters for hierarchical model. Because our dynamics of load cluster only contains *one* state, which is the current flow into the load cluster, the matrixes of system *A*, *B*, *C*, *D* are *one* dimension.

Firstly, take the load cluster $\mathcal{C}_1^{(1)}$ as an example to illustrate the dynamics calculation. The substation is considered to be an infinite-bus power system. So its output, $v_0(t)$, is not affected by the loads of the system. The transformer is considered to be an ideal transformer, and the input voltage of Layer 1 is

$$v_1^{(1)}(t) = v_{650}(t) / \gamma_{650}.$$

And the sets of node for the $\mathcal{C}_1^{(1)}$ is

$$\Phi_1^{(1)} = \{(632), (645, 671, 633),\ (646, 684, 680, 692, 634), (611, 652, 675)\}.$$

The complex power of Cluster $\mathcal{C}_1^{(1)}$ is:

$$S_1^{(1)} = \sum\nolimits_{j \in \Phi_1^{(1)}} S_j.$$

The S_j is the complex power (load) of node *j*. The equivalent impedance of the cluster is:

$$Z_1^{(1)} = \frac{V_1^{(1)} \overline{V}_1^{(1)}}{\overline{S}_1^{(1)}}.$$

Note that $V_1^{(1)}$ is the phasor of the variable $v_1^{(1)}(t)$, and $\overline{V}_1^{(1)}$ is the complex conjugate of $V_1^{(1)}$.

The impedance of the load cluster, $Z_1^{(1)}$, is represented by a resistance $R_1^{(1)}$ and a inductance $L_1^{(1)}$ connected in series,

$$Z_1^{(1)} = R_1^{(1)} + j\omega L_1^{(1)}.$$

Finally, the dynamics of $\mathcal{C}_1^{(1)}$ is:

$$\begin{cases} \dot{x}(t) = -435.382x(t) + 71.711u(t) \\ y(t) = -0.527x(t) + 0.864u(t) \end{cases}.$$

We give out the dynamics of all the load clusters at each layer in different situations.

1) PV systems are not embedded into the IEEE-13 feeder.

TABLE 2-9 DYNAMIC MODEL OF LOAD CLUSTERS WITHOUT PV GENERATIONS EMBEDDED

Dynamic model of load cluster	Matrix A	Matrix B	Matrix C	Matrix D
$\mathcal{C}_1^{(1)}$:	-435.382	71.711	0.527	0.864
$\mathcal{C}_{1-1}^{(2)}$:	-545.706	2.927	0.737	0.994
$\mathcal{C}_{1-2}^{(2)}$:	-479.059	16.389	0.610	0.969
$\mathcal{C}_{1-3}^{(2)}$:	-450.808	53.041	0.557	0.899
$\mathcal{C}_{1-4}^{(2)}$:	-403.341	6.410	0.466	0.988
$\mathcal{C}_{1-2-1}^{(3)}$:	-424.479	6.771	0.507	0.987
$\mathcal{C}_{1-2-2}^{(3)}$:	-540.148	10.061	0.726	0.981
$\mathcal{C}_{1-3-1}^{(3)}$:	-535.063	16.989	0.717	0.968
$\mathcal{C}_{1-3-2}^{(3)}$:	-508.510	15.970	0.666	0.970
$\mathcal{C}_{1-3-3}^{(3)}$:	-363.034	6.339	0.390	0.988
$\mathcal{C}_{1-3-4}^{(3)}$:	-453.812	18.554	0.562	0.965
$\mathcal{C}_{1-4-1}^{(3)}$:	-356.123	4.648	0.377	0.991
$\mathcal{C}_{1-4-2}^{(3)}$:	-660.189	2.097	0.954	0.996
$\mathcal{C}_{1-3-2-1}^{(4)}$:	-655.142	8.606	0.945	0.984
$\mathcal{C}_{1-3-2-2}^{(4)}$:	-390.268	2.830	0.442	0.995
$\mathcal{C}_{1-3-2-3}^{(4)}$:	-464.873	5.429	0.583	0.990
$\mathcal{C}_{1-3-4-1}^{(4)}$:	-351.124	6.694	0.367	0.987

2) PV systems are embedded into the terminal nodes of IEEE-13 feeder. PV systems are

regarded as *PQ-specified* nodes.

TABLE 2-10 DYNAMIC MODEL OF LOAD CLUSTERS WITH PV GENERATIONS EMBEDDED, WHICH ARE REGARDED AS PQ-SPECIFIED NODE

Dynamic model of load cluster	Matrix A	Matrix B	Matrix C	Matrix D
$\mathcal{C}_1^{(1)}$:	-434.882	54.892	0.528	0.895
$\mathcal{C}_{1-1}^{(2)}$:	-545.735	2.889	0.737	0.995
$\mathcal{C}_{1-2}^{(2)}$:	-589.656	13.494	0.820	0.974
$\mathcal{C}_{1-3}^{(2)}$:	-490.522	38.674	0.632	0.927
$\mathcal{C}_{1-4}^{(2)}$:	-403.382	6.324	0.466	0.988
$\mathcal{C}_{1-2-1}^{(3)}$:	-424.530	6.672	0.507	0.987
$\mathcal{C}_{1-2-2}^{(3)}$:	-648.246	7.192	0.932	0.986
$\mathcal{C}_{1-3-1}^{(3)}$:	-535.397	16.539	0.717	0.969
$\mathcal{C}_{1-3-2}^{(3)}$:	-649.213	12.577	0.934	0.976
$\mathcal{C}_{1-3-3}^{(3)}$:	-526.130	3.506	0.700	0.993
$\mathcal{C}_{1-3-4}^{(3)}$:	-502.776	12.708	0.655	0.976
$\mathcal{C}_{1-4-1}^{(3)}$:	-356.147	4.585	0.377	0.991
$\mathcal{C}_{1-4-2}^{(3)}$:	-694.566	1.135	1.020	0.998
$\mathcal{C}_{1-3-2-1}^{(4)}$:	-693.447	4.636	1.018	0.991
$\mathcal{C}_{1-3-2-2}^{(4)}$:	-390.298	2.762	0.442	0.995
$\mathcal{C}_{1-3-2-3}^{(4)}$:	-679.324	3.940	0.991	0.993
$\mathcal{C}_{1-3-4-1}^{(4)}$:	-351.187	6.524	0.367	0.988

3) PV systems are embedded into the terminal nodes of IEEE-13 feeder. The embedded PV systems are regarded as *PV-specified* nodes.

TABLE 2-11 DYNAMIC MODEL OF LOAD CLUSTERS WITH PV GENERATIONS EMBEDDED, WHICH ARE REGARDED AS PV-SPECIFIED NODE

Dynamic model of load cluster	Matrix A	Matrix B	Matrix C	Matrix D
$\mathcal{C}_1^{(1)}$:	-629.704	66.632	0.896	0.873
$\mathcal{C}_{1-1}^{(2)}$:	-545.317	2.875	0.736	0.995
$\mathcal{C}_{1-2}^{(2)}$:	-590.061	13.476	0.821	0.974
$\mathcal{C}_{1-3}^{(2)}$:	-701.886	49.406	1.034	0.906
$\mathcal{C}_{1-4}^{(2)}$:	-631.197	6.744	0.899	0.987
$\mathcal{C}_{1-2-1}^{(3)}$:	-424.539	6.655	0.507	0.987

$C_{1-2-2}^{(3)}$:	-1257.309	10.436	2.089	0.980
$C_{1-3-1}^{(3)}$:	-535.506	16.392	0.717	0.969
$C_{1-3-2}^{(3)}$	-940.305	18.642	1.487	0.965
$C_{1-3-3}^{(3)}$:	-1123.423	7.285	1.835	0.986
$C_{1-3-4}^{(3)}$:	-593.498	15.427	0.828	0.971
$C_{1-4-1}^{(3)}$:	-604.654	5.580	0.849	0.989
$C_{1-4-2}^{(3)}$:	-853.965	1.271	1.323	0.998
$C_{1-3-2-1}^{(4)}$:	-1178.141	11.470	1.938	0.978
$C_{1-3-2-2}^{(4)}$:	-604.459	3.257	0.848	0.994
$C_{1-3-2-3}^{(4)}$:	-1151.381	5.775	1.888	0.989
$C_{1-3-4-1}^{(4)}$:	-1022.296	11.483	1.642	0.978

2.6 Conclusion

Construction method of the Hierarchical Fault Diagnosis Model was proposed in this chapter. Due to the complex structure of distribution network, using an entire model of it for fault diagnosis was very time consuming, therefore the HFD model for distribution network was set up. In the HFD model, the distribution network was built by first dividing it into multiple load clusters based on the locality and/or logical topology. Each cluster contained a number of load nodes. Then the clusters were subdivided successively into smaller load clusters. This produced both a multilayer structure and a hierarchical model of the system. Fault diagnosis was carried out from the top down through the layers to gradually locate a fault and to identify its type. The parameters of HFD model were calculated by the Backward and Forward Sweep (BFS) power flow calculation algorithm. Meanwhile, in the power calculation the PV system can be classified into two types: the PV specified nodes type and the PQ specified node type, thus we improved the BFS algorithm to adapt them.

The IEEE-13 feeder was selected to illustrate how to construct the hierarchical model. The hierarchical framework of IEEE-13 feeder was given out, and then the BFS algorithm was applied to calculate the model parameters exactly. The dynamic models for all the load clusters are obtained finally.

Chapter References

[2-1] **A. Barua and K. Khorasani.** *Hierarchical Fault Diagnosis and Health Monitoring in Satellites Formation Flight,* IEEE Transactions on Syst., Man and Cyber., vol. 41, no. 2, pp. 223-239, Mar. 2011

[2-2] **A. Barua and K. Khorasani.** *A hierarchical fault diagnosis and fuzzy rule-based reasoning for satellites formation flight*, IEEE Trans. Aerosp. Electron. Syst., vol. 47, no. 4, pp: 2435-2456, Oct. 2010.

[2-3] **J. Bansiya and C.G. Davis.** *A hierarchical model for object-oriented design quality assessment,* IEEE Transactions on Software Engineering, vol. 28, no.1, pp. 4-17, Jan. 2002.

[2-4] **C. S. Cheng and D. Shirmohammadi.** *A three-phase power flow method for real-time distribution system analysis,* IEEE Trans. Power Syst., vol. 10, no. 2, pp. 671-679, May 1995.

[2-5] **D. Shirmohammadi, H. W. Hong, A. Semlyen and G.X. Luo.** *A Compensation-based Power Flow Method for Weakly Meshed Distribution and Transmission Networks,* IEEE Trans. Power Syst., vol. 3, no. 2, pp.753-762, May 1988.

[2-6] **A. Augugliaro, L. Dusonchet, S. Favuzza, M. G. Ippolito, and E. Riva Sanseverino.** *A Multi-Port Approach to Solve Distribution Networks with Meshes and PV Nodes,* in Proc. of IEEE Power Tech., pp. 92 - 97. Jul. 2007.

[2-7] **W. Xu, J. R. Marti and H. W. Dommel.** *A Multiphase Harmonic Load Flow Solution Technique,* IEEE Trans. on Power Syst., vol. 6, no. 2, pp. 174-182, Feb 1991.

[2-8] **D. Rajicic, A. Dimitrovski.** *A new method for handling PV nodes in backward/forward power flow for radial and weakly meshed networks,* in Proc. of IEEE Power Tech., 2001.

[2-9] **G. W. Chang, S. Y. Chu and H. L. Wang.** *An Improved Backward/Forward Sweep Load Flow Algorithm for Radial Distribution Systems,* IEEE Trans. Power Syst. vol. 22, no. 2, pp. 882-884, May 2007.

[2-10] **Z. Wang, F. Chen and J. Li.** *Implementing Transformer Nodal Admittance Matrices Into Backward/Forward Sweep-Based Power Flow Analysis for Unbalanced Radial Distribution Systems,* IEEE Trans. Power Syst. vol. 19, no. 4, pp. 1831-1836, Nov. 2004.

[2-11] **E. Bompard, E. Carpaneto, G. Chicco and R. Napoli.** *Convergence of the backward/forward sweep method for the load-flow analysis of radial distribution systems,* Electrical Power and Energy Systems, vol. 22, vol. 7, pp. 521-530. Oct. 2000.

[2-12] **A.V.Bakshi and U.A.Bakshi.** *Network analysis and Synthesis*, Technical Publications Pune, India, 2008.

[2-13] **W. H. Kersting.** *Radial distribution test feeders,* IEEE Trans. Power Syst., vol. 6, no. 3, pp. 975-985, Oct. 2002.

Chapter 3
Fault Diagnosis Method of Power Distribution Networks Based on EID Approach

3.1 Chapter Introduction

The parameters fluctuation, unmodeled dynamics, measurement noise and the external disturbance always exist in the actual control system, beside the power system. In order to improve the robustness of the system and ensure the normal operation of the system, many control methods have been developed to eliminate the impact of these disturbances and maintain the system stable. However, if the disturbances are too large and exceed the tolerance range for system, the faults may occur at the system. Therefore, if the disturbances can be estimated, it can be used to diagnose the faults.

In control theory, a considerable number of studies have been devoted to the estimation and rejection of the disturbance. While most of these methods require the differentiation of measured outputs, the methods in [3-1]–[3-8] do not. However, in [3-1]–[3-3], rank conditions are imposed on the unknown inputs; [3-4] requires exact information on a disturbance; [3-5] and [3-6] consider only a special class of disturbances; and [3-7] and [3-8] use the inverse dynamics of the plant directly in the construction of the estimator. She et al. [3-9]-[3-11] devised an EID method that overcomes the drawbacks of these methods. In this method, the state of the plant is needed for the estimation. On the other hand, from the standpoint of the fault diagnosis, it is more reasonable to estimate a disturbance on the input channel, called equivalent-input-disturbance, than to estimate the disturbance itself because we can use the EID to assess the extent of the damage caused by a fault at different levels from the standpoint of its influence on the power supply.

The structure of this chapter is planned as follows:

Section 3.2: The definitions of EID for a system containing disturbances that may not necessarily be imposed on the control input channel are given out. And the EID estimation based on the control input and the output of the plant is described.

Section 3.3: The fault diagnosis method based on EID approach fault is explained in detail. The two key critical technologies: 1) Thresholds of EID, 2) Characteristics of fault, are proposed.

Section 3.4: The simulation results on a case study are presented to illustrate the effective of the fault diagnosis method based on EID.

.

3.2 Concept of EID Approach

This section first defines an EID, describes the configuration of an EID estimator and then designs the filter and state observer for EID estimator.

3.2.1 Definition of EID

Consider the linear time-invariant plant in Fig. 3-1

$$\begin{cases} \dfrac{dx_o(t)}{dt} = Ax_o(t) + Bu(t) + B_d d(t) \\ y_o(t) = Cx_o(t) \end{cases}. \tag{3.1}$$

Where $A \in \Re^{n\times n}$, $B \in \Re^{n\times n}$, $B_d \in \Re^{n\times n_d}$, $C \in \Re^{n_y\times n}$, $x_o(t) \in \Re^n$, $u(t) \in \Re^{n_u}$, $d(t) \in \Re^{n_d}$ and $y_o(t) \in \Re^{n_y}$.

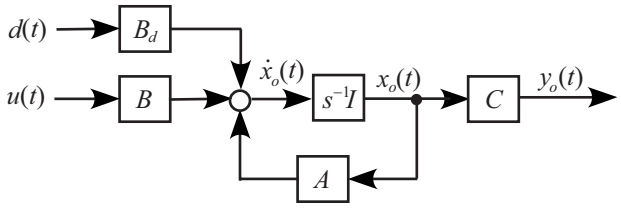

Fig. 3-1 Plant.

The following assumptions are made about the plant.

Assumption 3.1: (A, B, C) is controllable and observable.

Assumption 3.2: (A, B, C) has no zeros on the imaginary axis.

Remark 3.1: *Assumption* 3.1 is for simplicity. Since we want to use a control input to improve the tracking performance of the output, if the plant is not controllable and/or observable, then we only need to consider a controllable and observable subsystem of it.

Remark 3.2: *Assumption* 3.2 is necessary to guarantee the internal stability of a servo system and to allow the output of the plant to track a reference input without a steady-state error [3-12].

For simplicity, we only consider the single-input single-output (*SISO*) case, which means that $n_u = 1$ and $n_y = 1$. Note that, since B and B_d may have different dimensions, the disturbance may be imposed on a channel other than the control input channel, and the number of disturbances and associated input channels may also be larger than one. However, if we assume that a disturbance is imposed only on the control input channel, as shown in Fig. 3-2, then the plant is given by

$$\begin{cases} \dfrac{dx(t)}{dt} = Ax(t) + B\left[u(t) + d_e(t)\right] \\ y(t) = Cx(t) \end{cases} \tag{3.2}$$

An EID is defined as follows.

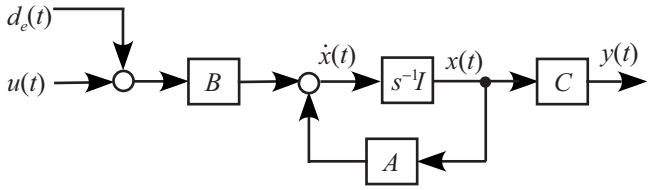

Fig. 3-2 Plant with EID.

Definition 3.1: Let the control input be $u(t) = 0$. Then, the output of the plant (3.1) for the disturbance $d(t)$ is $y_o(t)$, and the output of the plant (3.2) for the disturbance $d_e(t)$ is $y(t)$. The disturbance $d_e(t)$ is called an EID of the disturbance $d(t)$. if $y(t) \equiv y_o(t)$ for all $t \geq 0$.

Let

$$\Phi = \left\{ p_i(t) \sin\left(\omega_i t + \phi_i\right) \right\}, \qquad i = 0, \cdots n, \quad n < \infty \tag{3.3}$$

where $\omega_i (\geq 0)$ and ϕ_i are constants, and $p_i(t)$ denotes any polynomials in time t ($i = 0, \ldots, n$).

If the trajectory of the output caused by the disturbance $d(t)$ is $y_o(t) \in \Phi$, then, from the concept of stable inversion [3-13], it follows that there exists an EID $d_e(t) \in \Phi$ on the control input channel that produces the same trajectory. This leads to the following lemma.

Definition 3.2: Under Assumptions 3.1 and 3.2, there always exists an EID $d_e(t) \in \Phi$ on the control input channel of the disturbance $d(t)$ imposed on the plant (3.1), and the output it produces belongs to Φ.

Remark 3.3: Note that, since the stable-inversion approach computes a particular control input and a particular state trajectory that either does not excite the zeros of the system or excite them in a stable manner, this approach produces a satisfactory control input for a given output, even for a system with unstable zeros/poles.

Remark 3.4: Since we focus on the effect of disturbances on the output rather than on the disturbances themselves, the stable-inversion approach guarantees the existence of an EID, regardless of any difference in dimension between the control input matrix B and the disturbance input matrix B_d or any difference between the ranges of their linear transforms.

From the aforementioned *Definition 3.2*, we know that we can calculate an EID from the input and output of the plant. Since the calculation is complicated and also requires information

on future outputs, this approach cannot be directly used to obtain an EID. However, since this lemma clarifies that an EID exists, it gives us a theoretical guarantee of the meaningfulness of EID estimation. In the next section, we devise a simple method of estimating an EID. Considering the aforementioned lemma, we mainly use (3.2) as the model of the plant in the rest of this paper.

3.2.2 Estimation of EID

The configuration of an improved system is shown in Fig. 3-3, where

$$B^{+} := \left(B^{T}B\right)^{-1}B^{T}. \tag{3.4}$$

It can be viewed as a conventional servo system (internal model, state observer, and state feedback) combined with a disturbance estimator that produces an estimate of an EID. *K* is the observer gain, and *F*(*s*) is a low-pass filter that limits the angular-frequency band of the disturbance estimate. Since we know the exact form of the reference input, an internal model is employed in the control system to improve the tracking precision for the reference input. On the other hand, since the disturbance is assumed to be unknown, no internal model of it is contained in the control system, and we need to devise a method of suppressing its influence on the output. Note that the EID estimator makes use of the state observer instead of the inverse dynamics of the plant. This is a big difference in system structure between the disturbance-observer method and the one presented in this paper. In Fig. 3-3, for the state observer

$$\dot{\hat{x}}(t) = A\hat{x}(t) + Bu_{f}(t) + K\left[y(t) - C\hat{x}(t)\right] \tag{3.5}$$

holds. Letting

$$\Delta x(t) = \hat{x}(t) - x(t) \tag{3.6}$$

and substituting it into (3.2) yields

$$\dot{\hat{x}}(t) = A\hat{x}(t) + Bu(t) + \left\{Bd_{e}(t) + \left[\Delta\dot{x}(t) - A\Delta x(t)\right]\right\}. \tag{3.7}$$

Assume that there exists a control input $\Delta d(t)$ that satisfies

$$\Delta\dot{x}(t) - A\Delta x(t) = B\Delta d(t). \tag{3.8}$$

Substituting (3.8) into (3.7) and letting the estimate of the EID be

$$\hat{d}(t) = d_{e}(t) + \Delta d(t) \tag{3.9}$$

allow us to express the plant as

$$\dot{\hat{x}}(t) = A\hat{x}(t) + B\left[u(t) + \hat{d}(t)\right]. \tag{3.10}$$

Remark 3-5: Equations (3.9) and (3.10) mean that, if we take the state of the plant with an EID to be $\hat{x}(t)$, which is exactly the state of the observer, then the difference between the state of the plant and that of the observer is equivalent to the difference between the exact value and the estimate of the EID. Equation (3.10) plays a key role in the EID estimation.

Equations (3.5) and (3.10) yield

$$B \cdot \hat{d}(t) = KC\left[x(t) - \hat{x}(t)\right]. \tag{3.11}$$

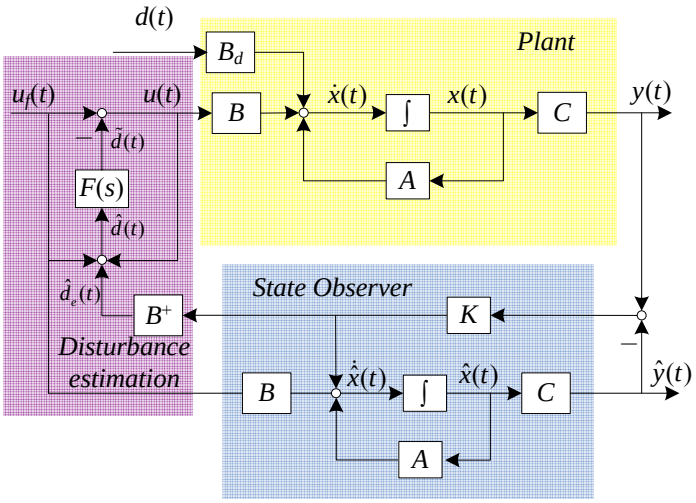

Fig. 3-3 Configuration of disturbance estimation.

If we solve (3.11) for $\hat{d}(t)$, then a least square solution is

$$\hat{d}(t) = B^{+}KC\left[x(t) - \hat{x}(t)\right] \tag{3.12}$$

$\hat{d}(t)$ is filtered by $F(s)$, which selects the angular-frequency band for disturbance estimation. Thus, the filtered disturbance estimate $\hat{d}(t)$ is given by

$$\tilde{D}(s) = F(s)\hat{D}(s) \tag{3.13}$$

where, $\tilde{D}(s)$ and $\hat{D}(s)$ are the Laplace transforms of $\tilde{d}(t)$ and $\hat{d}(t)$, respectively.

Remark 3-6: Since an estimate is obtained for an EID, the channel on which the EID is imposed might be different from that of the actual disturbance. Therefore, generally speaking, a full-order state observer must be used to estimate the state of the plant because, if a disturbance exists, then the estimated state of the plant might be different from the actual state, which

includes the effects of the disturbance. This difference degrades the tracking precision if we directly use the available states. In order to obtain an EID with a high precision, it is important to guarantee that $\hat{y}(t)-y(t)$ converges to zero. Therefore, using a full-order state observer is desirable.

3.2.3 Design of Filter and State Observer

The state observer gain K and the low-pass filter $F(s)$ should be designed so that they do not destroy the stability of the system. Regarding stability, if we let

$$r(t)=0, \quad d(t)=0 \tag{3.14}$$

then the plant (3.2) is

$$\dot{x}(t)=Ax(t)+Bu(t). \tag{3.15}$$

Combining (3.5), (3.6), and (3.14) with the aforementioned equation yields

$$\Delta\dot{x}(t)=(A-KC)\Delta x(t)+B\tilde{d}(t). \tag{3.16}$$

On the other hand, (3.12) is equivalent to

$$\hat{d}(t)=-B^{+}KC\Delta x(t)+\tilde{d}(t). \tag{3.17}$$

Using the relationships (3.14) – (3.17), equations (3.16) and (3.17) yield the transfer function from $\tilde{d}(t)$ to $\hat{d}(t)$

$$\begin{aligned} G(s) &= 1-B^{+}KC\left[sI-\left(A-KC\right)^{-1}\right]B \\ &= B^{+}(sI-A)\left[sI-(A-KC)\right]^{-1}B \end{aligned}. \tag{3.18}$$

Note that the stabilized dynamics in Fig. 3-3 are unobservable from the dynamics of plant, thus do not appear in the transfer function (3.18). For this system, we obtain the following from the small-gain theorem [3-14].

Theorem 3-1: For a suitably designed state-feedback, the control law guarantees the stability of the control system under the following conditions.

1) $A-KC$ is stable.

2) $\|GF\|_{\infty}<1$, where $\|GF\|_{\infty}:=\sup_{0\le\omega\le\infty}\sigma_{\max}\left[G(j\omega)F(j\omega)\right]$, and $\sigma_{\max}(G)$ means the maximum singular value of G.

Remark 3-7: The stability conditions for the improved servo system can be broken down into two parts (Separation Theorem [3-15]). First, the state-feedback servo system is stable.

Second, the conditions in Theorem 3-1 hold. Since the only parameters in those conditions are K and $F(s)$, their design is much simpler than the design of parameters in the disturbance-observer method [3-16], which requires a low-pass filter to guarantee the stability of the whole system.

On the other hand, for the dual system of the plant

$$\begin{cases} \dot{x}_L(t) = A^T x_L(t) + C^T u_L(t) \\ y_L(t) = B^T x_L(t) \end{cases}. \tag{3.19}$$

Consider the state feedback parameterized by a scalar $\rho > 0$

$$u_L(t) = K_\rho^T x_L(t). \tag{3.20}$$

If $\left(A^T, C^T, B^T\right)$ [and, thus, $\left(A, B, C\right)$] is a minimum-phase system, then, based on the concept of perfect regulation [3-17], [3-18], we can obtain an K_ρ^T that ensures

$$\lim_{\rho\to\infty}\left[sI - \left(A - K_\rho C\right)\right]^{-1} B = 0. \tag{3.21}$$

Note that $\left[sI - \left(A - K_\rho C\right)\right]^{-1} B$ is part of $G(s)$, which means that a large enough ρ makes $\left|G(j\omega)\right|$ sufficiently small for all $\omega \in [0, \infty)$. Therefore, based on the concept of perfect regulation, for a given $F(s)$, we can obtain an K that satisfies the conditions in *Theorem* 3-1.

We applied the Linear Quadratic Optimal Control method to calculate the gain K. Consider the m- input, n- state system with $x \in \Re^n, u \in \Re^m$:

$$\dot{x}(t) = Ax(t) + Bu(t), \quad x(t_0) = x_0, \quad t \in \left[t_0, t_f\right]. \tag{3.22}$$

Find open loop control $u(\tau)$, $\tau \in \left[t_0, t_f\right]$ such that the following objective function is minimized:

$$J\left(u, x_0, t_0, t_f\right) = \int_{t_0}^{t_f}\left[x^T(t)Qx(t) + u^T(t)Ru(t)\right]dt + x(t_f)^T Sx(t_f) \tag{3.23}$$

where Q and S are symmetric positive semi-definite $n\times n$ matrices, R is a symmetric positive definite $m\times m$ matrix. Notice that x_0, t_0, and t_f are fixed and given data.

The control goal generally is to keep $x(t)$ close to 0, especially, at the final time t_f, using little control effort u. To wit, notice in (3.23)

- $x^T(t)Qx(t)$ penalizes the transient state deviation,

- $x^T(t_f)Sx(t_f)$ penalizes the finite state,
- $u^T(t)Ru(t)$ penalizes control effort.

This formulation can accommodate regulating an output $y(t) = Cx(t) \in \Re^r$ at near 0. In this case, one choice for S and $Q(t)$ are $C^T(t)W(t)C(t)$ where $W(t) \in \Re^{r \times r}$ is symmetric positive definite matrix.

Theorem 3-2: The optimal control solution and the state observer gain K of the equation (3.20) is:

$$u^*(t) = -K^*(t)x(t), \quad K^*(t) = R^{-1}B^T P(t) \tag{3.24}$$

where, $P(t) \in \Re^{n \times n}$, is the solution to the following so called continuous time Riccati Differential Equation:

$$\begin{aligned} -\dot{P}(t) &= A^T P(t) + P(t)A + Q - P(t)BR^{-1}B^T P(t) \\ P(t_f) &= S, \quad t \in \left[t_0, t_f\right] \end{aligned} . \tag{3.25}$$

Moreover, the minimum cost achieved using the above control is:

$$J^*(x_0, t_0, t_f) := \min_{u(\cdot)} J(u, x_0) = x_0^T P(t_0) x_0 . \tag{3.26}$$

3.3 Key Technologies of Fault Diagnosis

In this section, three critical considerations in fault diagnosis method based on EID approach are

1) Fault disturbance;

2) Thresholds of the EIDs;

3) Characteristics of faults.

They are discussed below.

3.3.1 Fault Disturbance

In our method, we identify the faults by distinguishing the characteristics of the disturbances. If there is no any fault occurs at the system, the disturbance is the normal disturbances caused by load parameters variation, measurement noise or other regular reasons. If some faults occur at the system, the disturbance caused by the fault will impose to the normal disturbance. Furthermore, the characteristics of the normal disturbance and fault disturbance are different.

In order to analyze the characteristics of the two disturbances, a three-phase short-circuit fault is assumed to occur at the distribution feeder, as shown in Fig. 3-4 (a). Then, we constructed a short-circuit fault module by the MATLAB SIMULINK tool (Fig. 3-4) to carry out the simulation.

In the simulation, a three-phase short circuit fault occurs at the transmission line. The output voltage of three-phase source is 110 MV and frequency is 50 Hz. The load of three-phase series RLC Load is 5 MW. The total simulation time is 0.5*s*.

In the three-phase fault module, we set the short-circuit fault occurs at 0.1s. Once short-circuit occurs, the protection system will make the breaker trip immediately to isolate the fault position and protect the system. We set the fault recover at 0.4s.

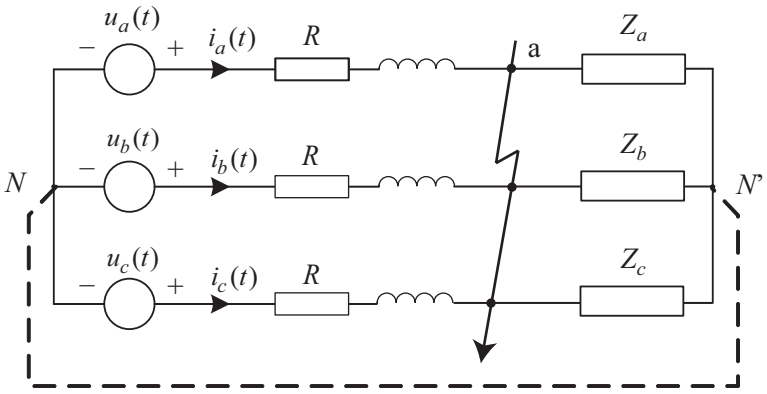

Fig. 3-4 (*a*) *Three-phase short circuit.*

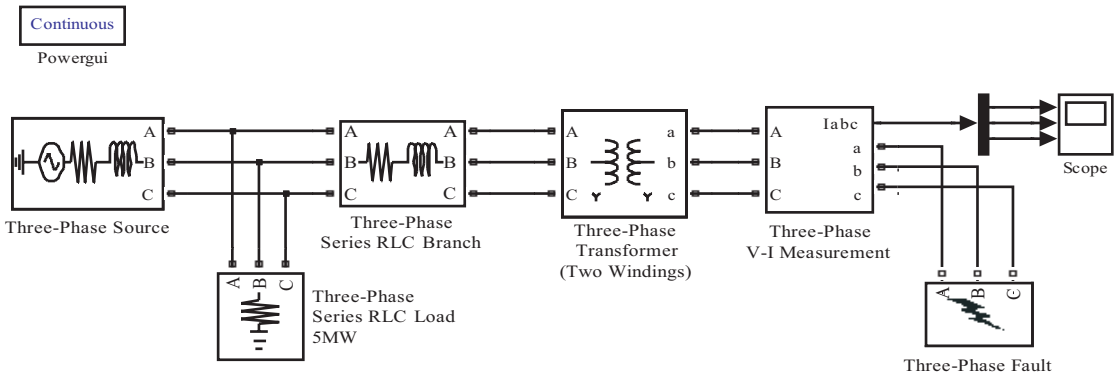

Fig. 3-4 (b) *Simulation structure for short-circuit fault*.

From the Fig. 3-5, the three-phase current experienced a rapid increase at 0.1s and the short-circuit current reached the stable at about 0.25s. At 0.4s, as the breaker tripped, the fault position is isolated and the short-circuit currents are disappeared. During the period [0.25s, 0.4s], the increased current bring a large disturbance to the system. In order to prove this, we introduce the disturbances to the system and apply the EID approach to estimate the disturbance.

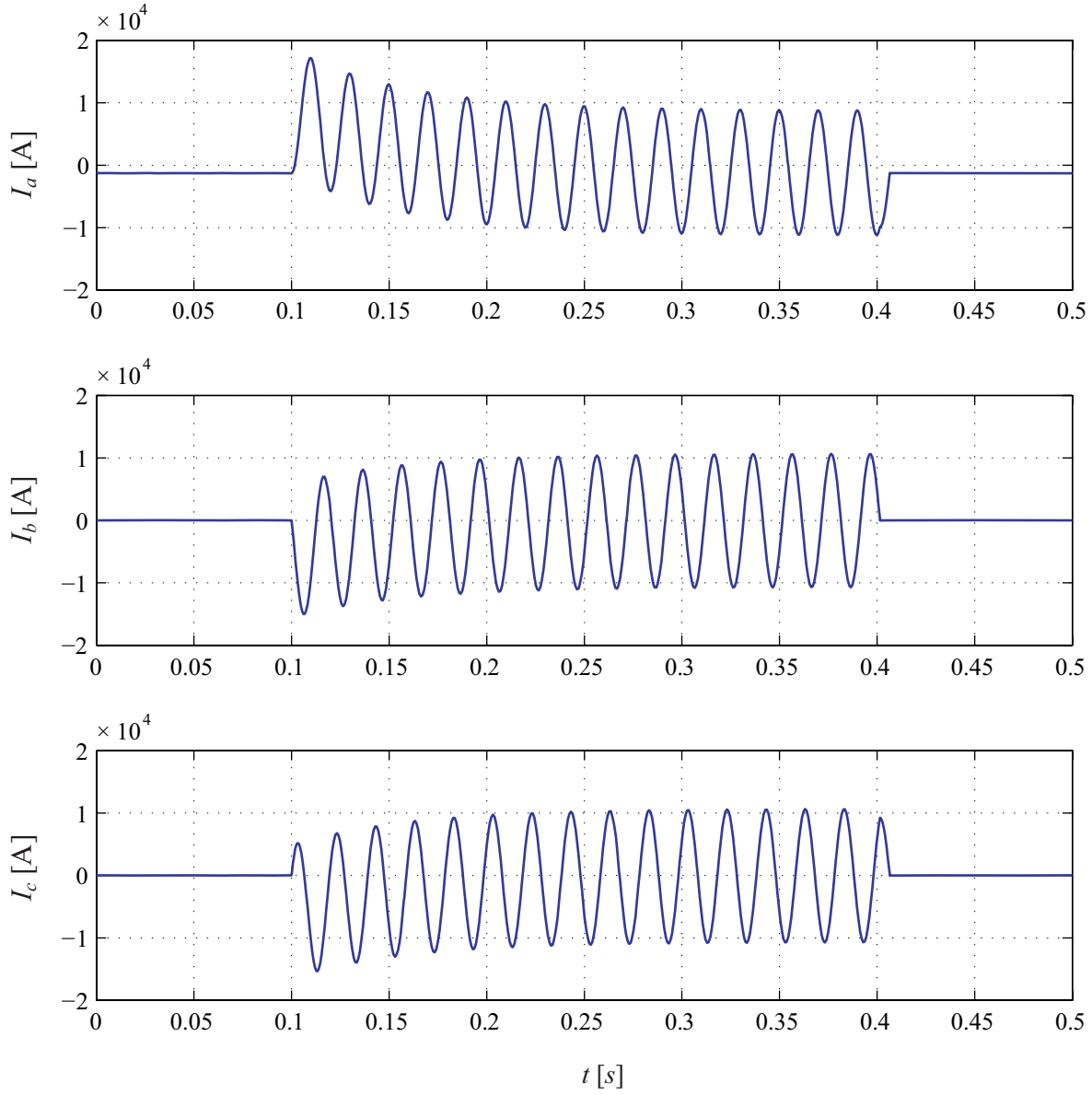

Fig. 3-5 Three-phase short circuit fault current.

In the Fig. 3-6, the simulation structure includes three modules:

1) Disturbance Design module. This module is the fault current simulator, which included all the components of Fig. 3-4. And the measurement of current is the output of this module.

2) Actual system. This module can simulate the actual system with parameters variation, measurement noise or other normal disturbance.

3) EID Estimator. This module is applied to estimate the EID, which has introduced in the Section 3.2.

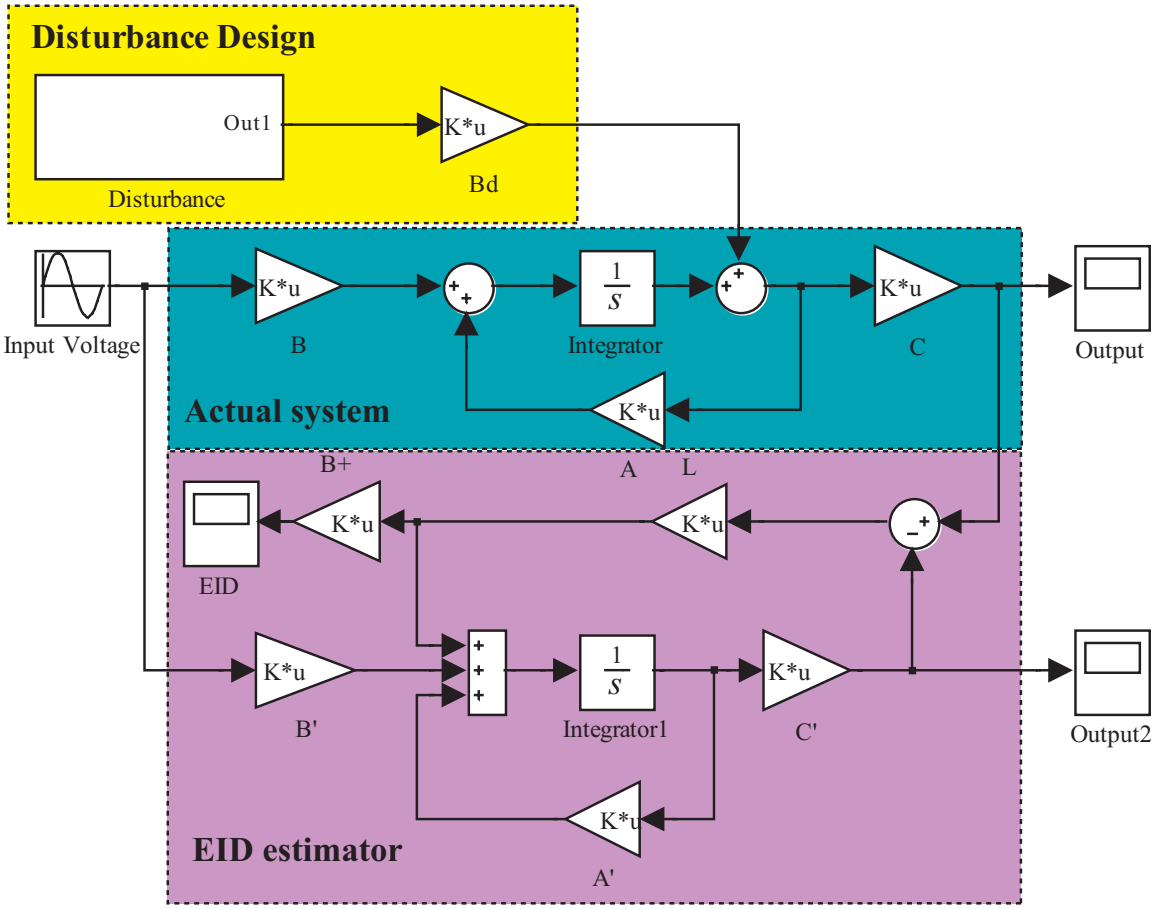

Fig. 3-6 Simulation structure for EID approach.

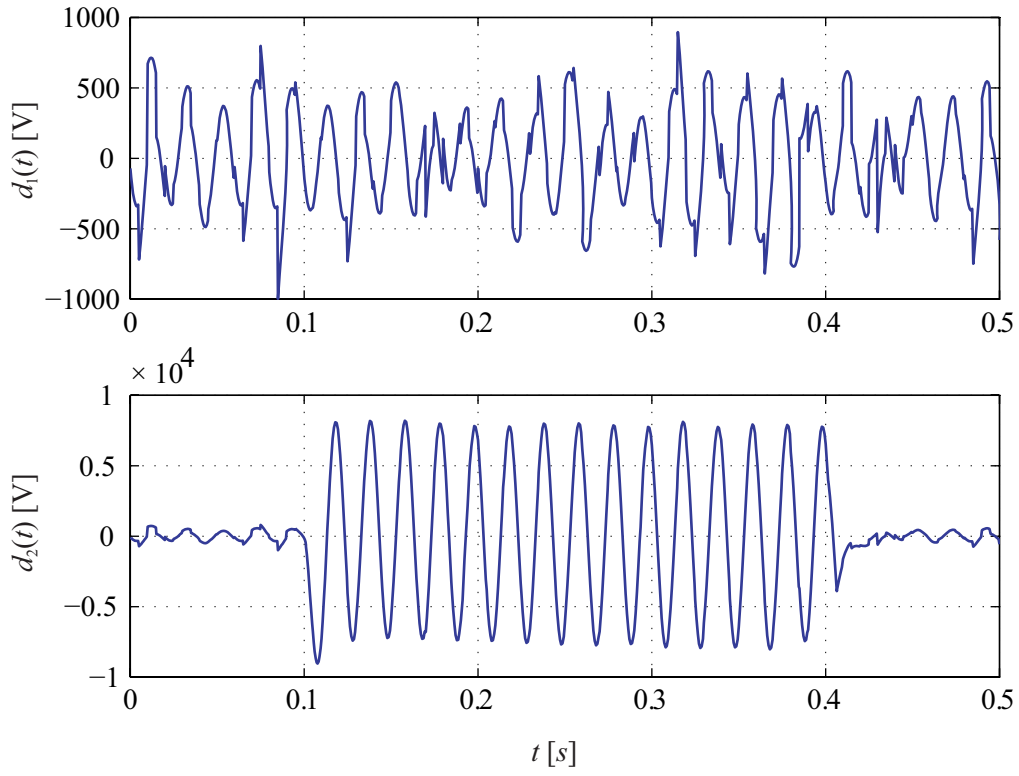

Fig. 3-7 EID of system in different situations.

In the Fig. 3-7, the $d_1(t)$ is the EID of the system in the normal condition and the $d_2(t)$ is the EID of the system when system suffered from a fault during the period [0.1s ,0.4s]. For the normal condition, the EID of system, $d_1(t)$, is small and stay in the range [-1000, 1000]. For the fault condition, the $d_2(t)$ increase remarkably and exceeded the range obviously during the fault period. This simulation result can prove two points:

1) The system disturbance can reflect the system operation condition, normal or fault.

2) The EID of system can be applied to diagnose the fault instead of the real system disturbance.

3.3.2 Thresholds of EIDs

The key point of the EID-based fault diagnosis method is that a fault is taken to be a disturbance. However, a system is constantly subjected to a variety of disturbances and parameter fluctuations. It is regarded as being in the normal state when the estimated EID is within a certain range. And the system is determined to suffer a fault only when either the estimated EID or the rate of change in the EID exceeds a certain value.

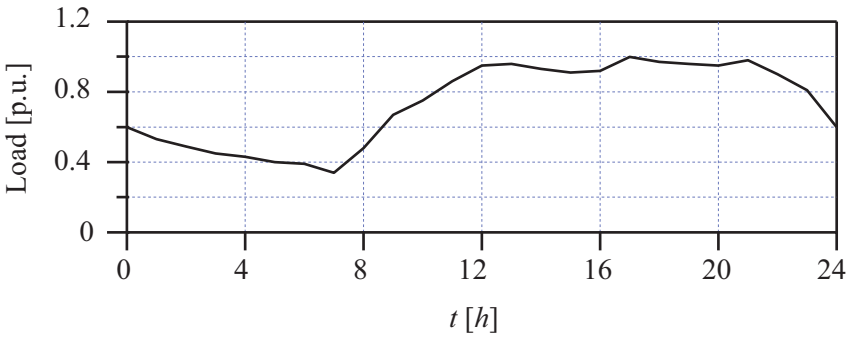

Fig. 3-8 Load variation of a node during a 24-hour period.

Fig. 3-8 shows the load variation of a node during a 24-hour period. Previously collected statistics are used to determine the minimum and maximum loads during a day, and the average load for a day, S_{L_avg}, for the load node.

$$S_{L\_min} = 0.4\ p.u.,\ S_{L\_max} = 1.2\ p.u.\ \text{and}\ S_{L\_avg} = 0.75\ p.u.. \tag{3.27}$$

Thus, the allowable range of loads is [S_{L_min}, S_{L_max}]. The allowable rate of change for the EID is determined based on the rate of change in S_L. Statistics are used to determine two fault detection thresholds for the EID in the dynamic model of Cluster $C_1^{(1)}$:

a) Absolute threshold, $d_{A\_e}(t)$: the smallest EID that indicates a fault; and

b) Differential threshold, $d_{D\_e}(t)$: the smallest rate of change in an EID that indicates a fault.

So, when either $\left|\hat{d}_{e\_L}(t)\right| \geq d_{A\_e}$ or $\left|\dot{\hat{d}}_{e\_L}(t)\right| \geq d_{D\_e}$, a fault is considered to have occurred.

3.3.3 Characteristics of Faults

After a fault has been pinpointed, its type must be determined. Actually, in the three-phase distribution networks, the faults can be classified into 7 categories: (1): Phase-to-earth fault; (2) Phase-to-phase fault; (3) Phase-to-phase-to-earth fault; (4) Three phase fault; (5) Three phase-to-earth fault; (6) Phase-to-pilot fault; (7) Pilot-to-earth fault. In our method, we only use the voltage and current information of fault node, not all the information of sensors. Therefore, it is almost impossible to identify the specific fault types. Note that a circuit failure (short or open) in a power system causes a change in the power supply, which is reflected in the change of the amplitude and phase of a node current. This type of fault can be determined by monitoring the current of a cluster, which is the state of its dynamics. However, it is usually impractical (if not impossible) to directly measure the states of all the parts of a system. So, it is necessary to build a state observer for the dynamics of each cluster. The state of Cluster $\mathcal{C}_n^{(k)}$ at Layer *k*, $\hat{i}_n^{(k)}(t)$, is taken as an example and is explained below.

a) Variation in Current Amplitude

The amplitude of the current of a cluster changes with the load. For example, let the minimum and maximum loads of Cluster $\mathcal{C}_n^{(k)}$ be $S_{n\_\min}^{(k)}$ and $S_{n\_\max}^{(k)}$, respectively. Since

$$\begin{aligned} I_{n\_\max}^{(k)} &= \left[S_{n\_\max}^{(k)} / U_n^{(k)} \right]^* \\ I_{n\_\min}^{(k)} &= \left[S_{n\_\min}^{(k)} / U_n^{(k)} \right]^* \end{aligned} \tag{3.28}$$

it is only necessary to observe the current, $\hat{I}_n^{(k)}$, and check whether

$$\hat{I}_n^{(k)} \in \left[I_{n\_\min}^{(k)}, I_{n\_\max}^{(k)} \right] \tag{3.29}$$

holds or not.

b) Variation in Current Phase

Generally speaking, the power factor should be in the range [0.86, 1] to guarantee the stability of a power system. That means that the power factor angle, φ, should satisfy

$$\varphi \in [-30^\circ, 30^\circ]. \tag{3.30}$$

This is also a criterion for fault detection.

3.4 Application to a Load Cluster

As an example to illustrate how to apply the EID approach to carry out for the cluster, we apply the method to the dynamics of Load Cluster $C_1^{(1)}$ at Layer 1, which was described in chapter 2, section 2.5.

The dynamic model of Load Cluster $C_1^{(1)}$ was:

$$\begin{cases} \dot{x}(t) = -480.06x(t) + 14.02u(t) \\ y(t) = -0.62x(t) + 0.97u(t) \end{cases}. \tag{3.31}$$

An optimal observer gain, $K_1^{(1)}$, was calculate for The equation (3.24) that minimized the performance index.

$$J_1^{(1)} = \int_0^\infty \left\{ \rho_1^{(1)} \left[x_1^{(1)}(t) \right]^T Q_1^{(1)} x_1^{(1)}(t) + \left[u_1^{(1)}(t) \right]^T u_1^{(1)}(t) \right\} dt .$$

Where $\rho_1^{(1)} = 3 \times 10^4$ and $Q_1^{(1)} = 1$. The parameters yielded

$$K_1^{(1)} = -554.56 . \tag{3.32}$$

The verification results for Layer 1 of the model (Fig. 3-9) show that the estimated error in the state, $\Delta i_1^{(1)}(t) = i_1^{(1)}(t) - \hat{i}_1^{(1)}(t)$, was very small (less than 1%). This means that, for fault diagnosis, the state of the system produced by the state observer can be used rather than the actual state, which may be unavailable.

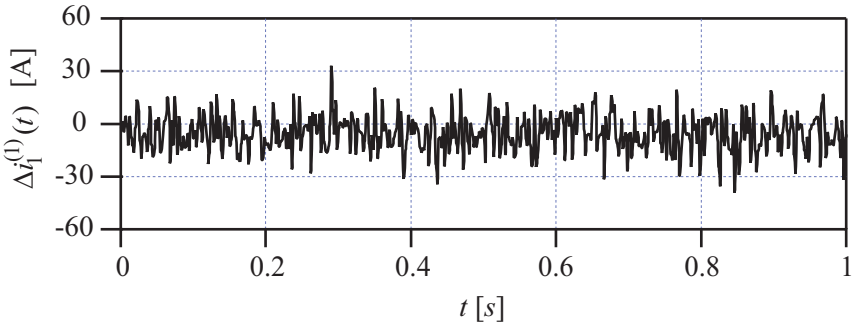

Fig. 3-9 Estimated state error, $\Delta i_1^{(1)}(t)$.

Next, we need to testify that the state observer gain $K_1^{(1)}$, calculated by the LQ method, can guarantee to satisfy the two conditions in *Theorem* 3-1.

Then, we introduce the normal load variation (Fig. 3-10) to the simulation and calculate the disturbance (Fig. 3-11) when system operates in normal conditions. The load variation varied from 1.3 p.u. to 0.35 p.u.. According to simulation result, the thresholds for Cluster $C_1^{(1)}$ were

set to

$$d_{A\_1e}^{(1)} = 2500,\ d_{D\_1e}^{(1)} = 80000. \tag{3.33}$$

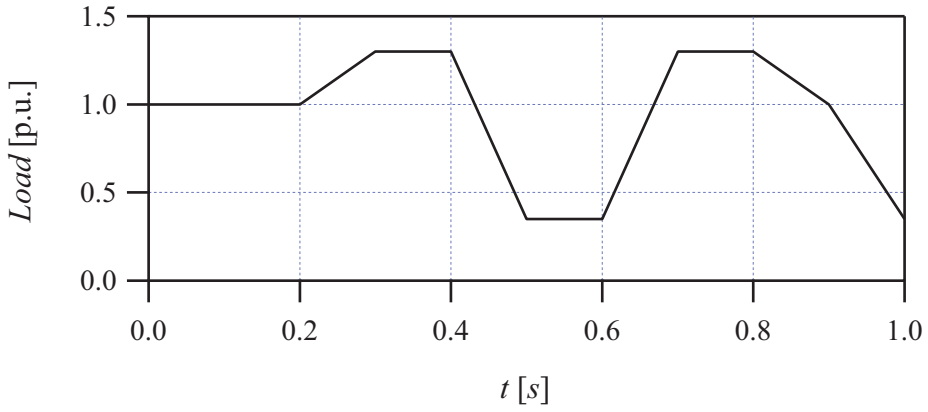

Fig. 3-10 Normal load variation.

There are two types of faults (Fig. 3-12): For one, the amplitude of the load exceeds the maximum; and for the other, both the amplitude and the power factor of the load are outside the allowable range. The two type faults were added to the cluster, respectively and testify whether the disturbances caused by the faults can be detected by EID approach.

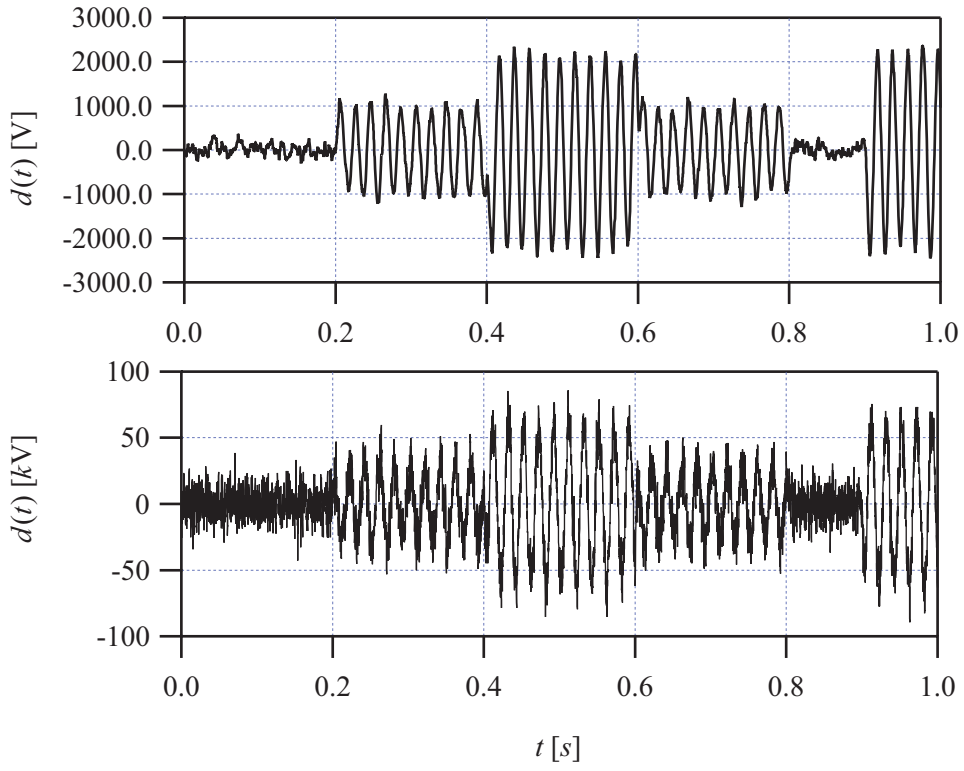

Fig. 3-11 Thresholds of EID.

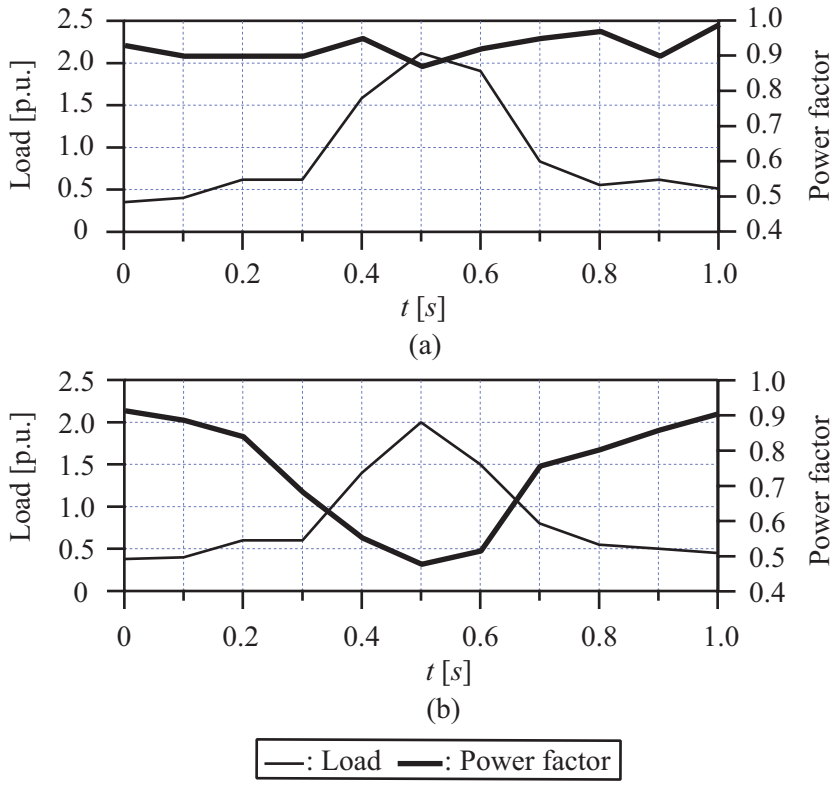

Fig. 3-12 Faults: (a) amplitude type and (b) phase type.

Applying the EID approach to Layer 1 yielded an estimate of the disturbance, $\hat{d}_{1e}^{(1)}(t)$ (Fig. 3-13). The value exceeded the absolute threshold during the periods $[0.3, 0.5]$, which means that faults occurred during that time.

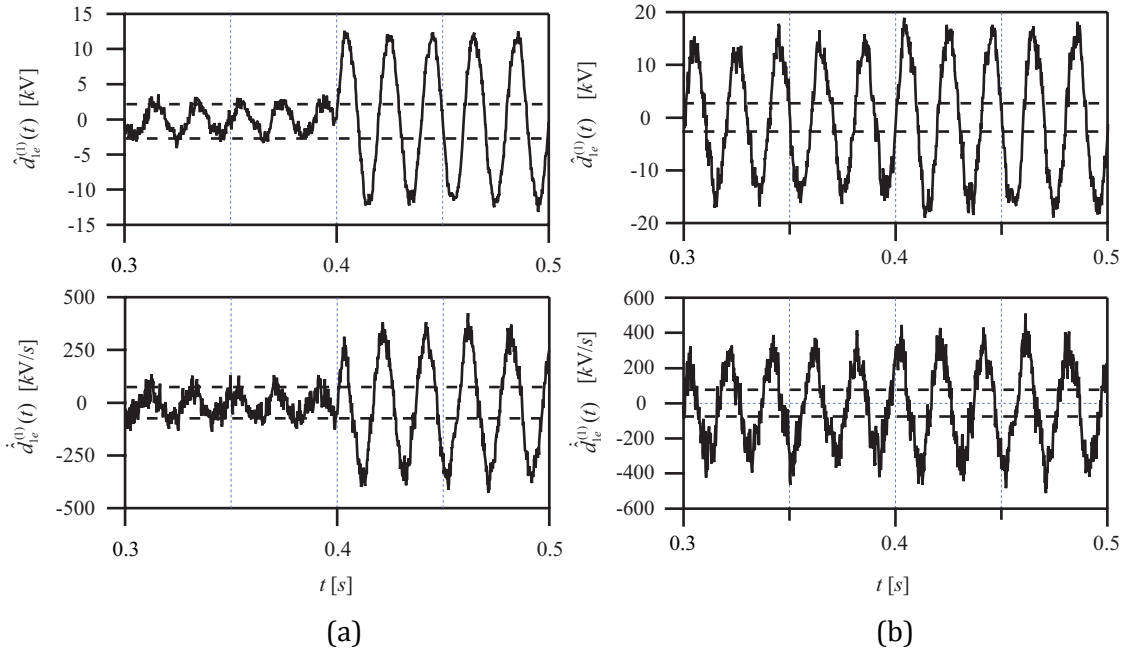

Fig. 3-13 EID estimate, $\hat{d}_{1e}^{(1)}(t)$ and $\dot{\hat{d}}_{1e}^{(1)}(t)$ of Cluster $C_1^{(1)}$ in layer 1.

(*a*) *EID for amplitude type fault;* (b) *EID for phase type fault.*

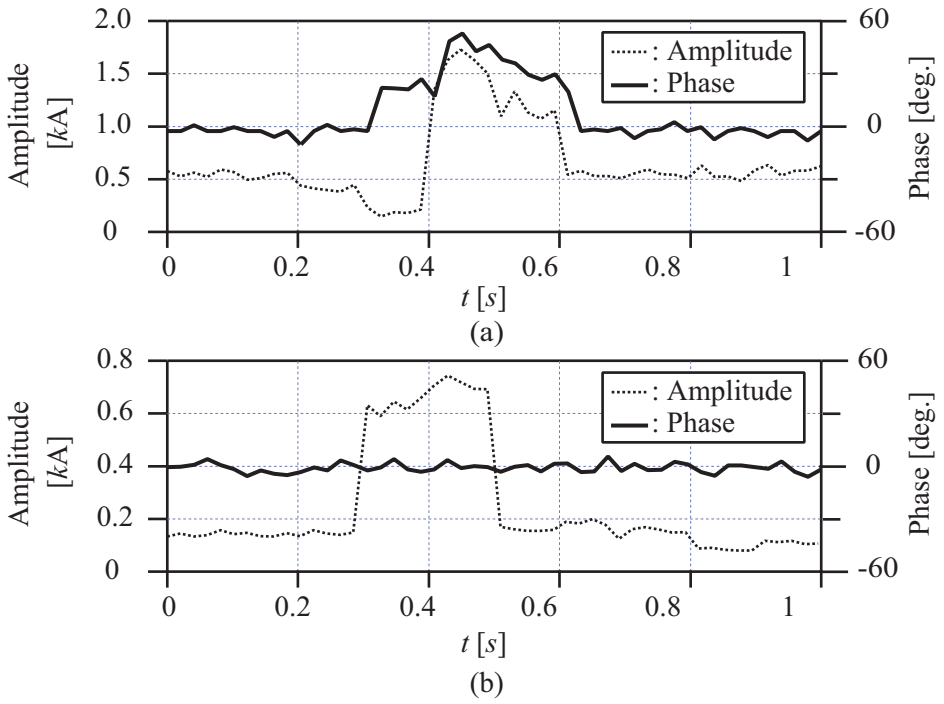

Fig. 3-14 Amplitudes and phases of $\hat{I}_1^{(1)}$.

It is clear from the result of EID, the disturbance and its differential can detect the faults. However, it is hard to distinguish the two type faults clearly only using the characteristics of disturbances. Next, this information is obtained from an analysis of the system states, that is, the currents, of the load cluster with faults. The calculated amplitudes and phases of the estimated states, $\hat{i}_1^{(1)}(t)$, yielded the following information (Fig. 3-14):

a) For Fig. 3-14 (a), the amplitude of the current was outside the allowable range, and the phase shifted so much that Condition (3.30) failed. So, both the amplitude and phase of the state were abnormal in this situation. The fault of (a) is the phase type fault.

b) For Fig. 3-14 (b), the large change in current during the period $[0.3, 0.5]$ was outside the allowable range; but the change in phase was small. So, only the amplitude of the state was abnormal in this situation. The fault of (b) is the amplitude type fault.

The infinity and Euclidean norms of the EIDs of different layers can be used to assess the damage caused by faults at different levels. More specifically, the infinity norm is related to maximum power, and the Euclidean norm is related to total energy. Equation (3.34) and (3.35) show the infinity norm and Euclidean norm of the EIDs for clusters, respectively.

$$\left\| d_{1e}^{(1)}(t) \right\|_2 = 21745 \tag{3.34}$$

$$\left\| d_{1e}^{(1)}(t) \right\|_\infty = 1884 . \tag{3.35}$$

3.5 Conclusion

The Equivalent-Input-Disturbance approach was applied to a fault diagnosis method for the load cluster in this chapter. From the viewpoint of system robustness, faults can be defined as: the disturbances exceed the allowable range and break the stability of system. Based on this idea, the EID approach, which can estimate the system disturbances, is applied to diagnose the faults. Firstly, the theory basis of EID approach and the definition of EID were introduced. According to the characteristics of dynamic model for load cluster, the design method of state observer gain was given out. Secondly, two critical considerations of fault diagnosis method based on EID approach, which are the thresholds of the EIDs and the characteristics of faults were discussed. Furthermore, after a fault was located, its type must be determined. This type of fault was determined by monitoring the current of a load cluster, which is the state of its dynamics. Lastly, the simulation results on the case study were presented to illustrate the effective of the fault diagnosis method.

Chapter References

[3-1] **M. Corless and J. Tu.** *State and input estimation for a class of uncertain systems.* Automatica, vol. 34, no. 6, pp. 757–764, 1998.

[3-2] **M. Hou and R. J. Patton.** *Optimal filtering for systems with unknown inputs,* IEEE Trans. Autom. Control, vol. 43, no. 3, pp. 445–449, Mar. 1998.

[3-3] **J.-L. Chang.** *Applying discrete-time proportional integral observers for state and disturbance estimations,* IEEE Trans. Autom. Control, vol. 51, no. 5, pp. 814–818, May 2006.

[3-4] **F.-J. Lin and P.-H. Shen.** *Robust fuzzy neural network sliding-mode control for two-axis motion control system,* IEEE Trans. Ind. Electron., vol. 53, no. 4, pp. 1209–1225, Jun. 2006.

[3-5] **M. Sun, Y. Wang, and D. Wang.** *Variable-structure repetitive control: A discrete-time strategy,* IEEE Trans. Ind. Electron., vol. 52, no. 2,pp. 610–616, Apr. 2005.

[3-6] **G. Cheng and K. Peng.** *Robust composite nonlinear feedback control with application to a servo positioning system,* IEEE Trans. Ind. Electron.,vol. 54, no. 2, pp. 1132–1140, Apr. 2007.

[3-7] **K. Ohnishi, N. Matsui, and Y. Hori.** *Estimation, identification, and sensorless control in motion control system,* Proc. IEEE, vol. 82, no. 8, pp. 1253–1265, Aug. 1994.

[3-8] **S. Katsura, K. Ohnishi, and K. Ohishi.** *Transmission of force sensation by environment quarrier based on multilateral control,* IEEE Trans. Ind. Electron., vol. 54, no. 2, pp. 898–906, Apr. 2007.

[3-9] **J.-H. She, Y. Ohyama, and M. Nakano.** *A new approach to the estimation and rejection of disturbances in servo systems,* IEEE Trans. Control Syst. Technol., vol. 13, no. 3, pp. 378–385, May 2005.

[3-10] **J. She, X. Xin and Y. Ohyama.** *Estimation of Equivalent Input Disturbance Improves Vehicular Steering Control,* IEEE Trans. Veh. Technol., vol. 56, no. 6, pp. 3722-3731, Nov. 2007.

[3-11] **J. She, X. Xin and Y. Pan.** *Equivalent-Input-Disturbance Approach – Analysis and Application to Disturbance Rejection in Dual-Stage Feed Drive Control System,* IEEE/ASME Trans. Mechatronics, vol. 16, no. 2, pp. 330-340, Apr. 2011.

[3-12] **W. S. Levine.** *The Control Handbook, Boca Raton*, FL: CRC Press, 1996.

[3-13] **L. R. Hunt, G.Meyer, and R. Su.** *Noncausal inverses for linear systems*, IEEE Trans. Autom. Control, vol. 41, no. 4, pp. 608–611, Apr. 1996.

[3-14] **K. Zhou, J. C. Doyle, and K. Glover.** *Robust and Optimal Control*, Englewood Cliffs, NJ: Prentice-Hall, 1996.

[3-15] **B. D. O. Anderson and J. B. Moore.** *Optimal Control—Linear Quadratic Methods.* Englewood Cliffs, NJ: Prentice-Hall, 1989.

[3-16] **K. Ohnishi, N. Matsui, and Y. Hori.** *Estimation, identification, and sensorless control in motion control system,* Proc. IEEE, vol. 82, no. 8, pp. 1253–1265, Aug. 1994.

[3-17] **H. Kwakernaak and R. Sivan.** *The maximally achievable accuracy of linear optimal regulators and linear optimal filters,* IEEE Trans. Autom. Control, vol. AC-17, no. 1, pp. 79–86, Feb. 1972.

[3-18] **H. Kimura.** *A new approach to the perfect regulation and the bounded peaking in linear multivariable control systems,* IEEE Trans. Autom. Control, vol. AC-26, no. 1, pp. 253–270, Feb. 1981.

Chapter 4
Fault Diagnosis of Distribution Networks with PV Generation Embedded

4.1 Chapter Introduction

In recent years, the renewable energy power such as solar energy, wind energy, fuel cells and etc. have experienced a remarkably rapid growth because they are pollution-free power sources. PV, as a kind of renewable energy, has been widely applied in the world. With the PV system installing to distribution network, although many benefits have brought to the both consumers and utility, some difficult problems also appeared. In particular, with the PV system injecting the power, the feeders get active and the short circuit fault current of feeders will be changed. The short circuit current of protection relay needs to be set again. What is worse, due to the fluctuation of PV output, the level of short circuit fault current will change with the variation of PV output. Therefore, the conventional protection turns out to be unsuitable.

Conventional methods are based on huge number information of protective relays and breakers in the system to identify the fault and locate fault position. If the false tripping or miss tripping of breakers frequently occur, it is hard to get the correct result for fault diagnosis. Recently many researchers begin to pay attention to the fault diagnosis of power distribution with PV connected. The paper [4-1] proposed a new protection scheme to solve the problem of protection mal-operation. However, in the new scheme, the installation location of protection device need to be changed and the amount of protection devices need to be increased.

In chapter 3, a new fault diagnosis method for the distribution network has been proposed, which not only can overcome the shortage of traditional methods, but also can avoid installing any new devices or modifying the exist protection system. However, before applying it to the network installed with PV system, the influence of PV system output fluctuation need to eliminate primarily.

The structure of this chapter is planned as follows:

Section 4.2: The impact of PV system to the distribution feeder is analyzed, including the reverse power, electrical line losses and malfunction of protection system.

Section 4.3: The dynamic model of load cluster with PV system is presented.

Section 4.4: The fault diagnosis method to the feeder with PV system embedded is proposed. In particular, the approach how to eliminate the PV's influence is given out.

Section 4.5: The simulation results are presented to testify the effective of our method.

4.2 Impacts of Grid-connected PV Generation

Before the fault diagnosis for the LC with PV system embedded, the impacts of Grid-connected PV system are analyzed, including the voltage variation, reverse power, electrical line losses and protection system malfunction.

4.2.1 Grid-connected PV Generation

A grid connected PV system [4-3] converts sunlight directly into AC electricity. The main purpose of the system is to reduce the electrical energy imported from the electric utility. Fig. 4-1 shows a general block diagram for a PV grid-connected system with feedback current control and two PWM blocks provided by inverter manufacturer: PWM Maximum power point tracking (MPPT) for maximum power generation and PWM (DC–AC) for DC–AC converter in current mode. The main components consist of:

(a) A PV panel which generates direct current from sunlight;

(b) DC–DC with isolated transformer designed for achieving the maximum power with PWM control produced by a simple method, namely Perturbation and Observation technique (P&O) (dP/dv=0) where P represents the PV output active power and V the voltage of PV;

(c) DC–AC full-bridge converter, which is used to generate AC waveform from DC signal with current-mode PWM scheme;

(d) Switching filter, used for eliminating the unwanted signal; and

(e) Other parts, for example Phase Lock Loop (PLL) and load in parallel connection.

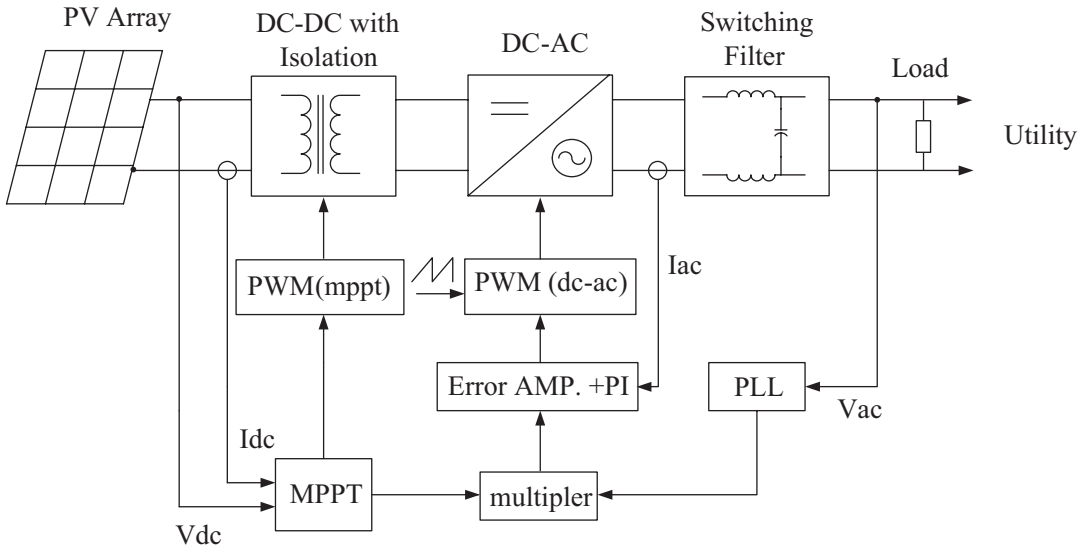

Fig. 4-1 Block diagram of a PV grid-connected generation.

The direct current and voltage from the PV panel are measured and formed as inputs for the MPPT block to generate a PWM signal for the dc–dc converter in order to operate in maximum power generation. The current amplitude at maximum operation from the MPPT block is multiplied with in-phase sinusoidal unit-vector waveform which is produced from the PLL block. The result is designated as current reference signal. At the output of dc–ac converter stage, the actual current from the inductor current flowing through the filter is sensed and compared with the current reference, and then the error is compensated with the PI controller. This stage is called error amplification. Finally, this output is compared with the saw-tooth signal to generate a PWM signal for the gate drive of dc–ac converter in the comparison stage.

With the PV system connected to distribution network, many benefits will bring to the both electricity consumer and utility. For the consumers, they can save money as well as improve their power supply reliability by installing PV grid-connected systems, because they can generate and use the solar energy at the peak demand when power is at its highest price of the day. For the utility, they can improve the voltage profile and reduce the loading level of branches. In radial distribution networks, bus voltages decrease as the distance from the distribution transformer increases, and may become lower than the minimum voltage permitted by the utility. By installing PV grid-connected system near substation or the end of feeder, the power of PV will import to the feeder, so the voltage of node will improve and the load level of branches will decrease.

Because of these reasons, the installations of PV grid-connected systems in many countries have been supported by utilities and government agencies. In Japan, the installation target of PV grid-connected system is set at 28GW by 2020, and 53GW by 2030. Furthermore, because of the event of Japanese nuclear leak in Fukushima nuclear power station, the government revised the country's energy policy that decrease the nuclear power and increase the renewable energy. On such a background, it is estimated that a large-scale PV Grid-connected system will be installed in electrical power networks in the near future.

Despite all the benefits introduced by PV systems to electric utilities, these systems might lead to some operational problems [4-4]. One of the main factors that lead to such problems is the fluctuations of the output power of PV systems due to the variations in the solar irradiance caused by the movement of clouds. Such fluctuations lead to several operational problems and make the output power forecast of PV systems a hard task. In addition, the high cost of these systems limits the possible solutions that can be adopted by electric utilities to reduce the severity of the operational problems that might arise due to these fluctuations.

The PV grid-connected system installed at Honjo campus in Waseda University in Tokyo,

Japan is studied. The electrical characteristics of the PV grid-connected system will be used in the study of the influence of PV installation to distribution network. The PV array is made of amorphous silicon. The rated capacity of the PV is 55 MVA, which supplies local loads, mainly electricity for fluorescent lighting, air conditioning units at the point of common coupling. The load is essentially inductive. The system configuration is shown in Fig. 4-1.

The most important factor for the output of PV system is the solar irradiance. Therefore, the electricity from PV is varying with the different season and weather. We collected and analyzed the fluctuations of PV output for one year.

The table 1 shows the average of PV output among different season and weather. Compared with cloudy and rain day, the PV can have obviously higher output power in sunny day. Meanwhile, the PV output power in spring and summer was larger than fall and winter. The maximum of PV output appeared on the sunny day of spring, not in summer, because the weather in spring is fine and typhoons frequently happens in summer. In the opposite, the minimum of PV output appeared on the rain day of fall.

TABLE 4-1 DATA OF PV DURING ONE YEAR PERIODS

Season	Weather	days	Average Output of PV	standard deviation
Spring	Sunny	49	0.808	0.175
	Cloudy	26	0.322	0.216
	Rain	13	0.239	0.214
Summer	Sunny	42	0.660	0.141
	Cloudy	41	0.334	0.202
	Rain	9	0.170	0.123
Fall	Sunny	67	0.432	0.112
	Cloudy	16	0.201	0.144
	Rain	9	0.063	0.063
Winter	Sunny	61	0.521	0.147
	Cloudy	22	0.251	0.183
	Rain	7	0.208	0.204
Total	Sunny	219	0.605	0.144
	Cloudy	105	0.277	0.187
	Rain	38	0.170	0.151

According to the average data of PV output in different season and weather, we can get the fluctuations of PV output power model as Fig. 4-2. Although PV output powers have different patterns in different season and weather, we also can find some common ground with them. The

output of the PV System has been captured for a period in a day from 6:00 am to 19:00 pm. It can be seen from Fig. 4-2 that the peak values occur around 12:00am.

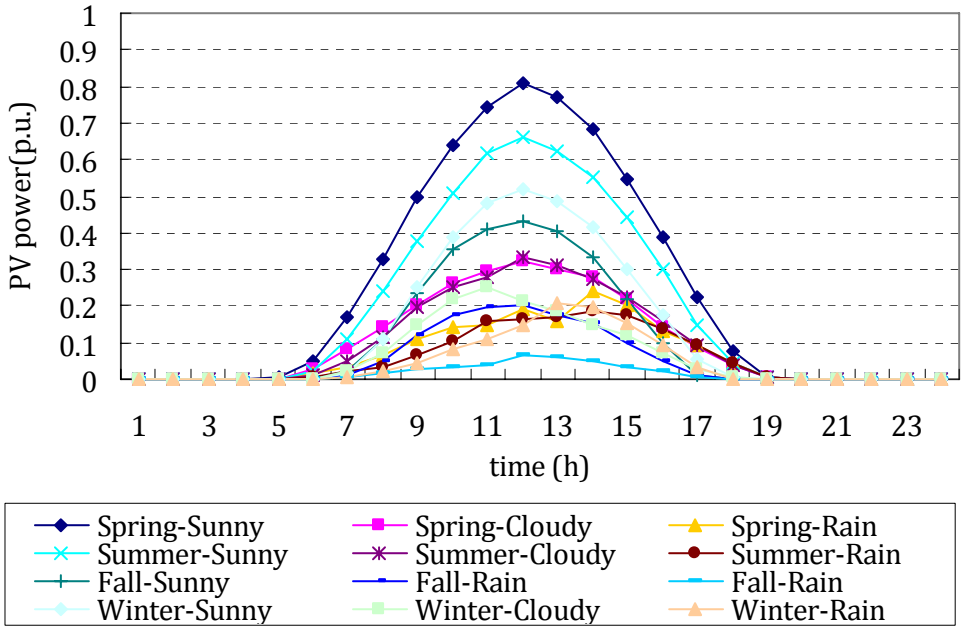

Fig. 4-2 PV output model.

In order to evaluate the impact of PV installation to distribution network, we need obtain the load fluctuation without the installation of PV grid-connected at first. In this section, a variety of load cases are adopted. The load data, which collected from the Honjo campus in Waseda University, were assumed in four patterns, including seasons of spring, summer, fall, winter as Fig. 4-3. From Fig. 4-3, the spring load and winter load was maximum and minimum load respectively. And it was obviously that the maximum and minimum of PV output also appeared in spring and winter. So we make the PV penetration in spring and winter to be the typical model to research.

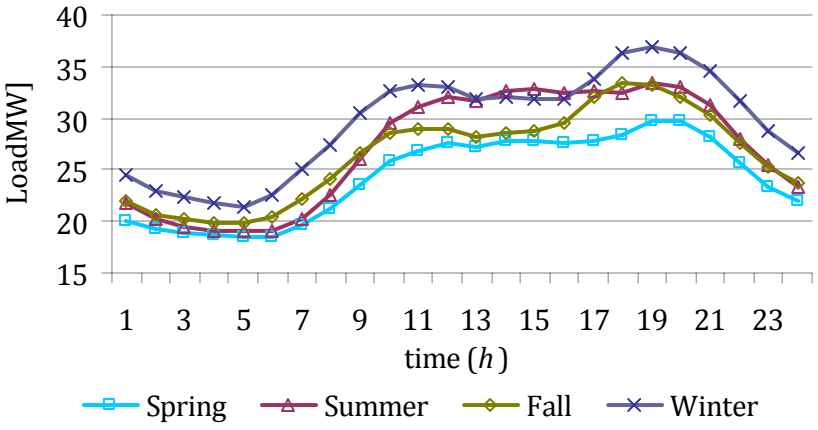

Fig. 4-3 Load model.

Then, we assume various scenarios of PV installation in distribution networks and show evaluation of the influence of PV installation on distribution networks to find the best scenarios for PV installation. The same value as the peak of the load was assumed to be 100% PV output, and the cases of 30%, 50%, 70%, 100% are also simulated for comparison. The Fig 4-4, 4-5 shows the spring and winter load model with the cases of 0%, 30%, 50%, 70%, 100% of PV penetration. By using these data, active power and reactive power are changed along with the load curve, while keeping the power factor constant.

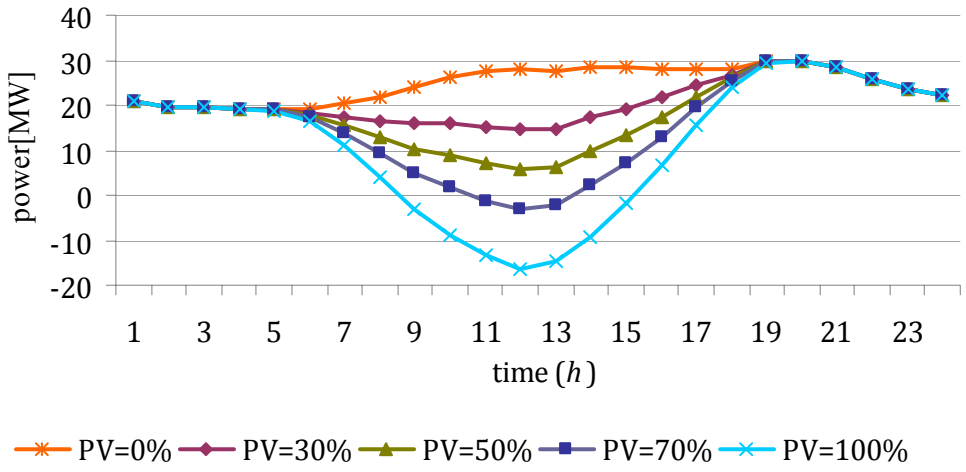

Fig. 4-4 Load with PV penetration in spring model.

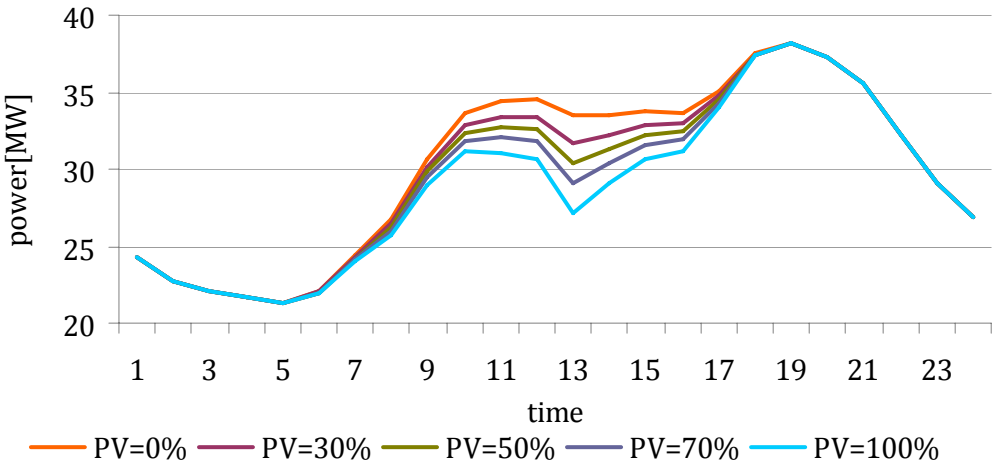

Fig. 4-5 Load with PV penetration in winter model.

4.2.2 Reverse Power

It was assumed to introduce load pattern and PV model in spring and winter to all the nodes in feeder and to keep the voltages on adequate range (±5%) by the tap control. The

profile of sending voltage, terminal voltage and the changing of tap position are drawn in spring and winter model.

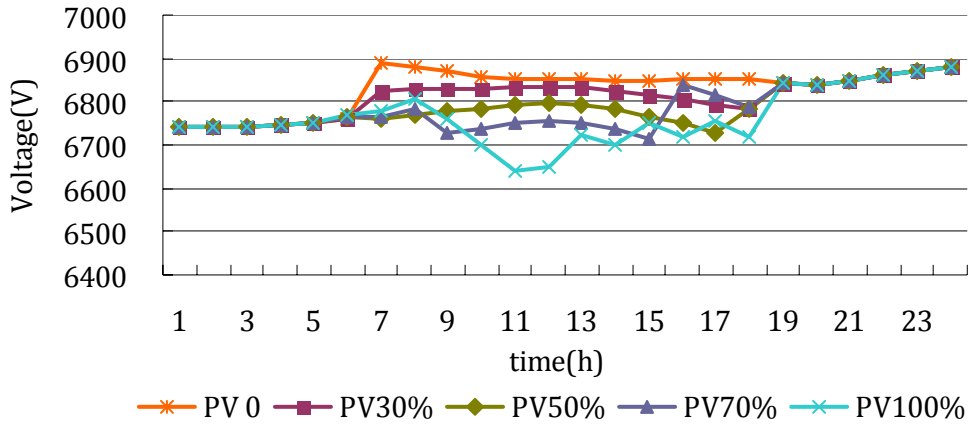

Fig. 4-6 Sending voltage curve in spring model.

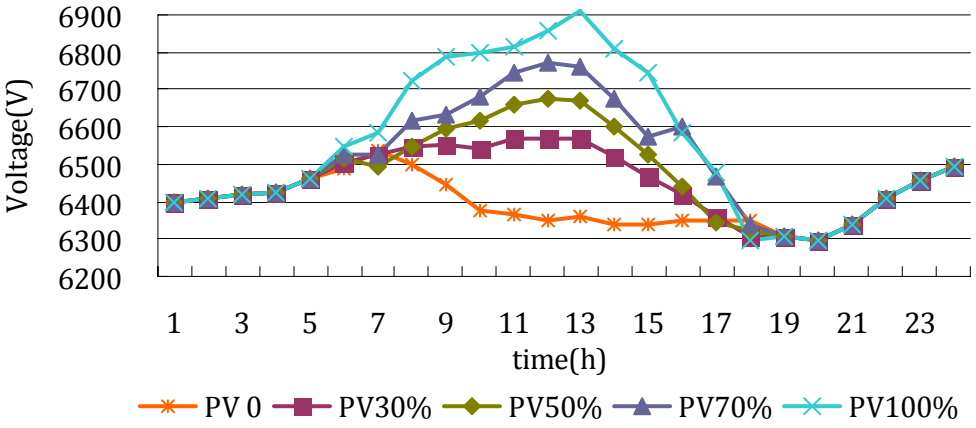

Fig. 4-7 Terminal voltage curve in spring model.

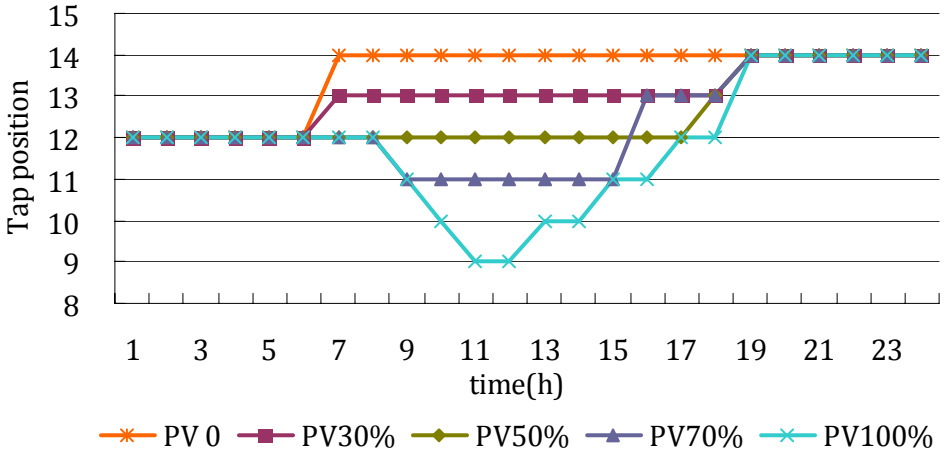

Fig. 4-8 Tap position.

The different kinds level of PV penetration in distribution networks in spring are shown in

Fig. 4-6 – 4-8. These figures are sending voltage (V_1), and terminal voltage (V_{12}), tap position, respectively. Sending voltage is controlled in order to keep terminal voltage near the normal voltage of 6600V, and tap change frequency is limited as few times as possible.

--First, in the scenarios of 100% PV installation, the terminal voltage was raised excessively at peak time of PV output because larger numbers of PV power import to feeder. The terminal voltage was kept in an adequate range by dropping the sending voltage enough. The frequency of tap changing increased because the sending voltage was rebounded in night time.

--Second, in the case of 70% PV installation, the sending voltage profile was similar to the one at 100%, however the terminal voltage was smaller than former, because the PV power poured in to the feeder was lower. Meanwhile, the frequency of tap changing was comparatively few because the load was offset by the PV output at the PV output peak time.

--Third, in the case of PV installation 50%, 30%, tap position was regulated so that the sending voltage was kept high at each time. The range of tap control had allowance because PV output power compensated voltage drop.

As a result, the node voltages can be controlled within an adequate range by changing taps. However, if the capacity of PV installation exceeds the allowable range, which is 100% of peak load in this case, the tap changes frequently. Furthermore, we can get the conclusion that when the capacity of PV installation larger than 70% of peak load, the reverse power will happen. Specifically, 0.93MW reverse power flow occurred on 70% PV case, 4.3MW reverse power flow occurred on 100% PV case.

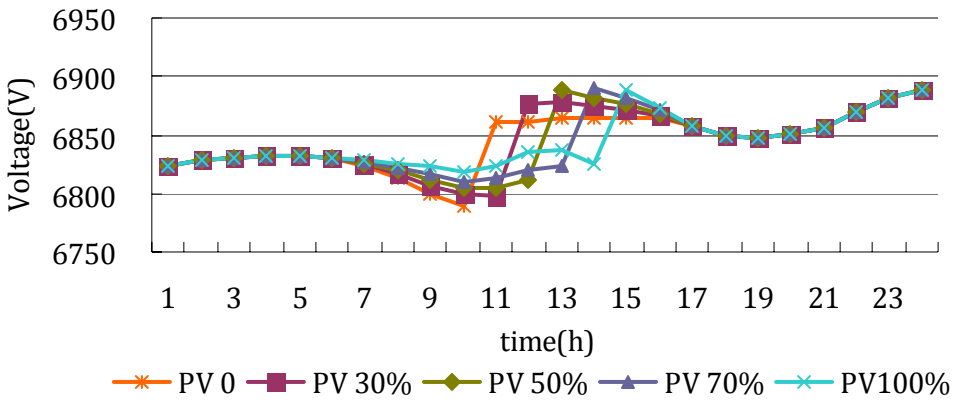

Fig. 4-9 Sending voltage curve in winter model.

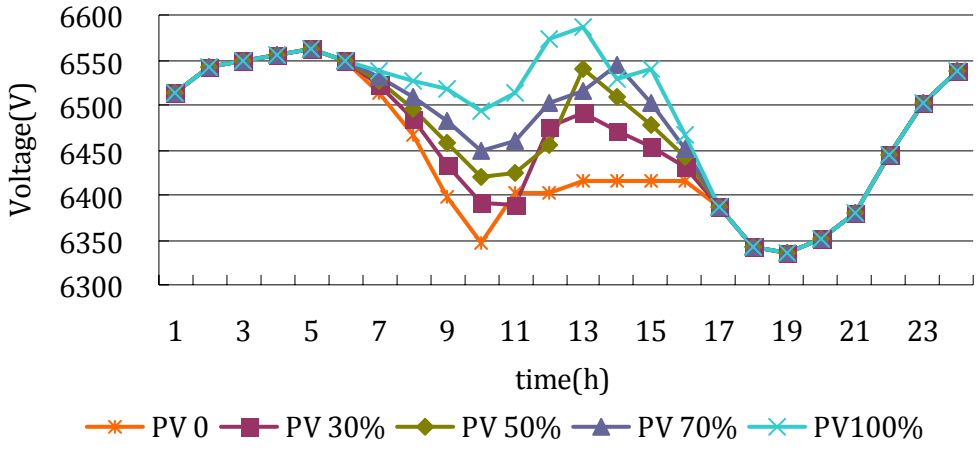

Fig. 4-10 Terminal voltage curve in winter model.

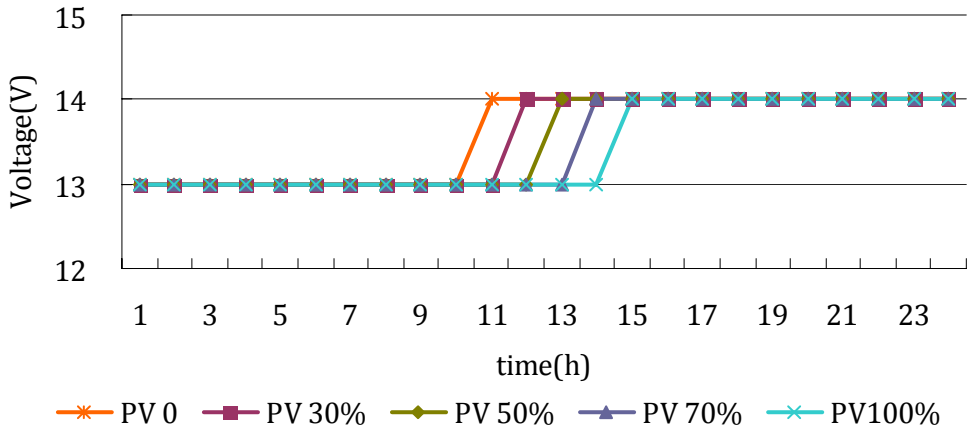

Fig. 4-11 Tap position.

In winter model, the simulation results are shown as Fig. 4-9 – 4-11. The sending voltages were basically consistent in all scenarios of PV installation and the terminal voltage kept in a low voltage level, because the low PV power poured into the distribution network. The tap change infrequently, just once a day. The reverse power flow of feeder did not occur in all of PV installation cases.

4.2.3 Electrical line losses

Electrical line losses occur as current flows through conductors, transformers and other transmission and distribution system devices [4-5]. The magnitude of the losses is related to current flow and resistance of the devices. Thus, line losses can be decreased by reducing either the resistance or the current.

With the introduction of PV, the current flows through the conductors are decreased. For this reason, the electrical line losses of distribution feeder are decreased simultaneously. Fig 4-12 shows electrical line losses with 0%, 30%, 50%, 70%, 100% of PV penetration,

respectively. Loss reduction, due to installation capacity, was shown to be in the order of hundreds of kilowatts for 0%, 30%, 50%, 70%, 100% penetration. So we can get the conclusion that the installation capacity of PV has considerable effects on system losses, higher PV penetration lower electrical line losses. However, when the PV penetration exceed the 70% of load, the reduction of losses was not obvious. And we also can note that the decrease of losses was not obvious in winter because of lower PV ouput power.

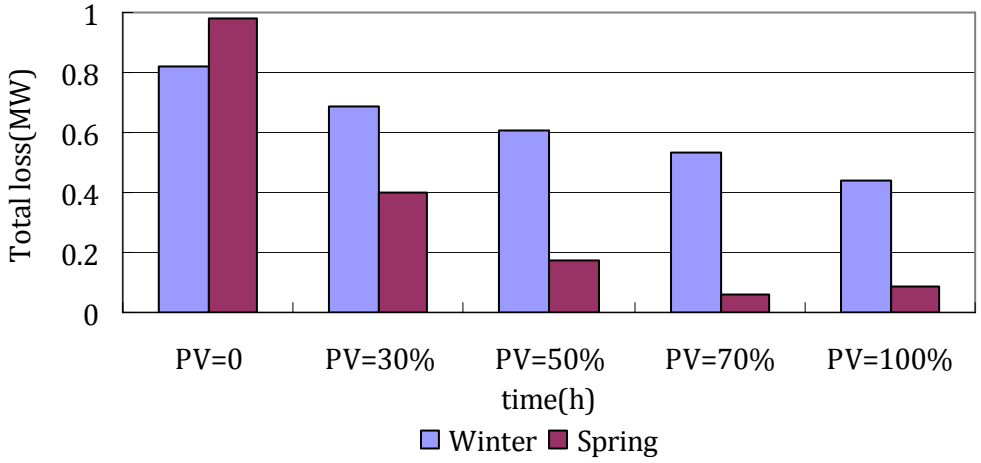

Fig. 4-12 Electrical line losses of distribution feeder

4.2.4 Protection System Malfunction

The fault current level describes the effect of faults in terms of current or power. It gives an indication of the short circuit current or (apparent) power boost. In [4-2] the fault level in p.u. is defined as

$$fl = i = \frac{1}{Z_{th}}. \tag{4.1}$$

Where, i is the fault current related to the nominal current and Z_{th} is the inner impedance of the Thevenin representation of the network in *p.u.*. Example for this value are given in [4-2], typical fault levels in distribution networks are in a range of 10-15 *p.u.*, where 1 *p.u.* corresponds to the rated current.

The fault current has to be distinguishable from the normal operational current for the relay triggers. If for example, a remote part of a distribution network is equipped with large PV installations, it could happen that in case of a failure there is almost no significant rise of the phase current and the fault is therefore not detected from the over-current protection system. With PV embedded in the network, the fault impedance Z_{th} can also decrease due to parallel circuits, therefore the fault level increase and there could be unexpected high fault currents in

case of a failure. This situation puts components at risk since they were not designed to operate under that circumstance.

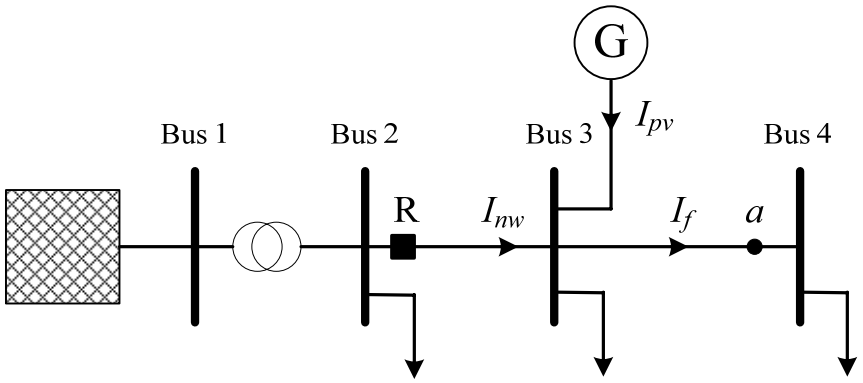

Fig. 4-13 Short circuit at a. Current from transmission network I_{nw}, current from embedded PV generator I_{pv}

For correct operation it is also important that relay measures the real fault current which was expected and taken under consideration when relay was configured. Fig. 4-13 shows d distribution feeder with an embedded PV generator that supplies part of the local loads. Assuming a short circuit at point *a*, the generator will also contribute to the total fault current

$$I_f = I_{nw} + I_{pv}. \tag{4.2}$$

But the relay *R* will only measure the current coming from the network from the network infeed I_{nw}. This is, the relay detects only a part of the real fault current and may therefore not trigger properly. There is an increased risk especially for high impedance faults that overcurrent protection with inverse time-current characteristic may not trigger in sufficient time.

In order to prove this, we constructed a simulation of short-circuit current analysis for Fig. 4-14 is the simulation structure in the MATLAB Simulink. The voltage of utility source is 110kV and the ratio of the transformer is 110kV/11kV. The PV source embedded in the Bus 3 and the voltage of PV output is 11 kV keeping the same with the network voltage. The three phase short circuit fault occurs at Bus 4. The simulation time is 0.5 *s* and the fault occurs at 0.2 *s*.

1) The PV source is not embedded into the bus 3.

The fault current measured of breaker *R* at bus 2 is shown in Fig. 4-15 (a). The short-circuit current is suffered a sharply increase at 0.2 *s*, caused by the fault. Therefore, the fault is easy to be detected by the protection relay according to the change of current and the breaker *R* can trigger timely to protect the networks.

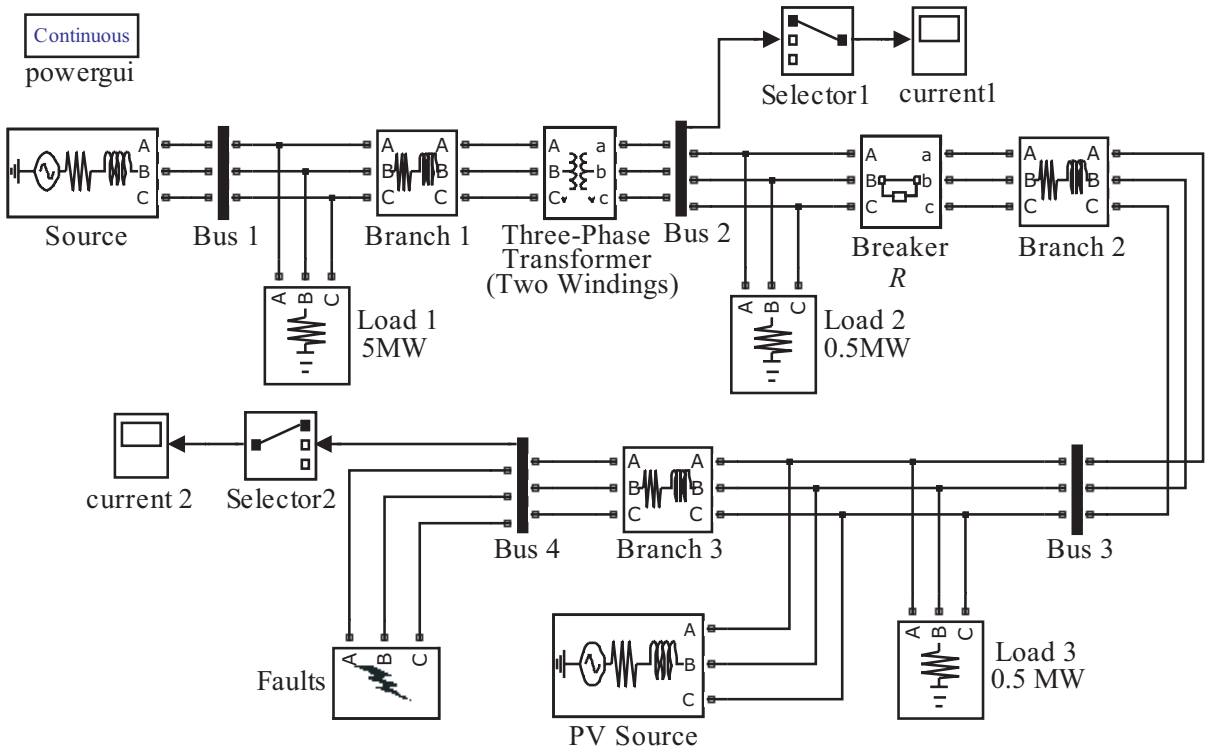

Fig. 4-14 Simulation structure of short circuit fault with PV generation embedded.

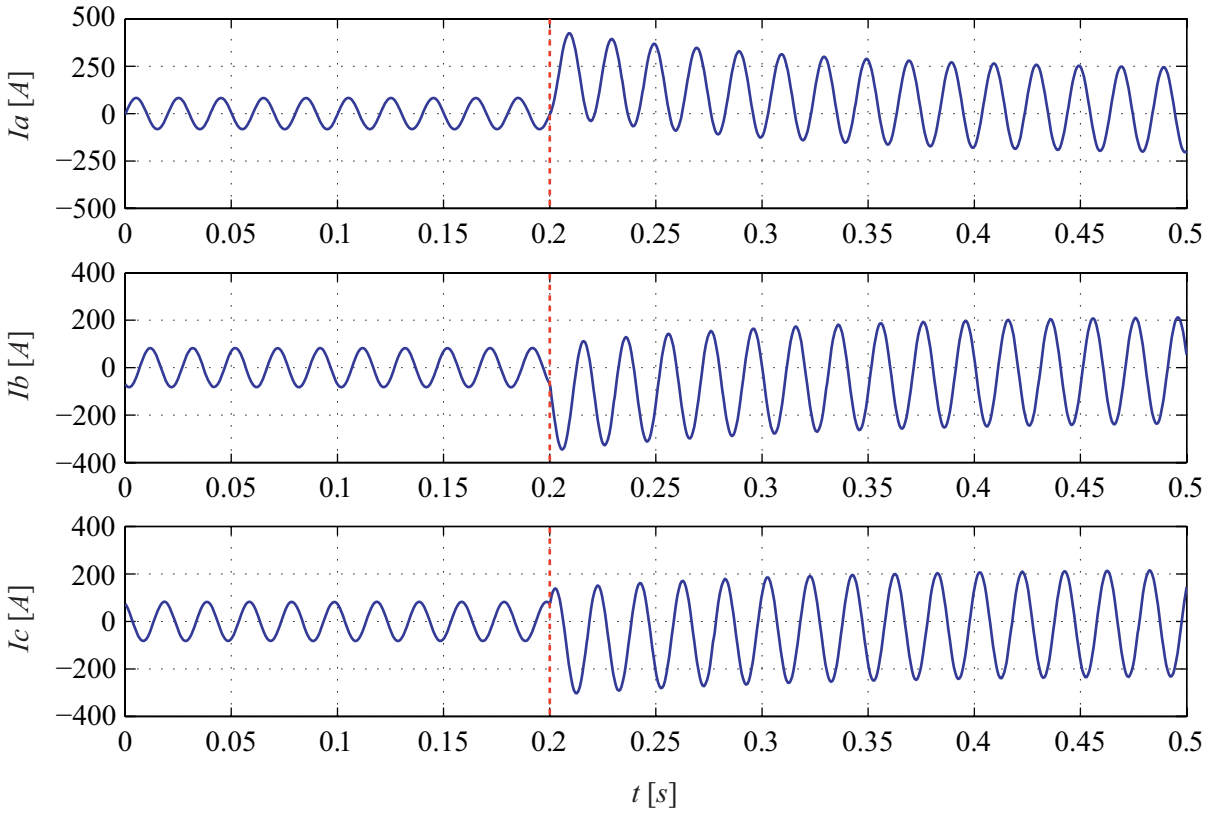

(a) Without PV generation

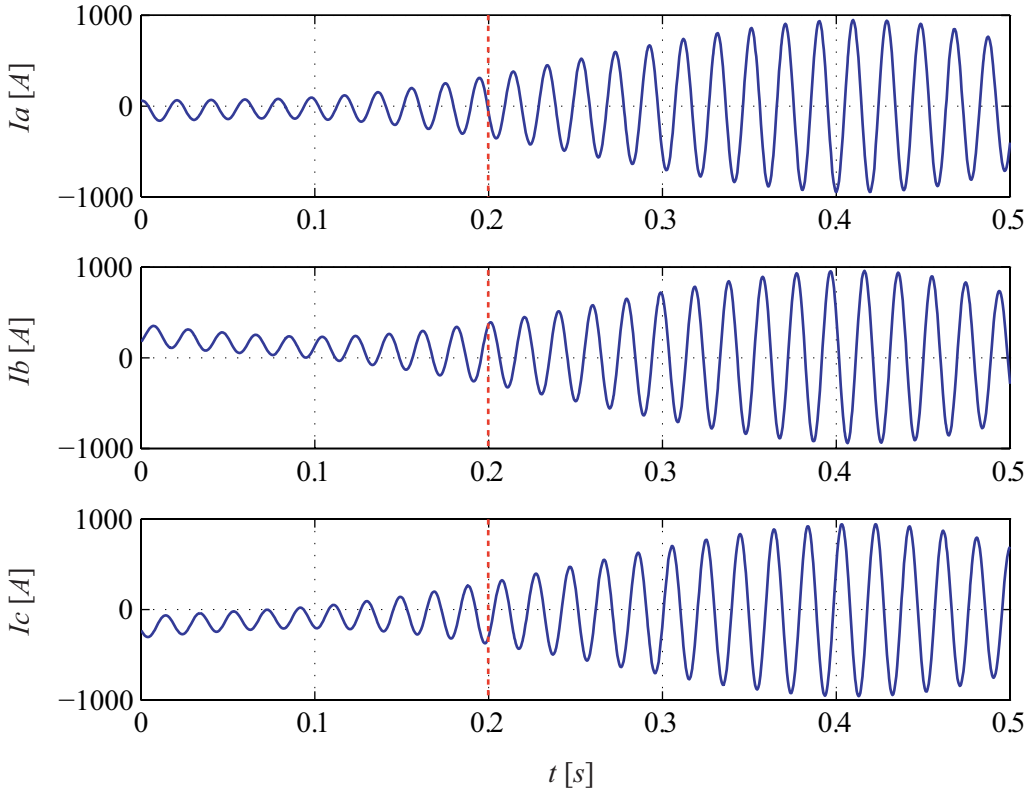

(b) PV generation embedded

Fig 4-15 Fault current of Relay R.

2) The PV source is embedded into the bus 3.

The fault current of breaker *R* with PV source is shown in Fig. 4-15 (b). The changes of fault current are not as large as the situation 1). The PV source, I_{pv} supplied the partial short-circuit current to the fault position to make the current at breaker *R*, I_{nw}, increase slowly. Therefore, the breaker may not trigger properly and protection relay may malfunction in this situation.

4.3 Dynamic Model of Distribution Network with PV Generation

In Fig. 4-16, the load consumers can be supplied power from both the utility grid and PV generator simultaneously.

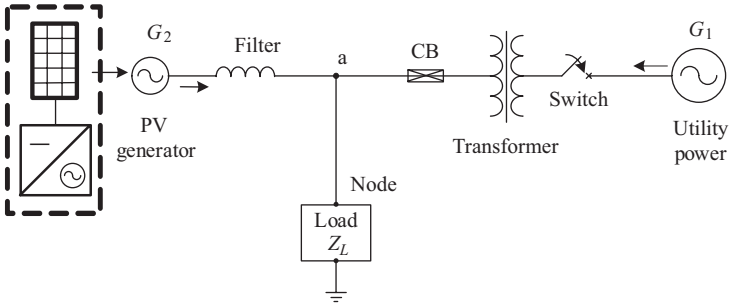

Fig. 4-16 Block diagram of feeder with PV system connected.

PV systems, consisting of PV arrays and an inverter, are connected to the distribution feeder at point "a" and inject the current to the feeder. Therefore, one part of load consumption is come from the PV systems (G_2), and the rest is supported by the utility power (G_1). The filter, installed at the PV side, can eliminate high frequency harmonic signals from the inverter. And compared to the PV generator, the utility power source could be regarded as an infinity power, which can supply the large enough power to the load. But for the PV generator, due to the limited power support, it can be regarded as a controlled source, of which the output current was limited and usually determined by the weather. Then the equivalent circuit of feeder with PV system connected was shown in Fig. 4-17.

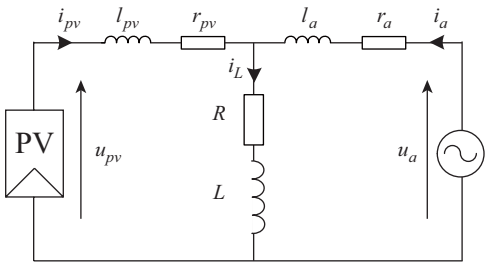

Fig. 4-17 Equivalent circuit of Fig. 4.16.

As we mentioned in Chapter 2, PV system can be regarded as a *PV-specified* node. If the voltage of PV system is specified to the voltage of utility source, u_{pv}=u_a, then the dynamic of equivalent circuit of feeder is given by

$$\begin{cases} \dot{x}(t) = Ax(t) + Bu(t) \\ y(t) = Cx(t) \end{cases}. \tag{4.3}$$

Where, $x(t) = [i_{pv}(t), i_a(t)]^T$, $u(t) = u_a(t)$, $y(t) = i_L(t)$. $i_{pv}(t)$ and $i_a(t)$ are the current of PV and utility source, respectively; $u_a(t)$ is the input voltage, and the $i_L(t)$ is the output current to node; and

$$A = \begin{bmatrix} -\dfrac{l_a R + r_{pv} L + r_{pv} l_a}{l_{pv} L + l_a L + l_{pv} l_a} & \dfrac{r_a L - l_a R}{l_{pv} L + l_a L + l_{pv} l_a} \\ \dfrac{r_{pv} L - l_p vR}{l_{pv} L + l_a L + l_{pv} l_a} & -\dfrac{l_{pv} R + l_{pv} r_a + r_a L}{l_{pv} L + l_a L + l_{pv} l_a} \end{bmatrix}, \quad B = \begin{bmatrix} \dfrac{l_a}{l_{pv} L + l_a L + l_{pv} l_a} \\ \dfrac{l_{pv}}{l_{pv} L + l_a L + l_{pv} l_a} \end{bmatrix}, \quad C = [1 \ 1]. \tag{4.4}$$

Where r_{pv}, r_a are the equivalent resistances of the line from the PV generator and utility source to load node respectively; l_{pv} is the equivalent inductance of filter; and the *R*, *L* is the equivalent resistance and reactance, respectively of load Z_L.

The complex power of the node is S_L. The equivalent impedance of it is:

$$Z_L = \frac{U_L \bar{U}_L}{\bar{S}_L}. \tag{4.5}$$

Note that U_L is the phasor of the variable u_L, and $\bar{U}_L$ is the complex conjugate of U_L.

Let the equivalent impedance of a passive two-port network, *N*, be $Z_L = R + jX$; that is, it is the equivalent resistance, *R*, and the reactance, *X*, connected in series. *N* is an inductive load when $X > 0$, a capacitive load when $X < 0$, and a pure resistive load when $X = 0$. Actual power systems are usually inductive, which means that $X > 0$ in most cases. Then we obtain:

$$Z_L = R + j\omega L. \tag{4.6}$$

If the PV system operates in *PQ-specified* node type, the voltage of PV system is not controlled. In this situation, we can regard the PV voltage as an input of system and a new formulation of system can be obtained.

$$\begin{cases} \dot{\bar{x}}(t) = A\bar{x}(t) + B\bar{u}(t) \\ \bar{y}(t) = C\bar{x}(t) \end{cases} \tag{4.7}$$

where $\bar{x}(t) = [i_{pv}(t), i_a(t)]^T$, $\bar{u}(t) = [u_a(t), u_{pv}(t)]^T$, $y(t) = i_L(t)$. $i_{pv}(t)$ and $i_a(t)$ are the current of PV and utility source, respectively; $u_{pv}(t)$ and $u_a(t)$ is the input voltage of PV system and utility source, and the $i_L(t)$ is the output current to node. And

$$A = \begin{bmatrix} -\frac{l_a R + r_{pv} L + r_{pv} l_a}{l_{pv} L + l_a L + l_{pv} l_a} & \frac{r_a L - l_a R}{l_{pv} L + l_a L + l_{pv} l_a} \\ \frac{r_{pv} L - l_p vR}{l_{pv} L + l_a L + l_{pv} l_a} & -\frac{l_{pv} R + l_{pv} r_a + r_a L}{l_{pv} L + l_a L + l_{pv} l_a} \end{bmatrix}, \quad B = \begin{bmatrix} \frac{L + l_a}{l_{pv} L + l_a L + l_{pv} l_a} & \frac{-L}{l_{pv} L + l_a L + l_{pv} l_a} \\ \frac{-L}{l_{pv} L + l_a L + l_{pv} l_a} & \frac{L + l_{pv}}{l_{pv} L + l_a L + l_{pv} l_a} \end{bmatrix} \quad C = [1 \ 1] \tag{4.8}$$

where the parameters is the same with equation (4.4).

4.4 Eliminate the Impacts of PV Generation

In this research, the fault diagnosis objective is the load node. According to the fault diagnosis method based on EID approach in chapter 3, the EID of load should be obtained at first. Due to the PV system installing, the situation changed.

4.4.1 Impacts of PV Disturbances on Fault Diagnosis

As mentioned in the chapter 3, the system of the feeder with disturbance is given by

$$\begin{cases} \dot{x}(t) = Ax(t) + Bu(t) + B_d d(t) \\ y(t) = Cx(t) \end{cases}. \tag{4.9}$$

1) If the PV system is regarded as *PV-specified* node, $d(t)$ consists of two parts: the

disturbance of load variation and disturbance caused by PV output fluctuation, as shown in (4.8).

$$d(t) = d_L(t) + d_{pv}(t)\,. \tag{4.10}$$

Where, $d_L(t)$ is the load disturbance and $d_{pv}(t)$ is the PV disturbance, which are explained as following.

a). The load *disturbance*, $d_L(t)$.

The load disturbance is caused by the power consumers. The disturbance of load, $d_L(t)$, can be divided into two portions (4.9): normal disturbance and fault disturbance.

$$d_L(t) = d_{Lf}(t) + d_{Ln}(t)\,. \tag{4.11}$$

Where, $d_{Ln}(t)$ is fault disturbance, and $d_{Lf}(t)$ is normal disturbance.

For an actual power system, the power consumption of a node always changed. Therefore, we regard the disturbance caused by the variation of power consumption as parameter disturbances, which is normal disturbance. If a fault occurs, the system will suffer from a sharply variation and a large disturbance would be generated to the system. The method, how to distinguish the normal disturbance and fault disturbance, was proposed at chapter 3.

b) $d_{pv}(t)$ is PV disturbance.

The output power of PV systems is not stable and changed with the weather and irradiation. The variation of PV output will lead to the disturbance to the utility network, and we call it PV disturbance. We should note that, the PV disturbance is not a fault to the system, but it will result in a serious impact on the fault diagnosis based on EID approach. For a feeder with PV system installed:

(1) If the PV output is stable and unchanged, the PV disturbance is small and almost to zero. The disturbance of system, $d(t)$, is approximate to $d_L(t)$. Therefore, the EID of $d(t)$, $d_e(t)$, estimated by EID approach can applied to distinguish the fault.

(2) If the PV output varied frequently, the PV disturbance can not be ignored even very large, and cause the $d(t)$ become large, too. Although the fault do not occurred to the system, as the $d(t)$ is too large to below the allowable range of system, the diagnosis result would be mistake.

Therefore, in this situation when PV system embedded, we should eliminate the PV disturbance at first, and then the proposed fault diagnosis method can be applied properly.

2) If the PV system is regarded as *PQ-specified* node, $d(t)$ is the disturbance of load to the

system and can be represented as:

$$d(t) = \left[d_{L\_pv}(t) \;\; d_{L\_a}(t) \right]^T . \tag{4.12}$$

Where, the $d_{L\_pv}(t)$ is the disturbance of load to the PV system and $d_{L\_a}(t)$ is the disturbance of load to the utility source. They can reflect the influence of load to the power supply, according to the definition of EID approach, therefore both of them should be used to diagnose the fault.

4.4.2 Calculate the EID of PV Disturbances

Form the disturbance equation (4.10), the disturbances of PV, $d_{pv}(t)$, need to be separated primarily. We assume that the power consumption of node is not changed, (R, L are constants), then $d_L(t)$. Substituting it into the equation (4.11), yield:

$$d_e(t) = d_{e\_pv}(t). \tag{4.13}$$

Putting (4.13) into (4.9) and applying the EID approach, the estimation of $d_{pv}(t)$, $d_{e\_pv}(t)$ can be calculated.

For the PV generator, the output voltage, u_{pv} strictly keeps the same with the utility voltage, u_a, by a voltage controller, and the output current, i_{pv}, changes with the output power of PV generator. In order to maintain the output voltage stability, the voltage controller will change the value of resistance of PV, r_{pv} with variation of i_{pv}. Under this situation, the parameter fluctuation of PV, r_{pv}, will bring disturbances to the system. However, the r_{pv} can not be measured directly and the i_{pv} will be measured instead. We use the measurable i_{pv} to evaluate the parameter r_{pv}.

From the system (4.9), yield the equation (4.14):

$$r_{pv}(t) = \frac{l_a \cdot \dot{i}_a(t) + r_a \cdot i_a(t) - l_{pv} \cdot \dot{i}_{pv}(t)}{\dot{i}_{pv}(t)}. \tag{4.14}$$

Discretize it, yield:

$$r_{pv}(k) = \frac{l_a \Delta i_a(k) + r_a i_a(k)}{\Delta i_{pv}(k)} - l_{pv} \tag{4.15}$$

where $\Delta i_a(k) = \dfrac{i_a(k) - i_a(k-1)}{\Delta t}$, $\Delta i_{pv}(k) = \dfrac{i_{pv}(k) - i_{pv}(k-1)}{\Delta t}$ and Δt is the sampling interval time, $\Delta t = t(k) - t(k-1)$.

Until now, the parameter of r_{pv} can be calculated, and substitute it into the EID estimator (4.15), finally, the $d_{e\_pv}(t)$ can be obtained.

4.4.3 Thresholds of EID

For the different dynamic model for a load cluster with PV generation embedded, the thresholds of EID are different.

1) If the dynamic model is the fashion as the model (4.3), two fault detection thresholds for the EID are set.

a) Absolute threshold, $d_{A\_e}(t)$: the smallest EID that indicates a fault;

b) Differential threshold, $d_{D\_e}(t)$: the smallest rate of change for the EID that indicates a fault.

When either $\left|\hat{d}_{e\_L}(t)\right| \geq d_{A\_e}$ or $\left|\dot{\hat{d}}_{e\_L}(t)\right| \geq d_{D\_e}$, a fault is considered to have occurred.

2) If the dynamic model is the fashion as the model (4.7), the dynamic model has two input channel: voltage of PV generation and voltage of utility power. Therefore, the EID estimations also have two dimensions concomitantly. In this situation, the thresholds need two dimensions.

a) Absolute threshold, $\left[d_{A1\_e}\ ,\ d_{A2\_e}\right]^T$: the smallest EID in two input channel. If both $\left|\hat{d}_{e\_L}(t)\right| \geq d_{A1\_e}$ and $\left|\hat{d}_{e\_L}(t)\right| \geq d_{A2\_e}$, the absolute threshold condition is broken.

b) Differential threshold, $\left[d_{D1\_e}\ ,\ d_{D2\_e}\right]^T$: the smallest rate of change of EIDs that indicates a fault. If both $\left|\dot{\hat{d}}_{e\_L}(t)\right| \geq d_{D1\_e}$ and $\left|\dot{\hat{d}}_{e\_L}(t)\right| \geq d_{D2\_e}$, the differential threshold condition are broken.

When either absolute threshold or differential threshold is broken, a fault is considered to have occurred.

4.5 Application to a Test Model

Simulations were carried out in MATLAB Simulink tools to demonstrate the validity of the EID-based Fault diagnosis method.

4.5.1 Data of Test Model

The parameters of system are list in Table 5-1, and the system matrixes of (4.4) were

$$A=\begin{bmatrix}-377.4 & 377.4\\ -1193 & -3297\end{bmatrix},\ B=\begin{bmatrix}0\\ 1349\end{bmatrix},\ C=\begin{bmatrix}1 & 1\end{bmatrix}. \tag{4.16}$$

TABLE 4-2 PARAMETERS OF TEST SYSTEM

Variable	Description	Value
U_a	The utility voltage	110 V
r_a	The resistance of utility line	1 Ω
U_{pv}	The PV output voltage	$=U_a$
r_{pv}	The resistance of PV line	1 Ω
L_{pv}	The inductance of filter	2.65 mH
P_{avg}	The average of *active power*	283 kW
Q_{avg}	The average of *reactive power*	219 kVAR

An optimal observer gain, *K*, was calculated for (4.7) that minimized the performance index:

$$J = \int_0^\infty \left\{ \rho \left[x(t) \right]^T Qx(t) + \left[u(t) \right]^T u(t) \right\} dt. \tag{4.17}$$

Where, $\rho = 2 \times 10^6, Q = \begin{bmatrix} 1 & 0 \\ 0 & 10^2 \end{bmatrix}$. The parameters yielded:

$$K = \left[416, 935 \right]^T. \tag{4.18}$$

4.5.2 Thresholds Setting

Before the fault diagnosis, the suitable thresholds of EIDs must be set at first. The normal load variation was introduced into the simulation, and the EIDs of system and its rate of change are shown in Fig 4-18. It is clear from the figure, the EIDs were consistent in the range of [8 V, -8 V] and the differential of the EIDs were kept in the range of [3000 V/*s*, -3000 V/*s*]. Therefore, the thresholds of EID were set to:

$$d_{A\_e} = 8,\ d_{D\_e} = 3000. \tag{4.19}$$

4.5.3 Components and Structure of Simulations

The simulation architecture of the method was shown in Fig. 4-19. The system includes four function modules,

a) *Fault Disturbance Design (FDD) module*. Generate the normal or fault disturbances and introduce them into the system disturbance estimation module.

b) *System Disturbance Estimation* (*SDE*) *module*. Apply the EID approach, estimate the EIDs

of the system, $d_e(t)$.

c) *PV Resistance Evaluation (PVRE) module*. According to the measurement of PV output current, i_{pv}, evaluate the equivalent resistance of transmission line from PV generator to load node, r_{pv}.

d) *PV Disturbance Estimation (PVDE) module*. Estimate the EIDs of PV generator by EID approach, d_{epv}(t).

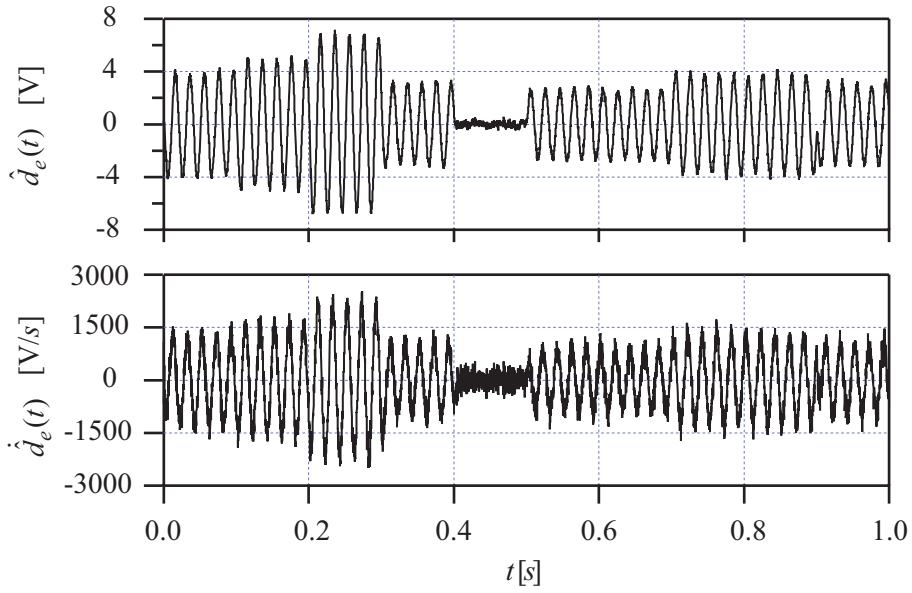

Fig. 4-18 EID estimates of system, $\hat{d}_e(t)$, $\dot{\hat{d}}_e(t)$, while the load varied in normal. To simulate easily, the simulation time shorten to 1s proportionally.

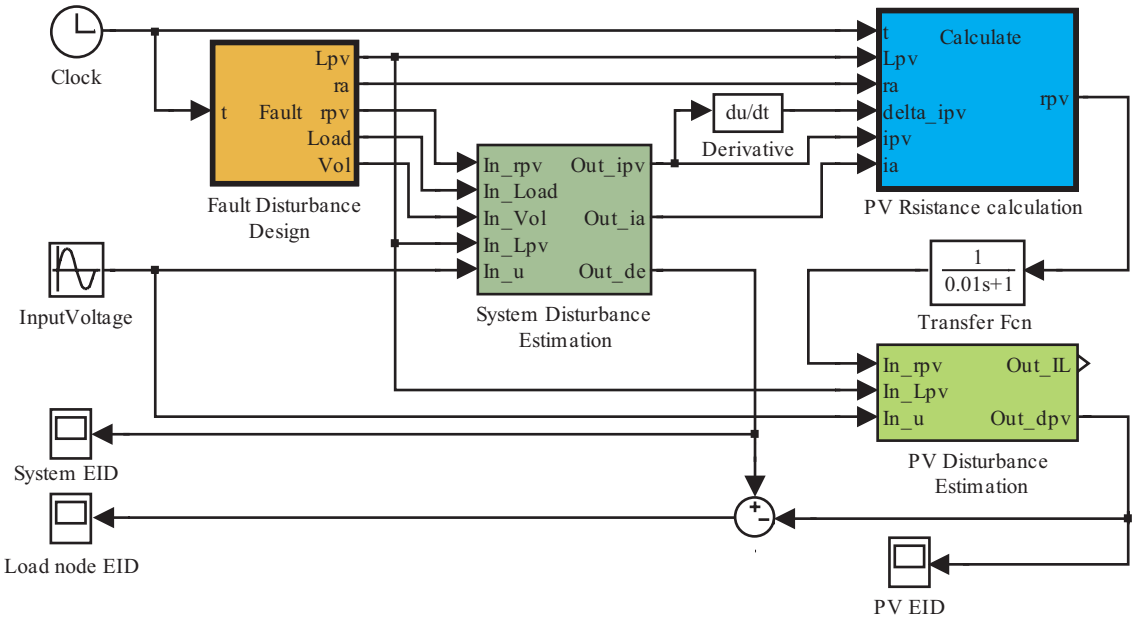

Fig. 4-19 Simulation structure of fault diagnosis method based on EID approach.

4.5.4 Simulation Results

In this study, we concern the short circuit fault occurs at the load node. From the viewpoint of power supply, the short circuit fault at the node causes an instantaneous load increasing quickly. As shown in Fig. 4-20, there is a sharp increment at 0.3 *s*. This kind of fault disturbance combined with the normal disturbances was added to the FDD module to test whether our method can identify the fault successfully, and to verify whether our method can eliminate the parameters influence of the PV generator. Simulations were divided into the following two scenarios.

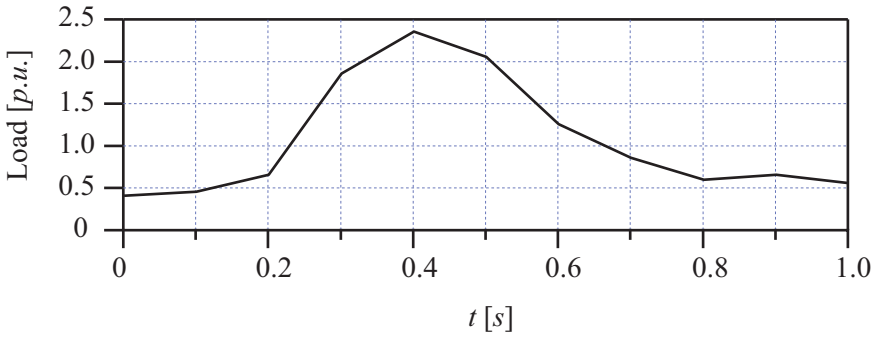

Fig. 4-20 Load parameter variations when the short circuit fault occurs.

a) Simulations for Invariable r_{pv}

We assumed that the PV output current was stable and the resistance, r_{pv}, is a constant. Applying the EID approach yielded the EID of system, $\hat{d}_e(t)$, and its differential, $\dot{\hat{d}}_e(t)$ (Fig. 4-21).

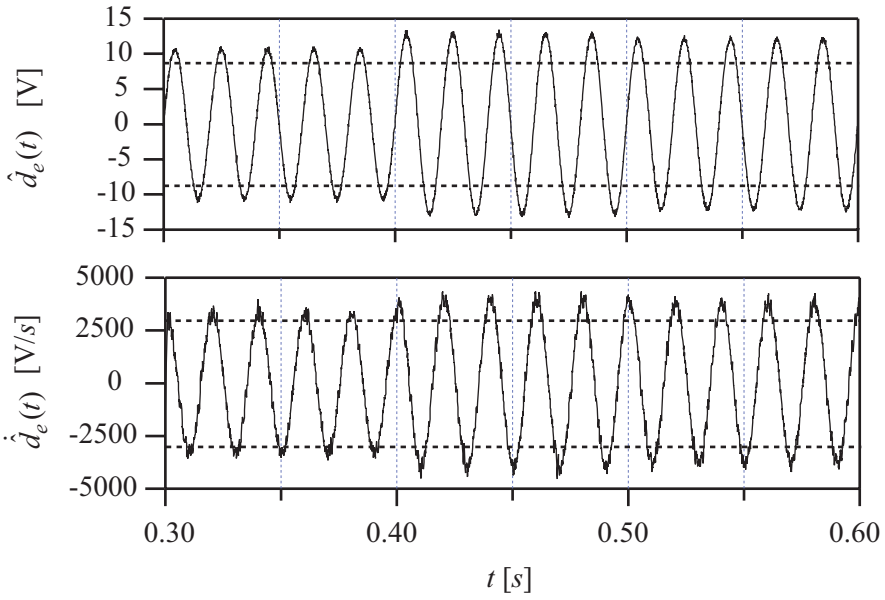

Fig. 4-21 EID estimates of system, $\hat{d}_e(t)$, $\dot{\hat{d}}_e(t)$, while the PV output is stable.

It is clear from the Fig. 4-21, both the value of $\hat{d}_e(t)$ and $\dot{\hat{d}}_e(t)$ exceeded the absolute and differential thresholds during the periods [0.3 *s*, 0.6 *s*]. These mean that a fault occurred during that time. The diagnosis results were consistent with the fault disturbance designed previously. Meanwhile, the EID of PV is nearly equal to 0 (Fig. 4-22). Therefore, the influence of PV can be ignored for fault diagnosis.

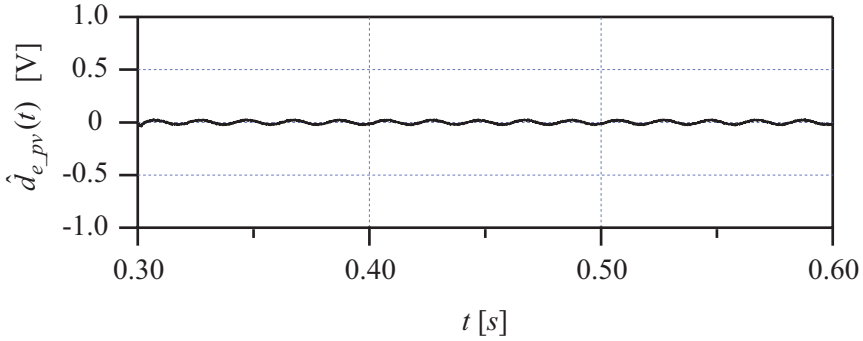

Fig. 4-22 EID estimates of PV generator, $\hat{d}_{pv}(t)$, while the PV output is stable.

b) Simulations for variable r_{pv}

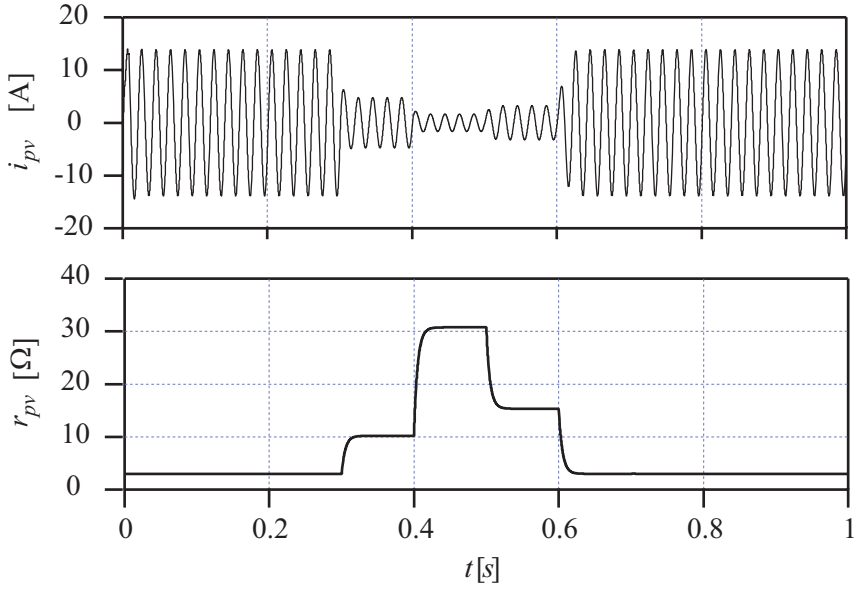

Fig. 4-23 PV variation, i_{pv} and r_{pv}.

The influence of PV fluctuation was considered in this scenario. Fig. 4-23 shows the variation of PV output current, i_{pv}, and the equivalent resistance, r_{pv}. i_{pv} decreased during the periods [0.3 *s*, 0.6 *s*] and at the same time, r_{pv} increased to keep the PV output voltage stable.

In this situation, both the EID, $\hat{d}_e(t)$, and its differential, $\dot{\hat{d}}_e(t)$, (Fig. 4-24) reduced, and returned to the allowable range. So, we may not find a correct result if the EID is used to diagnose the faults. Fig. 4-25 shows the EID of the PV generator. Clearly, the big fluctuation of

the PV parameters during the periods [0.3 *s*, 0.6 *s*] produced a large EID, $\dot{\hat{d}}_e(t)$, and it mixes with EID of load node, $\hat{d}_{e\_L}(t)$ (4.8), so that the EID, $\hat{d}_e(t)$, reduced. Therefore, in this situation, the EID of the load node should be used to diagnose the fault instead.

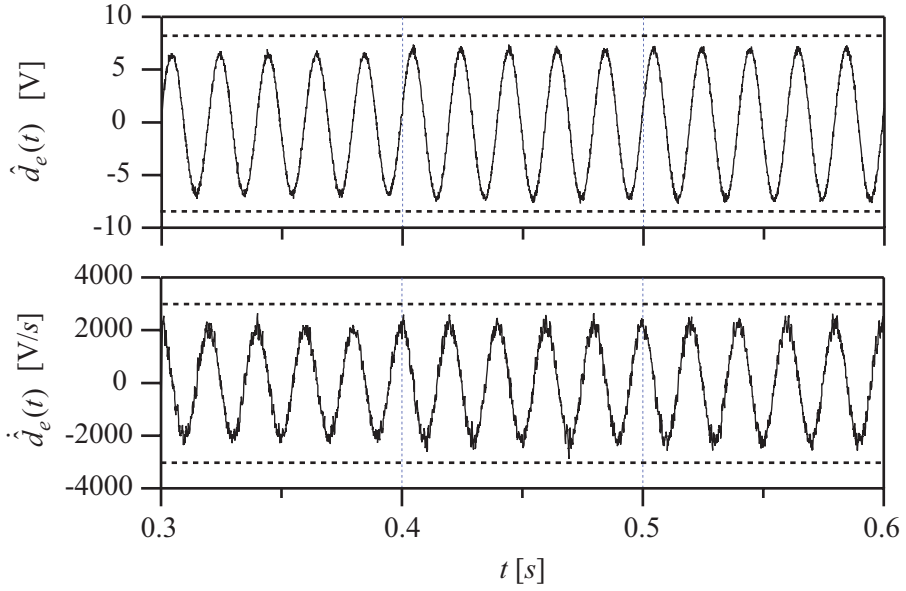

Fig. 4-24 EIDs estimates of system, $\hat{d}_e(t)$, $\dot{\hat{d}}_e(t)$, while the PV output is variable.

According to equation (4.9), we calculated the EID of the load node, $\hat{d}_{e\_L}(t)$, which represents the disturbance only from the load node and eliminates the influence of the PV generator. Fig. 4-26 shows that, during the periods [0.3 *s*, 0.6 *s*], $\hat{d}_{e\_L}(t)$ and $\dot{\hat{d}}_{e\_L}(t)$ was out of the allowable range. This gives the correct diagnosis results.

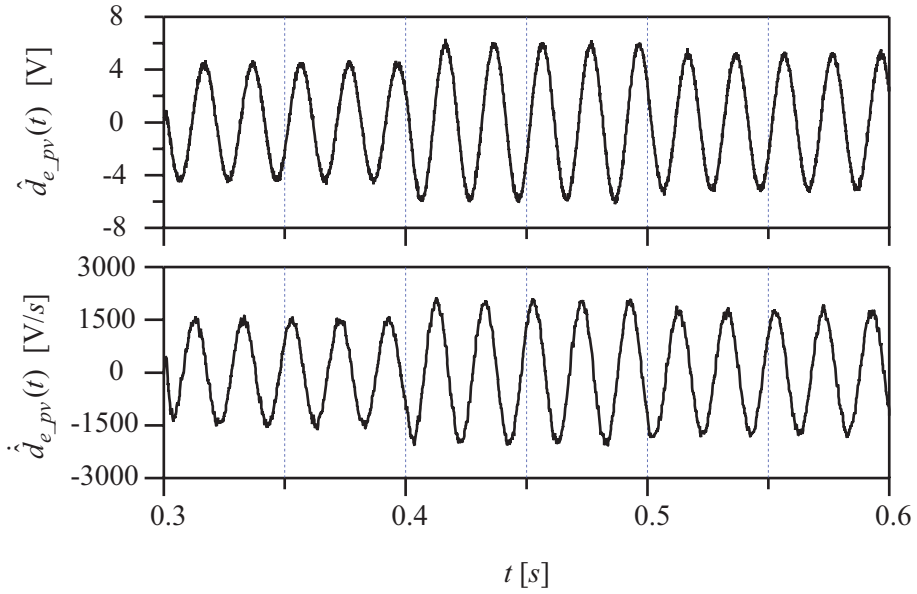

Fig. 4-25 EIDs estimates of PV $\hat{d}_{e\_pv}(t)$, $\dot{\hat{d}}_{e\_pv}(t)$, while the PV output is variable.

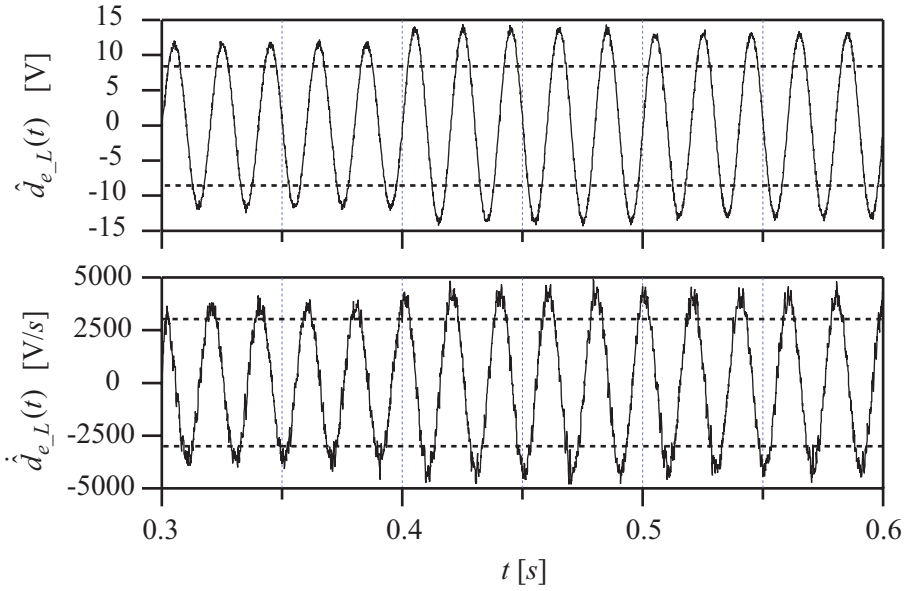

Fig. 4-26 EIDs estimates of load node, $\hat{d}_{e\_L}(t)$, $\dot{\hat{d}}_{e\_L}(t)$, *while the PV output is variable.*

From $\hat{d}_e(t)$ at the first scenario and $\hat{d}_{e\_L}(t)$ at the second scenario, we calculated the error, $\Delta d(t) = d_e(t) - d_{e\_L}(t)$ (Fig. 4-27). It is clear from the figure that the error is small. It means that the influence of the fluctuation of the PV parameters to the fault diagnosis was eliminated almost completely.

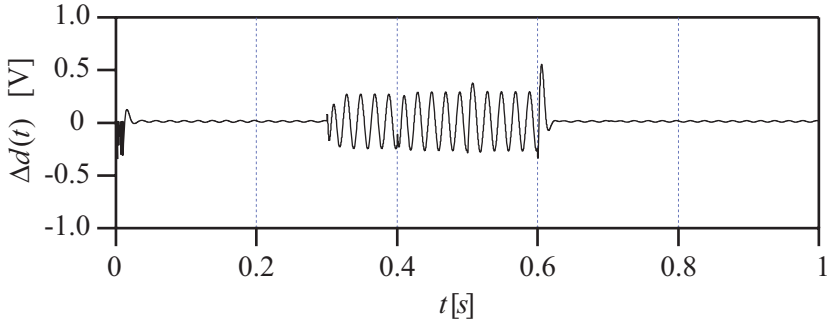

Fig. 4-27 Errors of EID estimates between $d_e(t)$ *of scenario* 1) *and* $d_{e\_L}(t)$ *at the second scenario* 2).

4.6 Conclusion

In this chapter, a new fault diagnosis method based on EID approach for a load cluster with PV system embedded was describes. With the PV systems installed in the distribution network as distributed generators, many new problems, such as fluctuation of PV output and malfunction of relays caused by PV power injected, appears to the conventional fault diagnosis method. Firstly, based on the PV output power data collected from the PV systems installed at Honjo campus of Waseda University, the impact of PV system on the distribution network such as the voltage profile improving, electrical losses, and reverse power were analyzed. Secondly, the fault diagnosis method based on

EID approach for the load cluster with PV system connected was proposed. The fluctuation of PV output lead to the disturbance to the utility grid and this disturbance mixed with the fault signal, which brings a negative impact on the fault diagnosis method based on EID approach. To eliminate the PV influence, a PV output disturbance estimator was designed. By measuring the PV system output current and make it as an input to the PV output disturbance estimator, the disturbance of PV can be calculated and the fault signal was abstracted successfully.

Simulation results on the test model demonstrate the validity of the method. The results show that the influence of PV system was eliminated, and the fault is correctly identified successfully using the EID of load. Comparing with other methods, our method does not need to install any new device or modify the setting of existing device. It can save the cost for power grid upgrade when installing a large scale of grid-connected PV systems.

Chapter References

[4-1] **S.A.M. Javadian, M.R. Haghifam.** *Implementation of a New Protection Scheme on a Real Distribution System in Presence of DG*. POWERCON 2008, Oct. 2008.

[4-2] **N. Jenkins et al.** *Embedded generation*. IEE, 2000. ISBN 0-85296-774-8.

[4-3] **C. Nattapong, K. Krissanapong, M. Veerapol, J. Chiya, C. Dhirayut.** *DC–AC switching converter modelings of a PV grid-connected system under islanding phenomena*. Renewable Energy, vol. 34 pp. 536–2544, 2009.

[4-4] **W. Yang, X. Zhou, Feng X..** *Impacts of Large Scale and High Voltage Level Photovoltaic Penetration on the Security and Stability of Power System.* Power and Energy Engineering Conference (APPEEC), pp.1-5, Apr. 2010.

[4-5] **M. E. Baran, H. Hooshyar, Z. Shen and A. Huang.** *Accommodating High PV Penetration on Distribution Feeders.* IEEE Trans. smart grid. vol. 3, no. 2, pp. 1039-1046, Jun. 2012.

Chapter 5
EID-based HFD Method Applied to the IEEE 37 Nodes Test Feeder

5.1 Chapter Introduction

The hierarchical fault diagnosis method based on EID approach has been described detailedly in the former chapters. In the chapter 2, the construction method of HFD model was proposed. The HFD model was divided into multiple load clusters and multiple layers. The fault diagnosis could be carried out from the top down through the layers of the HFD model to gradually locate a fault. In our method, the load cluster is the basic unit for fault diagnosis and the fault could be located at node number finally. In the chapter 3, the fault diagnosis method based on EID was explained. This method was used to diagnose the fault of the load cluster. In order to eliminate the influence of PV system to our fault diagnosis method, a fault signal was abstracted from the EID by removing the fluctuation caused by the PV system, in chapter 4.

In this chapter, in order to make the procedure of HFD Method easy to understand and demonstrate our method is effective and valid, the IEEE 37 nodes test feeder model [5-1] is used as an example. The structure of this chapter is planned as follows:

Section 5.2: The IEEE 37 nodes test feeder model structure and data is given out.

Section 5.3: The HFD model structure, the model parameter and dynamics for each load cluster are given out.

Section 5.4: Procedures of fault diagnosis method for the IEEE 37 nodes test feeder model are explained. The simulation and results are discussed.

5.2 Data of IEEE-37 Feeder

The IEEE 37 nodes test feeder model is an actual feeder located in California [5-1]- [5-3]. In this feeder, all the loads are spot load and consisting of constant *PQ*, constant current and constant impedance. The feeder contains two transformers and the data are shown in Table 5-1. In this feeder, Node 799 is the power substation, and the other nodes are loads. A step-down transformer connects the substation to each load, and another transformer is used between Nodes 709 and 755. The transformer between Nodes 709 and 755 is considered to be a simple gain factor to simplify modeling and is ignored in the analysis of fault diagnosis. The output voltages from the transformer are balanced three-phase of 1.03 per unit.

TABLE 5-1 TRANSFORMER DATA OF IEEE-37 FEEDER

	kVA	kV-high	kV-low	R - %	X - %
Substation:	2,500	230 D	4.8 D	2	8
XFM -1	500	4.8 D	0.480 D	0.09	1.81

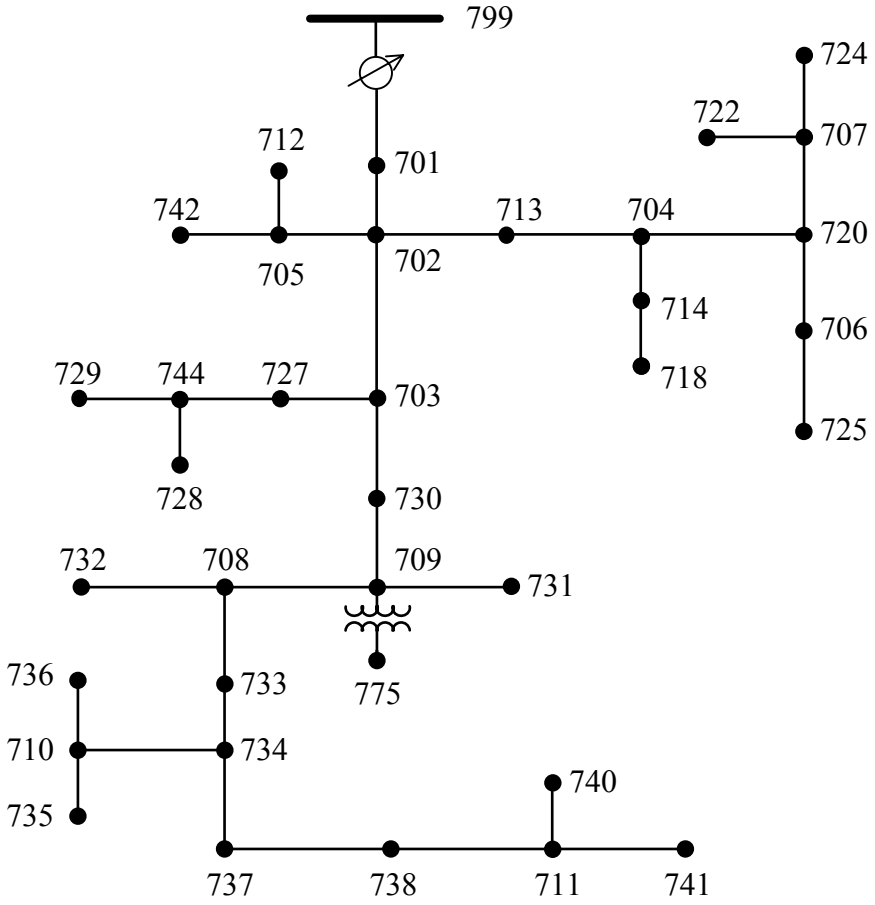

Fig. 5-1 IEEE 37 Nodes test feeder (IEEE-37 feeder).

Table 5-2 gives the Line Section Data for this system.

TABLE 5-2 LINE SECTION DATA OF IEEE-37 FEEDER

Node A	Node B	Length(ft.)	Config.
701	702	960	722
702	705	400	724
702	713	360	723
702	703	1320	722
703	727	240	724
703	730	600	723

704	714	80	724
704	720	800	723
705	742	320	724
705	712	240	724
706	725	280	724
707	724	760	724
707	722	120	724
708	733	320	723
708	732	320	724
709	731	600	723
709	708	320	723
710	735	200	724
710	736	1280	724
711	741	400	723
711	740	200	724
713	704	520	723
714	718	520	724
720	707	920	724
720	706	600	723
727	744	280	723
730	709	200	723
733	734	560	723
734	737	640	723
734	710	520	724
737	738	400	723
738	711	400	723
744	728	200	724
744	729	280	724
775	709	0	XFM-1
799	701	1850	721

Table 5-3 gives the Overhead Line configuration codes for this system.

TABLE 5-3 OVERHEAD LINE CONFIGURATIONS OF IEEE-37 FEEDER

Configuration.	Phasing	Cable	Spacing ID
721	A B C	1,000,000 AA, CN	515
722	A B C	500,000 AA, CN	515
723	A B C	2/0 AA, CN	510
724	A B C	#2 AA, CN	510

Table 5-4 gives the Bus Load Data of the system.

TABLE 5-4 BUS LOAD DATA OF IEEE-37 FEEDER

Node	Load	Ph-1	Ph-1	Ph-2	Ph-2	Ph-3	Ph-4
	Model	kW	kVAr	kW	kVAr	kW	kVAr
701	D-PQ	140	70	140	70	350	175
712	D-PQ	0	0	0	0	85	40
713	D-PQ	0	0	0	0	85	40
714	D-I	17	8	21	10	0	0
718	D-Z	85	40	0	0	0	0
720	D-PQ	0	0	0	0	85	40
722	D-I	0	0	140	70	21	10
724	D-Z	0	0	42	21	0	0
725	D-PQ	0	0	42	21	0	0
727	D-PQ	0	0	0	0	42	21
728	D-PQ	42	21	42	21	42	21
729	D-I	42	21	0	0	0	0
730	D-Z	0	0	0	0	85	40
731	D-Z	0	0	85	40	0	0
732	D-PQ	0	0	0	0	42	21
733	D-I	85	40	0	0	0	0
734	D-PQ	0	0	0	0	42	21
735	D-PQ	0	0	0	0	85	40
736	D-Z	0	0	42	21	0	0
737	D-I	140	70	0	0	0	0
738	D-PQ	126	62	0	0	0	0
740	D-PQ	0	0	0	0	85	40
741	D-I	0	0	0	0	42	21
742	D-Z	8	4	85	40	0	0
744	D-PQ	42	21	0	0	0	0
Total		727	357	639	314	1091	530

In this feeder, we assume that some PV systems are embedded into the feeder. The information of PV systems is shown in the Table 5-5.

TABLE 5-5 DATA OF PV GENERATION

PV number	Location node	Load of the nodes [kW] + *j* [kVAR]	PV capacities, [kW]+ *j* [kVAR]	PV operation model	Specified voltage
PV 1	741	42+ *j* 21	21+*j*10.5	*PQ-specified*	/
PV 2	735	85+ *j* 40	43+*j*20	*PQ-specified*	/
PV 3	732	42+ *j* 21	21+*j*0	*PQ-specified*	/
PV 4	725	42+ *j* 21	42+*j*10	*PQ-specified*	/

PV 5	728	126+ *j* 63	63+*j*0	*PV-specified*	0.95 p.u.
PV 6	742	85+ *j* 40	42.5+*j*0	*PV-specified*	0.95 p.u.

5.3 HFD Method for IEEE-37 Feeder

In this section, the HFD model and the procedures of HFD algorithm are given out.

5.3.1 HFD Model

Applied the construct method of HFD model, the hierarchical model of IEEE 37 nodes test feeder is given out in Table 5-6.

TABLE 5-6 HIERARCHICAL STRUCTURE OF IEEE-37 FEEDER

Layer 0			
$\mathcal{C}^{(0)}$	$\Rightarrow$	Whole network	Node *i*, $i \in \Phi$.
Layer 1			
$\mathcal{C}^{(0)}$	$\Rightarrow$	$\mathcal{C}_s^{(1)}$:	Root node (Node 799, which is the substation).
		$\mathcal{C}_1^{(1)}$:	Node 701.
		$\mathcal{C}_2^{(1)}$:	Node *i*, $i \in \Phi \backslash \{701, 799\}$.
Layer 2			
$\mathcal{C}_2^{(1)}$	$\Rightarrow$	$\mathcal{C}_{2-1}^{(2)}$:	Node 702.
		$\mathcal{C}_{2-2}^{(2)}$:	Nodes 705, 712 and 742.
		$\mathcal{C}_{2-3}^{(2)}$:	Node *i*, $i \in \Phi_1$.
		$\mathcal{C}_{2-4}^{(2)}$:	Node *i*, $i \in \Phi_2$.
Layer 3			
$\mathcal{C}_{2-2}^{(2)}$	$\Rightarrow$	$\mathcal{C}_{2-2-1}^{(3)}$:	Node 705.
		$\mathcal{C}_{2-2-2}^{(3)}$:	Node 712.
		$\mathcal{C}_{2-2-3}^{(3)}$	Node 742.
$\mathcal{C}_{2-3}^{(2)}$	$\Rightarrow$	$\mathcal{C}_{2-3-1}^{(3)}$:	Node 703.
		$\mathcal{C}_{2-3-2}^{(3)}$:	Nodes 727, 728, 729 and 744.
		$\mathcal{C}_{2-3-3}^{(3)}$:	Node *i*, $i \in \Phi_3$.
$\mathcal{C}_{2-4}^{(2)}$	$\Rightarrow$	$\mathcal{C}_{2-4-1}^{(3)}$:	Node 713.
		$\mathcal{C}_{2-4-2}^{(3)}$:	Node 704.
		$\mathcal{C}_{2-4-3}^{(3)}$:	Node 714 and 718.
		$\mathcal{C}_{2-4-4}^{(3)}$:	Node 706, 707, 720, 722, 724 and 725.
Layer 4			
$\mathcal{C}_{2-3-2}^{(3)}$	$\Rightarrow$	$\mathcal{C}_{2-3-2-1}^{(4)}$:	Node 727.
		$\mathcal{C}_{2-3-2-2}^{(4)}$:	Node 744, 728 and 729.
$\mathcal{C}_{2-3-3}^{(3)}$	$\Rightarrow$	$\mathcal{C}_{2-3-3-1}^{(4)}$	Node 730.
		$\mathcal{C}_{2-3-3-2}^{(4)}$	Node 709.
		$\mathcal{C}_{2-3-3-3}^{(4)}$	Node *i*, $i \in \Phi_4$.

		$\mathcal{C}^{(4)}_{2-3-3-4}$	Node 775.
		$\mathcal{C}^{(4)}_{2-3-3-5}$	Node 731.
$\mathcal{C}^{(3)}_{2-4-3}$	$\Rightarrow$	$\mathcal{C}^{(4)}_{2-4-3-1}$:	Node 714.
		$\mathcal{C}^{(4)}_{2-4-3-2}$:	Node 718.
$\mathcal{C}^{(3)}_{2-4-4}$	$\Rightarrow$	$\mathcal{C}^{(4)}_{2-4-4-1}$:	Node 720.
		$\mathcal{C}^{(4)}_{2-4-4-2}$:	Node 707, 722 and 724.
		$\mathcal{C}^{(4)}_{2-4-4-3}$:	Node 706 and 725.
Layer 5			
$\mathcal{C}^{(4)}_{2-3-2-2}$	$\Rightarrow$	$\mathcal{C}^{(5)}_{23221}$:	Node 744.
		$\mathcal{C}^{(5)}_{23222}$:	Node 728.
		$\mathcal{C}^{(5)}_{23223}$:	Node 729.
$\mathcal{C}^{(4)}_{2-3-3-3}$	$\Rightarrow$	$\mathcal{C}^{(5)}_{23331}$:	Node 708.
		$\mathcal{C}^{(5)}_{23332}$:	Node 732.
		$\mathcal{C}^{(5)}_{23333}$:	Node i, $i \in \Phi_5$.
$\mathcal{C}^{(4)}_{2-4-4-2}$	$\Rightarrow$	$\mathcal{C}^{(5)}_{24421}$:	Node 707.
		$\mathcal{C}^{(5)}_{24422}$:	Node 722.
		$\mathcal{C}^{(5)}_{24423}$:	Node 724.
$\mathcal{C}^{(4)}_{2-4-4-3}$	$\Rightarrow$	$\mathcal{C}^{(5)}_{24431}$:	Node 706.
		$\mathcal{C}^{(5)}_{24432}$:	Node 725.
Layer 6			
$\mathcal{C}^{(5)}_{23333}$	$\Rightarrow$	$\mathcal{C}^{(6)}_{233331}$:	Node 733.
		$\mathcal{C}^{(6)}_{233332}$:	Node 734.
		$\mathcal{C}^{(6)}_{233333}$:	Node 710, 735 and 736.
		$\mathcal{C}^{(6)}_{233334}$:	Node 737, 738, 711, 740 and 741.
Layer 7			
$\mathcal{C}^{(6)}_{233333}$	$\Rightarrow$	$\mathcal{C}^{(7)}_{2333331}$:	Node 710.
		$\mathcal{C}^{(7)}_{2333332}$:	Node 735.
		$\mathcal{C}^{(7)}_{2333333}$:	Node 736.
$\mathcal{C}^{(6)}_{233334}$	$\Rightarrow$	$\mathcal{C}^{(7)}_{2333341}$:	Node 737.
		$\mathcal{C}^{(7)}_{2333342}$:	Node 738.
		$\mathcal{C}^{(7)}_{2333343}$:	Node 736.
		$\mathcal{C}^{(7)}_{2333344}$:	Node 711.
		$\mathcal{C}^{(7)}_{2333345}$:	Node 741.

Where $\Phi = \{799, 701, 702, 705, 712, 742\} \bigcup \Phi_2 \bigcup \Phi_1$ is the set of all the nodes in the feeder and $n_\Phi = 37$. Φ_1, Φ_2, Φ_3, Φ_4, Φ_5 is the subset of the nodes.

$$\Phi_1 = \{703, 727, 744, 728, 729\} \bigcup \Phi_3 , \quad n_{\Phi_1} = 21$$

$$\Phi_2 = \{713, 704, 714, 718, 706, 707, 720, 722, 724, 725\} , \quad n_{\Phi_2} = 10$$

$$\Phi_3 = \{730, 709, 775, 731\} \bigcup \Phi_4 , \quad n_{\Phi_3} = 16$$

$$\Phi_4 = \{708, 732\} \bigcup \Phi_5 , \quad n_{\Phi_4} = 12$$

$$\Phi_5 = \{733, 734, (710, 735, 736), (737, 738, 711, 740, 741)\} , \quad n_{\Phi_5} = 10 .$$

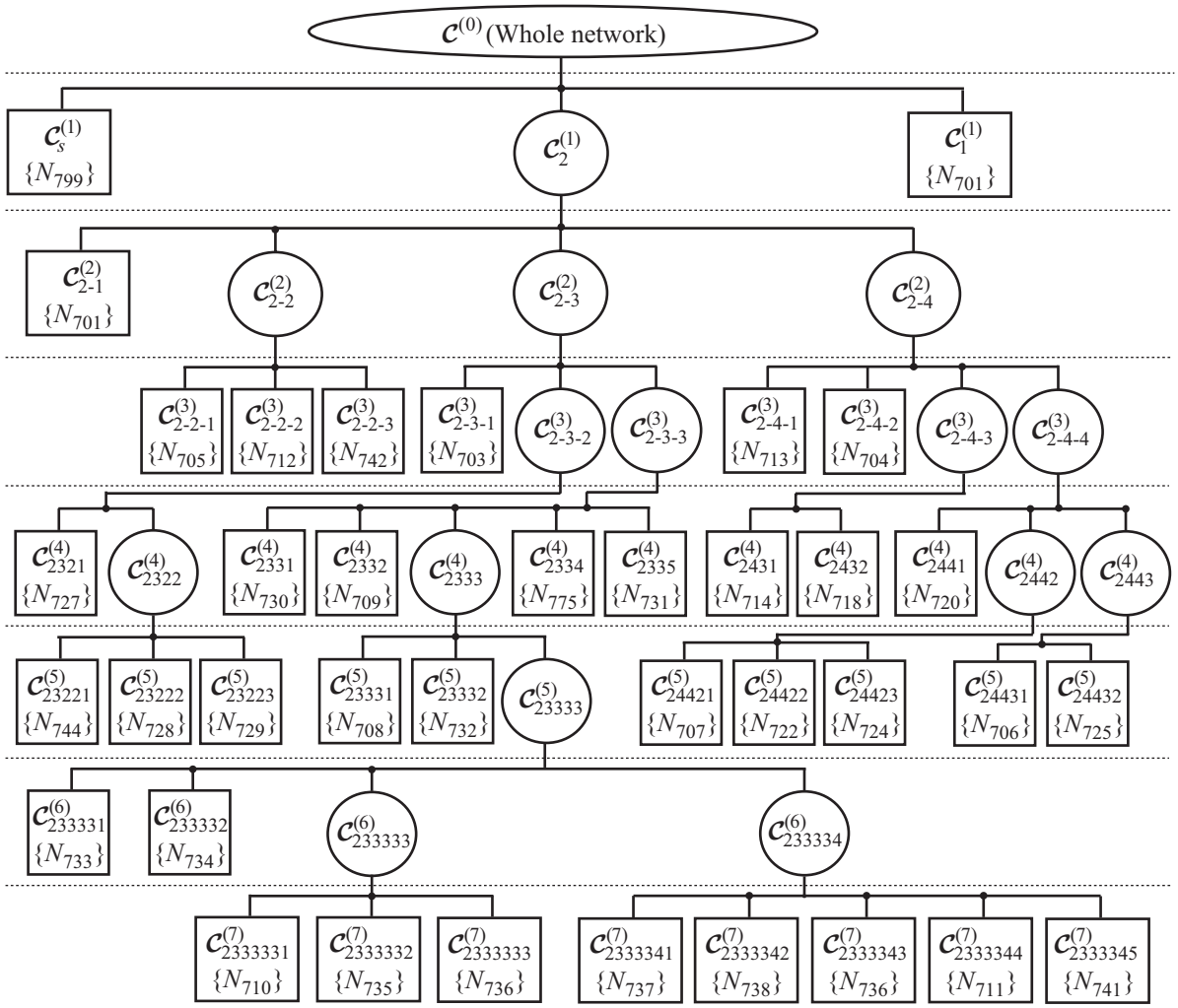

Fig. 5-2 Hierarchical structure of IEEE 37 nodes test feeder

Then the hierarchical structure of IEEE 37 nodes test feeder was constructed in Fig. 5-2. The hierarchical model contains 7 layers and each layer was divided into several load clusters, for example, there are 3 load clusters in layer 1 and 8 load clusters in layer 7. In the figure, there are two type of load cluster: square and circle. The squares type indicates single-node clusters, like the cluster $\mathcal{C}_{2-1}^{(2)}$, which can not be subdivided in the next layer. The circles type indicates

multi-node clusters, like the cluster $\mathcal{C}_2^{(1)}$, which can be subdivided in the next layer. The fault diagnosis will be located at the square type load cluster finally. The bottom of hierarchical model only contains square clusters.

Apply the aforementioned dynamic model calculation method in Chapter 2, all the dynamic models for the load cluster in IEEE-37 feeder are shown in Table 5-7.

TABLE 5-7 DYNAMIC MODEL OF LOAD CLUSTERS FOR IEEE-37 FEEDER

Dynamic model of load cluster	Matrix A	Matrix B	Matrix C	Matrix D
$\mathcal{C}_1^{(1)}$	-603.782	27.114	0.847	0.948
$\mathcal{C}_2^{(1)}$	-579.788	72.781	0.802	0.862
$\mathcal{C}_{2-1}^{(2)}$	-509.487	1.652	0.668	0.997
$\mathcal{C}_{2-2}^{(2)}$	-657.436	8.240	0.949	0.984
$\mathcal{C}_{2-3}^{(2)}$	-624.228	29.663	0.886	0.944
$\mathcal{C}_{2-4}^{(2)}$	-622.655	34.512	0.883	0.934
$\mathcal{C}_{2-2-1}^{(3)}$	-872.421	16.053	1.358	0.970
$\mathcal{C}_{2-2-2}^{(3)}$	-902.217	15.336	1.414	0.971
$\mathcal{C}_{2-2-3}^{(3)}$	-659.520	4.330	0.953	0.992
$\mathcal{C}_{2-3-1}^{(3)}$	-630.965	11.021	0.899	0.979
$\mathcal{C}_{2-3-2}^{(3)}$	-618.004	11.192	0.874	0.979
$\mathcal{C}_{2-3-3}^{(3)}$	-652.206	15.545	0.939	0.970
$\mathcal{C}_{2-4-1}^{(3)}$	-487.496	4.950	0.626	0.991
$\mathcal{C}_{2-4-2}^{(3)}$	-512.689	4.658	0.674	0.991
$\mathcal{C}_{2-4-3}^{(3)}$	-660.372	5.724	0.955	0.989
$\mathcal{C}_{2-4-4}^{(3)}$	-628.086	22.168	0.893	0.958
$\mathcal{C}_{2-3-2-1}^{(4)}$	-626.304	1.899	0.890	0.996
$\mathcal{C}_{2-3-2-2}^{(4)}$	-619.640	9.359	0.877	0.982
$\mathcal{C}_{2-3-3-1}^{(4)}$	-546.236	4.387	0.738	0.992
$\mathcal{C}_{2-3-3-2}^{(4)}$	-859.870	10.900	1.334	0.979
$\mathcal{C}_{2-3-3-3}^{(4)}$	-613.942	36.954	0.866	0.930
$\mathcal{C}_{2-3-3-4}^{(4)}$	-1413.470	15.769	2.386	0.970

$\mathcal{C}^{(4)}_{2-3-3-5}$	-1267.671	12.762	2.109	0.976
$\mathcal{C}^{(4)}_{2-4-3-1}$	-661.184	1.777	0.956	0.997
$\mathcal{C}^{(4)}_{2-4-3-2}$	-1119.493	10.070	1.827	0.981
$\mathcal{C}^{(4)}_{2-4-4-1}$	-969.202	7.702	1.541	0.985
$\mathcal{C}^{(4)}_{2-4-4-2}$	-629.501	12.911	0.896	0.975
$\mathcal{C}^{(4)}_{2-4-4-3}$	-648.235	5.841	0.932	0.989
$\mathcal{C}^{(5)}_{23221}$	-626.304	1.899	0.890	0.996
$\mathcal{C}^{(5)}_{23222}$	-622.948	5.656	0.884	0.989
$\mathcal{C}^{(5)}_{23223}$	-626.304	1.899	0.890	0.996
$\mathcal{C}^{(5)}_{23331}$	-969.202	7.702	1.541	0.985
$\mathcal{C}^{(5)}_{23332}$	-626.304	1.899	0.890	0.996
$\mathcal{C}^{(5)}_{23333}$	-618.816	28.237	0.876	0.946
$\mathcal{C}^{(5)}_{24421}$	-893.350	6.642	1.397	0.987
$\mathcal{C}^{(5)}_{24422}$	-625.411	7.232	0.888	0.986
$\mathcal{C}^{(5)}_{24423}$	-626.304	1.899	0.890	0.996
$\mathcal{C}^{(5)}_{24431}$	-740.414	4.777	1.107	0.991
$\mathcal{C}^{(5)}_{24432}$	-626.304	1.899	0.890	0.996
$\mathcal{C}^{(6)}_{233331}$	-663.404	3.974	0.960	0.992
$\mathcal{C}^{(6)}_{233332}$	-626.304	1.899	0.890	0.996
$\mathcal{C}^{(6)}_{233333}$	-649.827	9.727	0.935	0.982
$\mathcal{C}^{(6)}_{233334}$	-623.442	17.431	0.885	0.967
$\mathcal{C}^{(7)}_{2333331}$	-663.404	3.974	0.960	0.992
$\mathcal{C}^{(7)}_{2333332}$	-663.404	3.974	0.960	0.992
$\mathcal{C}^{(7)}_{2333333}$	-626.304	1.899	0.890	0.996
$\mathcal{C}^{(7)}_{2333341}$	-622.394	6.277	0.883	0.988
$\mathcal{C}^{(7)}_{2333342}$	-632.919	5.710	0.903	0.989
$\mathcal{C}^{(7)}_{2333343}$	-626.304	1.899	0.890	0.996
$\mathcal{C}^{(7)}_{2333344}$	-663.404	3.974	0.960	0.992
$\mathcal{C}^{(7)}_{2333345}$	-626.304	1.899	0.890	0.996

5.3.2 Procedures of HFD Algorithm

According to the HFD algorithm is described in Chapter 2. The fault diagnosis procedure for the IEEE 37 nodes test feeder is given out. The fault diagnosis starts from the layer 1.

Step 1) Monitor Layer 1 of the hierarchical model by estimating the EID in a real-time fashion. If a fault occurs (that is, if the estimated EID or its rate of change exceeds the threshold), then go to the next step.

Step 2) Go to Layer 2 and estimate the EID for each cluster in this layer to determine which cluster contains the fault ($\mathcal{C}_{2-3}^{(2)}$ in the example). If the cluster containing the fault has only one node, go to Step 7.

Step 3) Go to Layer 3 and estimate the EID for each cluster in this layer to determine which cluster contains the fault ($\mathcal{C}_{2-3-2}^{(3)}$ in the example). If the cluster containing the fault has only one node, go to Step 7.

Step 4) Go to Layer 4 and estimate the EID for each cluster in this layer to determine which cluster contains the fault ($\mathcal{C}_{2-3-2-2}^{(4)}$ in the example). If the cluster containing the fault has only one node, go to Step 7.

Step 5) Go to Layer 5 and estimate the EID for each cluster in this layer to determine which cluster contains the fault ($\mathcal{C}_{23222}^{(5)}$ in the example).

Step 6) Determine the type of fault by analyzing the amplitude and phase of the estimated state of the smallest cluster containing the fault ($\mathcal{C}_{23222}^{(5)}$ in the example), which was produced by the dynamic model.

5.4 Application to IEEE-37 Feeder Model

In this section, we assume the fault nodes and fault type to the feeder model. Apply the HFD method to diagnose the feeder to locate the fault node and detect the fault type according the procedures. Comparing the diagnosis result with the assumption, the effectiveness of our method can be testified.

5.4.1 Design of Fault Disturbances

From the aforementioned fault disturbance design, the fault will cause a remarkable increase in the magnitude of current. Meanwhile, the fault will cause the power factor of the node changing. Generally speaking, the power factor should be in the range [0.86, 1] to guarantee the stability of a power system. That means that the power factor angle,

$\varphi \in [-30^{\circ}, 30^{\circ}]$.

In the simulation, two types of faults (Fig. 5-3) are considered: For one, the amplitude of the load exceeds the maximum; and for the other, both the amplitude and the power factor of the load are outside the allowable range. The two type faults were added to the load cluster $\mathcal{C}^{(4)}_{2-3-4-2}$ and $\mathcal{C}^{(5)}_{23332}$, respectively and testify whether the disturbances caused by the faults can be detected by EID approach.

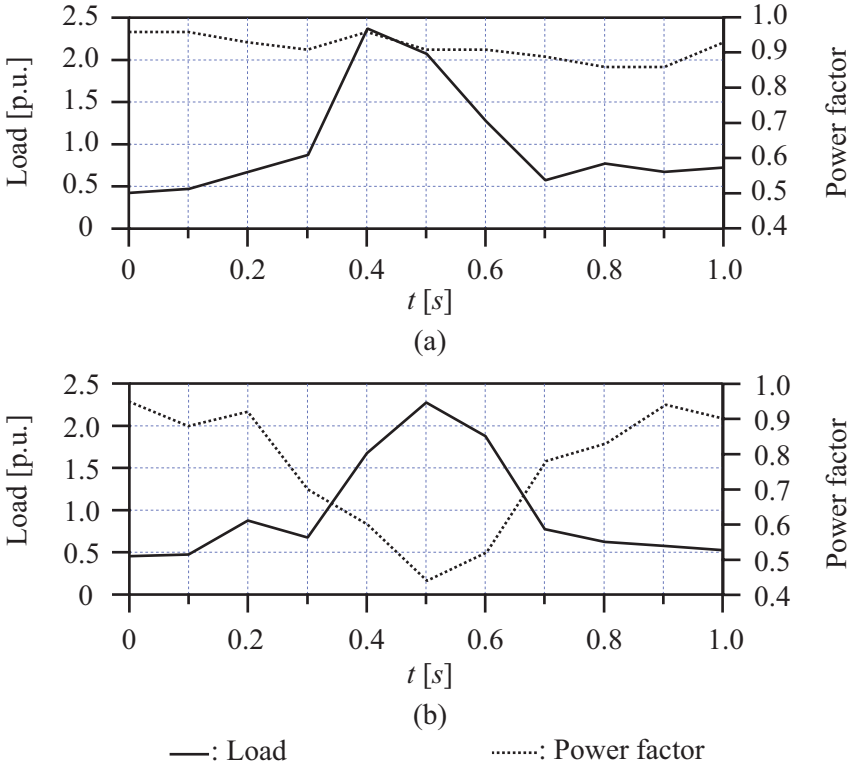

Fig. 5-3 Faults in IEEE-37 feeder: (a) amplitude type and (b) phase type.

5.4.2 Thresholds Setting for All Load Clusters

Simulations were carried out on the IEEE-37 feeder model to illustrate the fault diagnosis procedures of the EID-based HFD method and demonstrate the validity of the method. Measurement noise is a key factor that affects the precision of fault diagnosis in power systems [5-4]. To determine if our method is practical, simulations were carried out with white noise in the measurements, and the signal-noise ratio (SNR) was set to 30 dB.

According to thresholds setting method mentioned in chapter2, the allowable range of load is [S_{L_min}, S_{L_max}], and S_{L_min} = 0.4 *p.u.*, S_{L_max} = 1.2 *p.u.* and S_{L_avg} = 0.75 *p.u.* Then the thresholds for all the load cluster was set to

$$d_{A\_e} = 2500,\ d_{D\_e} = 80000. \tag{5.1}$$

5.4.3 Simulation Results Analysis

Applying the EID approach to Layer 1 yielded an estimate of the disturbance, $\hat{d}_{2e}^{(1)}(t)$ (Fig. 5-4). The value exceeded the absolute threshold during the period $[0.3s, 0.5s]$, which means that a fault occurred during that time.

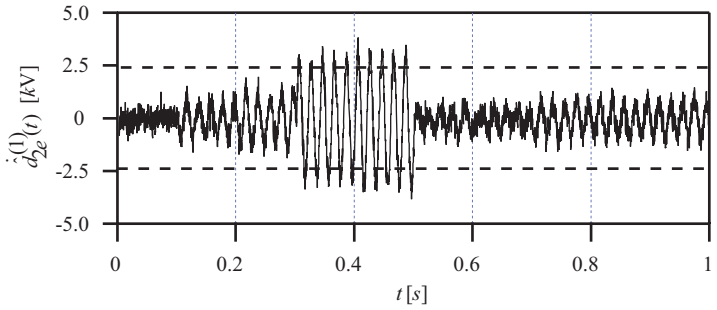

Fig. 5-4 EID estimate, $\hat{d}_{2e}^{(2)}(t)$, for Layer 1.

Next, Layer 2 was checked and estimates were obtained for the EIDs $\hat{d}_{2-1e}^{(2)}(t)$, $\hat{d}_{2-2e}^{(2)}(t)$, $\hat{d}_{2-3e}^{(2)}(t)$, and $\hat{d}_{2-4e}^{(2)}(t)$, for Clusters $\mathcal{C}_{2-1}^{(2)}$, $\mathcal{C}_{2-2}^{(2)}$, $\mathcal{C}_{2-3}^{(2)}$, and $\mathcal{C}_{2-4}^{(2)}$, respectively. Fig. 5-5 shows $\hat{d}_{2-je}^{(2)}(t)$ ($j=1,2,3,4$) and their derivatives with respect to time during the period $[0.3, 0.5]$. $\hat{d}_{2-3e}^{(2)}(t)$ and $\dot{\hat{d}}_{2-3e}^{(2)}(t)$, and $\hat{d}_{2-4e}^{(2)}(t)$ and $\dot{\hat{d}}_{2-4e}^{(2)}(t)$, were outside the allowable ranges, but the EIDs of the other clusters exhibited no abnormalities. This means that faults occurred in Clusters $\mathcal{C}_{2-3}^{(2)}$ and $\mathcal{C}_{2-4}^{(2)}$.

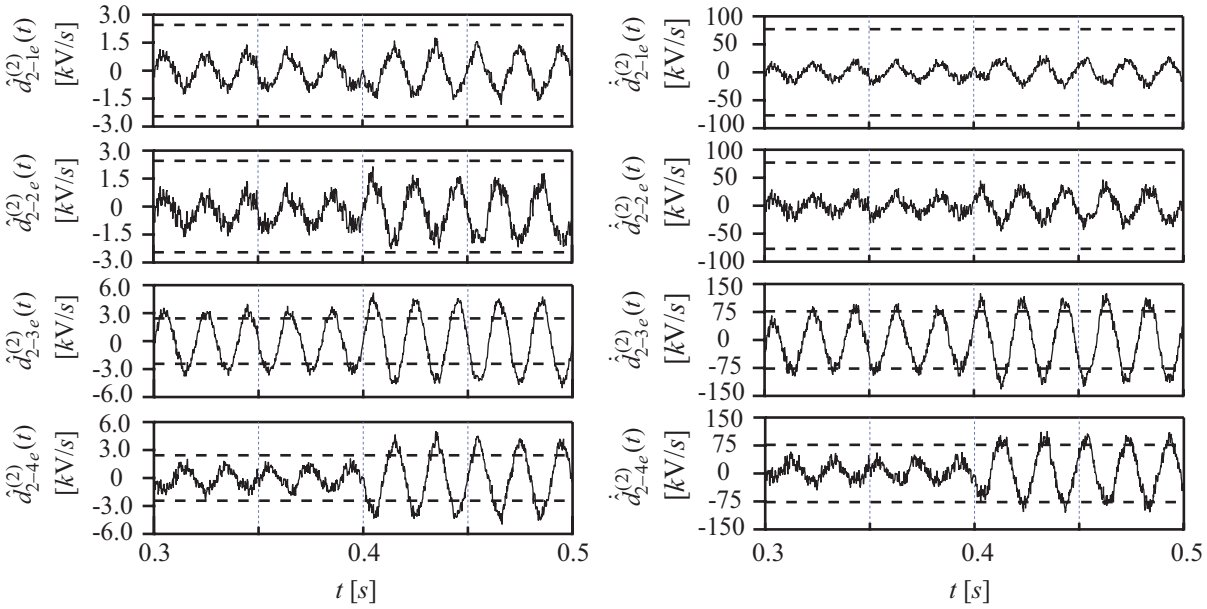

Fig. 5-5 EID estimates, $\hat{d}_{2-je}^{(2)}(t)$ and $\dot{\hat{d}}_{2-je}^{(2)}(t)$ ($j=1,2,3,4$), in Layer 2.

Two clusters in Layer 3 were analyzed to further locate the faults:

1) Regarding Cluster $\mathcal{C}_{2-3}^{(2)}$ (Fig. 5-6), $\hat{d}_{2-3-3e}^{(3)}(t)$ for Cluster $\mathcal{C}_{2-3-3}^{(3)}$ was outside the allowable range, which means that a fault occurred there.

2) Regarding Cluster $\mathcal{C}_{2-4}^{(2)}$ (Fig. 5-7), $\hat{d}_{2-4-3e}^{(3)}(t)$ for Cluster $\mathcal{C}_{2-4-3}^{(3)}$ was outside the allowable range, which means that a fault occurred there.

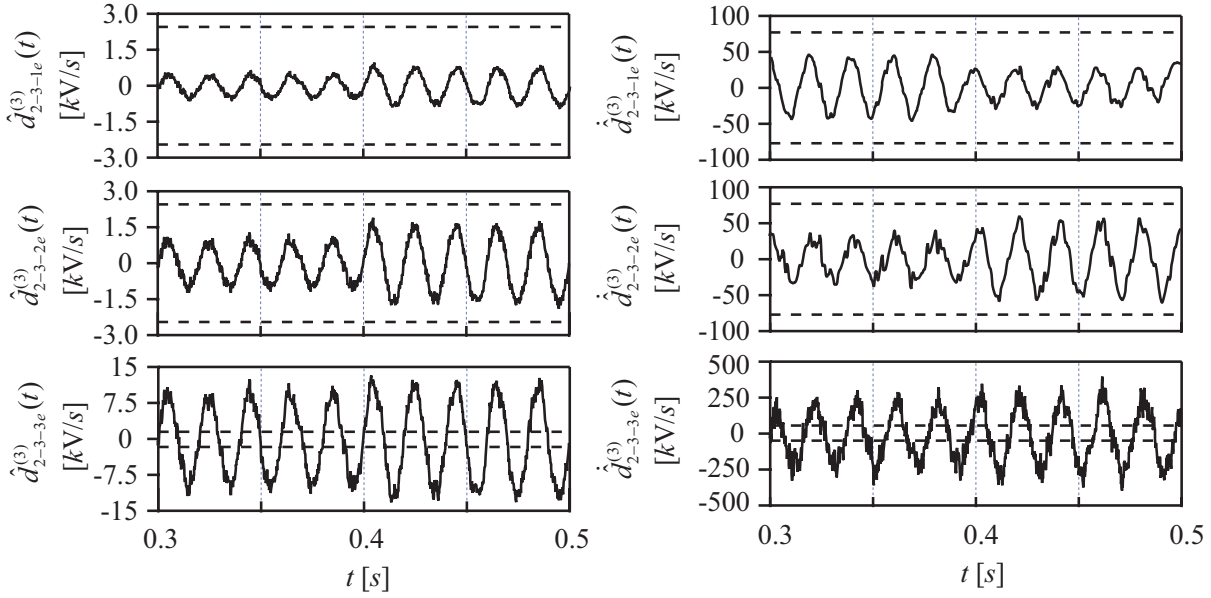

Fig. 5-6 EID estimates, $\hat{d}_{2-3-je}^{(3)}(t)$ and $\dot{\hat{d}}_{2-3-je}^{(3)}(t)$ $(j=1,2,3)$, in Layer 3.

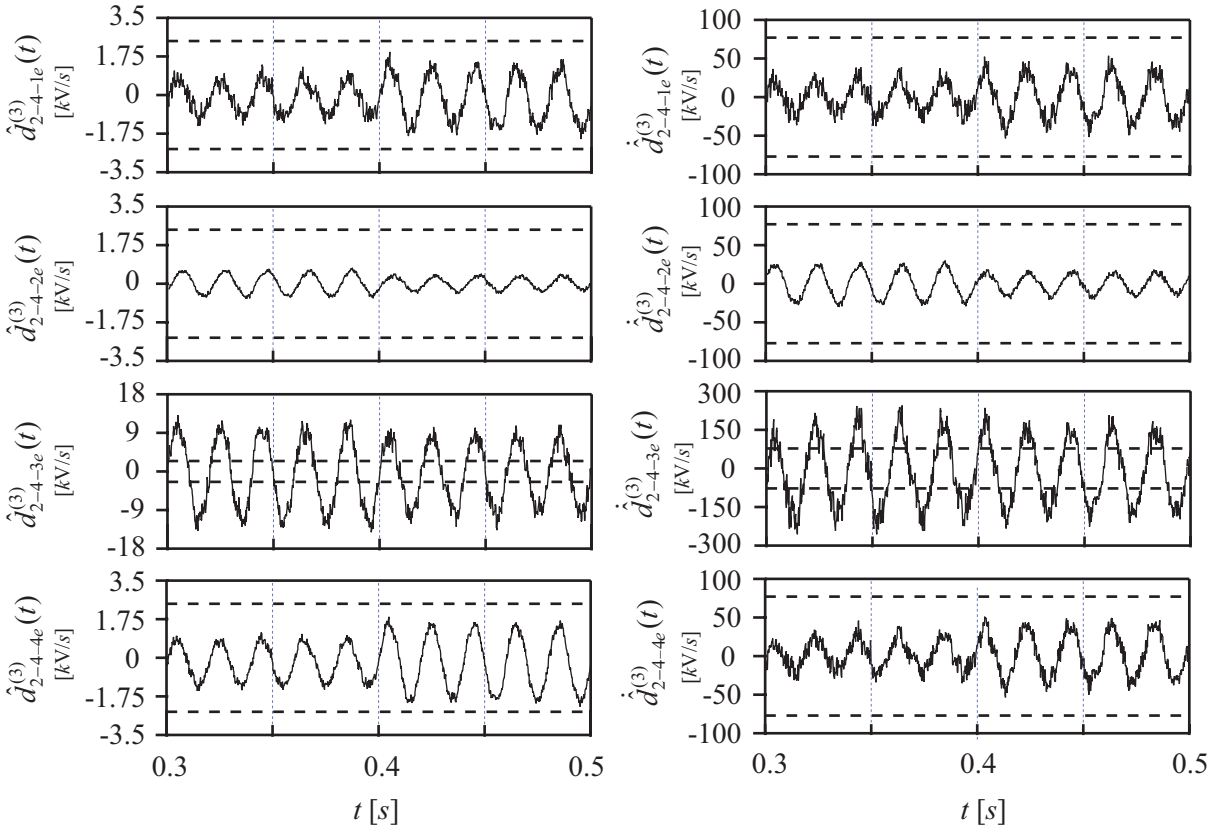

Fig. 5-7 EID estimates, $\hat{d}_{2-4-je}^{(3)}(t)$ and $\dot{\hat{d}}_{2-4-je}^{(3)}(t)$ $(j=1,2,3,4)$, in Layer 3.

Two clusters in Layer 4 were analyzed to further locate the faults:

1) Regarding Cluster $\mathcal{C}^{(3)}_{2-3-3}$ (Fig. 5-8), $\hat{d}^{(4)}_{2-3-3-3e}(t)$ for Cluster $\mathcal{C}^{(4)}_{2-3-3-3}$ was outside the allowable range, which means that a fault occurred there.

2) Regarding Cluster $\mathcal{C}^{(3)}_{2-4-3}$ (Fig. 5-9), $\hat{d}^{(4)}_{2-3-4-2e}(t)$ for Cluster $\mathcal{C}^{(4)}_{2-3-4-2}$ was outside the allowable range, which means that a fault occurred there.

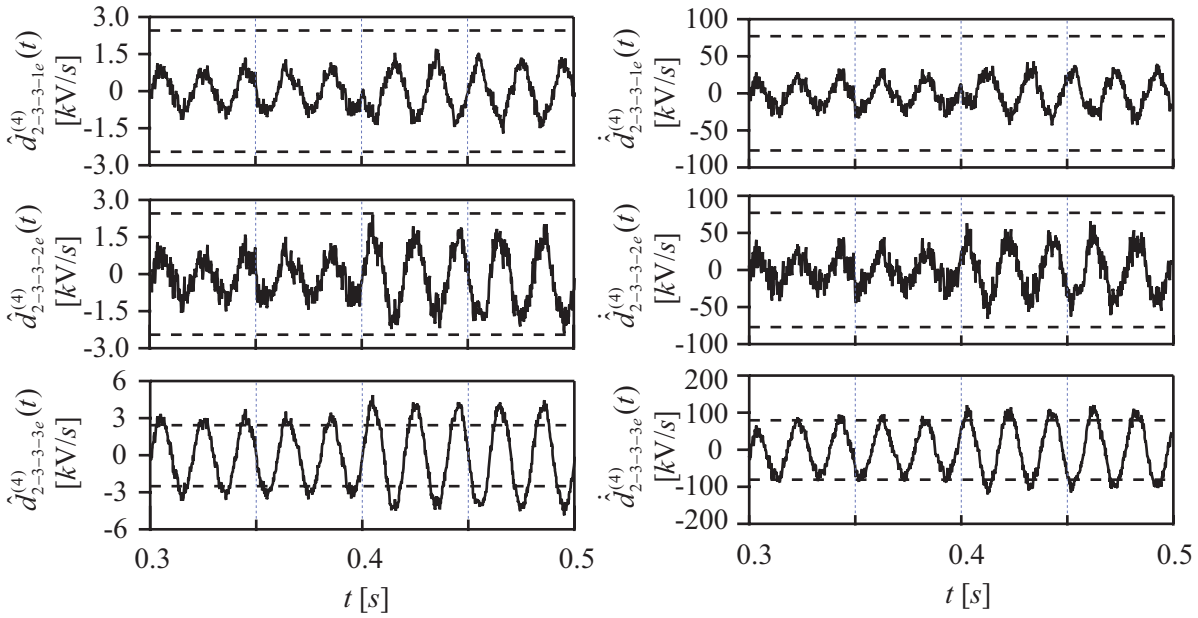

Fig. 5-8 EID estimates, $\hat{d}^{(4)}_{2-3-3-je}(t)$ and $\dot{\hat{d}}^{(4)}_{2-3-3-je}(t)$ $(j=1,2,3)$, in Layer 4.

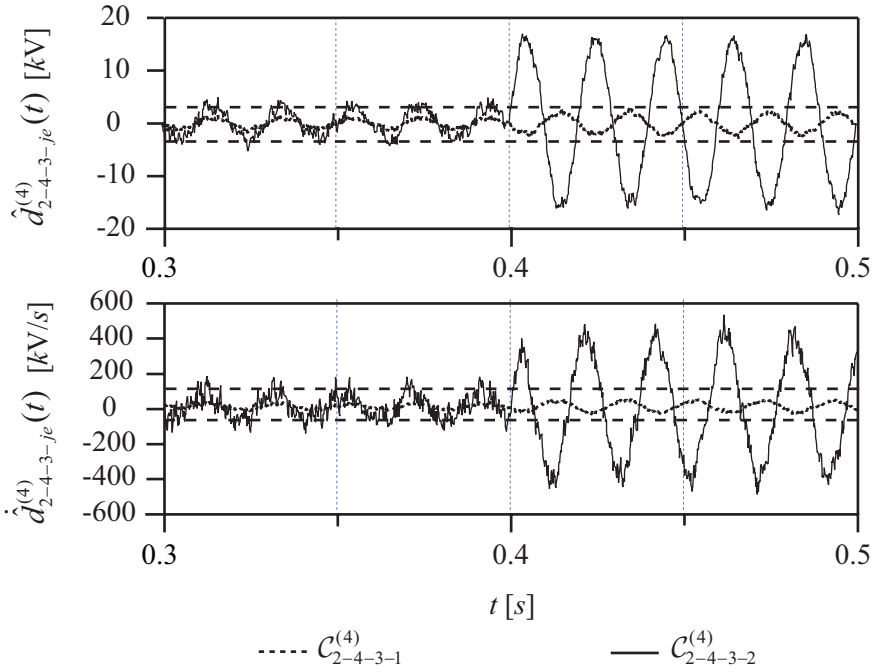

Fig. 5-9 EID estimates, $\hat{d}^{(4)}_{2-4-3-je}(t)$ and $\dot{\hat{d}}^{(4)}_{2-4-3-je}(t)$ $(j=1,2)$, in Layer 4.

Since Cluster $C^{(4)}_{2-3-4-2}$ contains only Node 718, this node must have a fault. On the other hand, $C^{(4)}_{2-3-3-3}$ contains three clusters; so more analysis is needed.

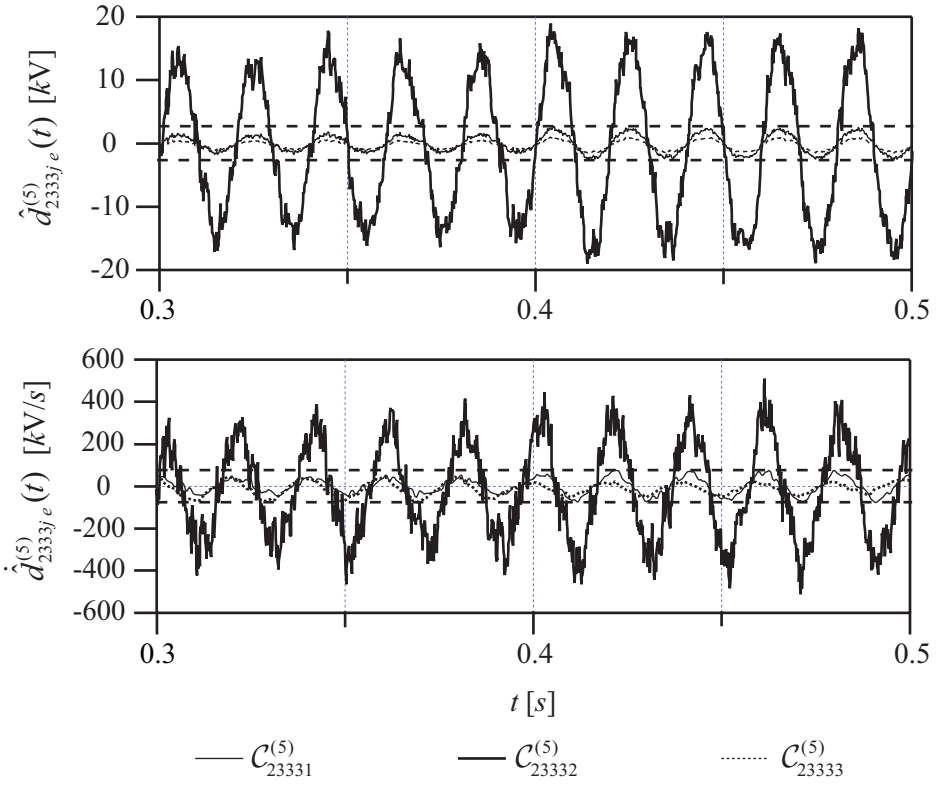

Fig. 5-10 EID estimates, $\hat{d}^{(5)}_{23332e}(t)$ and $\dot{\hat{d}}^{(5)}_{23332e}(t)$ $(j=1,2,3)$, in Layer 5.

The results for Cluster $C^{(4)}_{2-3-3-3}$ of Layer 4 (Fig. 5-10) show that $\hat{d}^{(5)}_{23332e}(t)$ for Cluster $C^{(5)}_{23332}$ was outside the allowable range. Since Cluster $C^{(5)}_{23332}$ contains only Node 732, that is where the fault is.

In this way, the locations of the faults were narrowed down to Nodes 718 and 732; but the types are still unknown. This information is obtained from an analysis of the system states, that is, the currents, of the layers with a fault (Fig. 5-11). The calculated amplitudes and phases of the estimated states, $\hat{i}^{(4)}_{2-3-4-2}(t)$ and $\hat{i}^{(5)}_{23332}(t)$, yielded the following information:

1) For Node 718, the amplitude of the current was outside the allowable range, and the phase shifted so much that Condition (5.1) failed. So, both the amplitude and phase of the state were abnormal.

2) For Node 732, the large change in current during the period $[0.3, 0.5]$ was outside the allowable range; but the change in phase was small. So, only the amplitude of the state was abnormal.

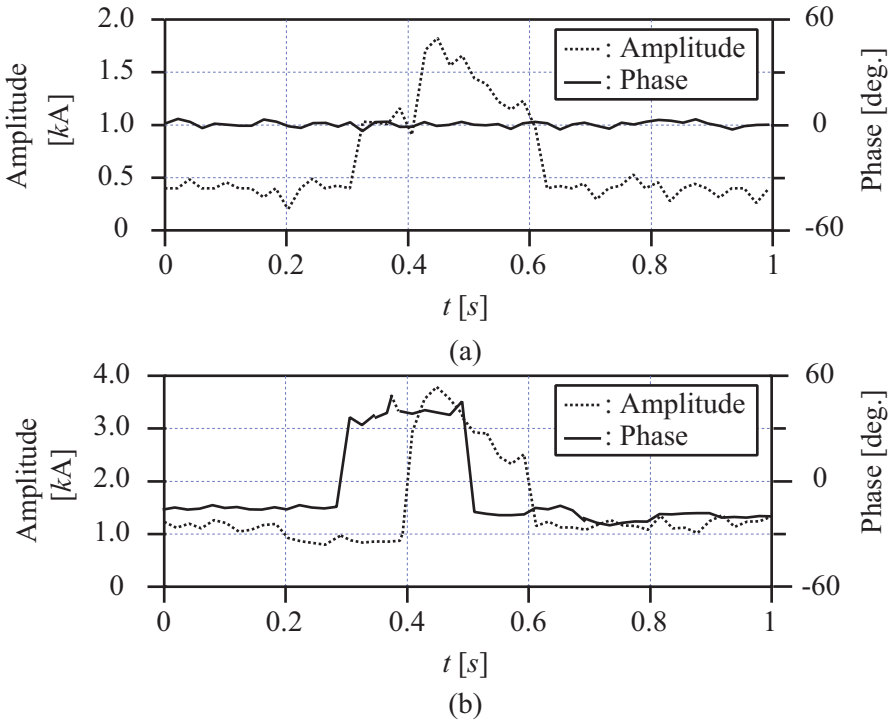

Fig. 5-11 Amplitudes and phases of (*a*) $\hat{I}^{(4)}_{2-3-4-2}$ (*Node* 718) and (*b*) $\hat{I}^{(5)}_{23332}$ (*Node* 732).

The infinity and Euclidean norms of the EIDs of different layers can be used to assess the damage caused by faults at different levels [5-5] - [5-7]. More specifically, the infinity norm is related to maximum power, and the Euclidean norm is related to total energy. Tables 5-7 and 5-8 show the infinity norm and Euclidean norm of the EIDs for faulty and normal load clusters, respectively, in different layers.

The tables tell us two things. One is that the norms of the EIDs are much larger for faulty clusters than for normal ones. The other is that the norms of the EIDs of faulty clusters increase with the depth of the layer. This means that a fault strongly affects a local network, but has less effect on other parts of the system. Since an EID is the input signal for a layer, its norms show what impact a fault has on power supply at different levels. This can aid a decision system in making appropriate choices for system recovery.

TABLE 5-8 INFINITY AND EUCLIDEAN NORMS OF ESTIMATED EIDS OF FAULTY LOAD CLUSTERS

Layer	Load Cluster	Infinity norm	Euclidean
1	$\mathcal{C}_2^{(1)}$:	3856	47757
2	$\mathcal{C}_{2-3}^{(2)}$	4915	64088
2	$\mathcal{C}_{2-4}^{(2)}$	4865	59326
3	$\mathcal{C}_{2-3-3}^{(3)}$	12811	172305

3	$\mathcal{C}_{2-4-3}^{(3)}$	13693	201428
4	$\mathcal{C}_{2-3-3-3}^{(4)}$	18762	263513
4	$\mathcal{C}_{2-4-3-2}^{(4)}$:	17658	227991
5	$\mathcal{C}_{23332}^{(5)}$:	24582	353370

TABLE 5-9 INFINITY AND EUCLIDEAN NORMS OF ESTIMATED EIDS OF NORMAL LOAD CLUSTERS

Layer	Load Cluster	Infinity norm	Euclidean norm	Layer	Load Cluster	Infinity norm	Euclidean norm
1	$\mathcal{C}_{1}^{(1)}$:	2367	29,257	-	-	-	-
2	$\mathcal{C}_{2-2}^{(2)}$:	2122	28,747	2	$\mathcal{C}_{2-1}^{(2)}$	1884	21,745
3	$\mathcal{C}_{2-2-2}^{(3)}$:	2222	29,399	3	$\mathcal{C}_{2-2-1}^{(3)}$	2281	28,503
3	$\mathcal{C}_{2-3-1}^{(3)}$:	1704	18,813	3	$\mathcal{C}_{2-2-3}^{(3)}$	2064	23,757
3	$\mathcal{C}_{2-4-1}^{(3)}$:	2423	31,387	3	$\mathcal{C}_{2-3-2}^{(3)}$	2388	31,815
3	$\mathcal{C}_{2-4-4}^{(3)}$:	1984	24,777	3	$\mathcal{C}_{2-4-2}^{(3)}$	2145	28,458
4	$\mathcal{C}_{2-3-2-2}^{(4)}$:	1822	23,413	4	$\mathcal{C}_{2-3-2-1}^{(4)}$	1279	14,925
4	$\mathcal{C}_{2-3-3-2}^{(4)}$	2226	21,253	4	$\mathcal{C}_{2-3-3-1}^{(4)}$	2124	31,049
4	$\mathcal{C}_{2-3-3-5}^{(4)}$	2323	27,620	4	$\mathcal{C}_{2-3-3-4}^{(4)}$	2400	33,689
4	$\mathcal{C}_{2-4-4-1}^{(4)}$:	2242	26,366	4	$\mathcal{C}_{2-4-3-1}^{(4)}$	2425	32,338
4	$\mathcal{C}_{2-4-4-3}^{(4)}$:	2040	21,703	4	$\mathcal{C}_{2-4-4-2}^{(4)}$	2190	31,377
5	$\mathcal{C}_{23222}^{(5)}$:	2478	29,042	5	$\mathcal{C}_{23221}^{(5)}$	2337	32,251
5	$\mathcal{C}_{23331}^{(5)}$:	2303	27,064	5	$\mathcal{C}_{23223}^{(5)}$	1602	19550
5	$\mathcal{C}_{24421}^{(5)}$:	2245	28,344	5	$\mathcal{C}_{23333}^{(5)}$	1897	20,713
5	$\mathcal{C}_{24423}^{(5)}$:	2182	25,167	5	$\mathcal{C}_{24422}^{(5)}$	1823	24,953
5	$\mathcal{C}_{24432}^{(5)}$:	1863	20,804	5	$\mathcal{C}_{24431}^{(5)}$	1873	26,511
6	$\mathcal{C}_{233332}^{(6)}$:	2157	23,814	6	$\mathcal{C}_{233331}^{(6)}$	2005	24,321
6	$\mathcal{C}_{233334}^{(6)}$:	2022	24,289	6	$\mathcal{C}_{233333}^{(6)}$	1725	21,786
7	$\mathcal{C}_{2333332}^{(7)}$:	1934	21,713	7	$\mathcal{C}_{2333331}^{(7)}$	2004	18,297
7	$\mathcal{C}_{2333341}^{(7)}$:	1712	19,072	7	$\mathcal{C}_{2333333}^{(7)}$	2196	23,598
7	$\mathcal{C}_{2333343}^{(7)}$:	1847	20,681	7	$\mathcal{C}_{2333342}^{(7)}$	2052	20,605
7	$\mathcal{C}_{2333345}^{(7)}$:	2227	25,570	7	$\mathcal{C}_{2333344}^{(7)}$	2131	22,006

5.5 Conclusion

In order to make the procedure of Hierarchical Fault Diagnosis Method easy to understand, the IEEE 37 nodes test feeder model was used as an example in this chapter. Firstly, the hierarchical model of the system and an EID estimator for the dynamic model of load cluster in each layer was constructed. Secondly, procedures of the HFD method were described. Fault diagnosis was carried out from the top down through the layers to gradually locate the fault nodes. Finally, after located the fault, the type of fault was identified using of the amplitude and phase of the estimated state.

Simulation results on the IEEE 37 nodes test feeder model show that our method is effective, and that faults were correctly diagnosed in spite of the noise. Furthermore, our method not only determined whether or not a fault occurred, but also can assess the damage caused by a fault at different levels of the system.

Chapter References

[5-1] **W. H. Kersting.** *Radial distribution test feeders.* IEEE Trans. Power Syst., vol. 6, no. 3, pp. 975-985, Oct. 2002.

[5-2] **IEEE PES Test Feeders.** http://ewh.ieee.org/soc/pes/dsacom/testfeeders/index.html.

[5-3] **J.M. Solanki, N.N. Schulz.** *Development of Three-Phase Unbalanced Power Flow Using PV and PQ Models for Distributed Generation and Study of the Impact of DG Models.* IEEE Trans. on Power Syst., vol. 22, no. 3, pp. 1019-1025, Aug. 2007.

[5-4] **J. A. Jiang, C. L. Chuang, Y. C. Wang, C. H. Hung, J. Y. Wang, C. H. Lee, and Y. T. Hsiao.** *A Hybrid Framework for Fault Detection, Classification, and Location–Part II: Implementation and Test Results*. IEEE Trans. Power Del., vol. 26, no. 3, pp. 1999-2008, Jul. 2011.

[5-5] **L.A. Zadeha and C.A. Desoer.** *Linear system theory*. NewYork: MeGraw-Hill, 1963.

[5-6] **D.Z. Zheng.** *Modern Control Theory*. Beijing: Tsinghua University Press, 2002.

[5-7] **M. Wu, Yong He and J. Hua.** *Stability Analysis and Robust Control of Time-Delay System*. Beijing: Springer, 2010

Chapter 6
Conclusions and Further Works

6.1 Conclusion

The thesis proposed a new HFD method based on EID approach for power system distribution network with PV system embedded.

In chapter 2, construction method of the HFD Model was proposed. Due to the complex structure of distribution network, using an entire model of it for fault diagnosis was very time consuming, therefore the HFD model for distribution network was set up. In the HFD model, the distribution network was built by first dividing it into multiple load clusters based on the locality and/or logical topology. Each cluster contained a number of load nodes. Then the clusters were subdivided successively into smaller load clusters. This produced both a multilayer structure and a hierarchical model of the system. Fault diagnosis was carried out from the top down through the layers to gradually locate a fault and to identify its type. The parameters of HFD model were calculated by the BFS power flow calculation algorithm. Meanwhile, in the power calculation the PV system can be classified into two types: the *PV-specified* nodes type and the *PQ-specified* node type, thus we improved the BFS algorithm to adapt them. The IEEE 13 nodes test feeder was selected to illustrate how to construct a hierarchical model.

In Chapter 3, the EID approach was applied to a fault diagnosis method for the load cluster. From the viewpoint of system robustness, faults can be defined as: the disturbances exceed the allowable range and break the stability of system. Based on this idea, the EID approach, which can estimate the system disturbances, is applied to diagnose the faults. Firstly, the theory basis of EID approach and the definition of EID were introduced. According to the characteristics of dynamic model for load cluster, the design method of state observer gain was given out. Secondly, two critical considerations of fault diagnosis method based on EID approach, which are the thresholds of the EIDs and the characteristics of faults were discussed. Furthermore, after a fault was located, its type must be determined. This type of fault was determined by monitoring the current of a load cluster, which is the state of its dynamics. Lastly, the simulation results on the case study were presented to illustrate the effective of the fault diagnosis method.

In Chapter 4: with the PV systems installed in the distribution network as distributed generators, many new problems, such as fluctuation of PV output and malfunction of relays caused by PV power injected, appears to the conventional fault diagnosis method. Firstly, based on the PV output power data collected from the PV systems installed at Honjo campus of

Waseda University, the impact of PV system on the distribution network such as the voltage profile improving, electrical losses, and reverse power were analyzed. Secondly, the fault diagnosis method based on EID approach for the load cluster with PV system connected was proposed. The fluctuation of PV output lead to the disturbance to the utility grid and this disturbance mixed with the fault signal, which brings a negative impact on the fault diagnosis method based on EID approach. To eliminate the PV influence, a PV output disturbance estimator was designed. By measuring the PV system output current and make it as an input to the PV output disturbance estimator, the disturbance of PV can be calculated and the fault signal was abstracted successfully. The simulation result on a case study showed the effectiveness of proposed method.

In Chapter 5, in order to make the procedure of Hierarchical Fault Diagnosis Method easy to understand, the IEEE 37 nodes test feeder model is used as an example. Firstly, applying the method mentioned above, the hierarchical model of the IEEE 37 nodes test feeder model was constructed and EID estimators for load clusters in each layer were designed. Secondly, monitoring Layer 1 of the hierarchical model by estimating the EID of load cluster in a real-time fashion, if a fault was detected at any load cluster, then go to the next layer of the fault load cluster. If the load cluster only contains one load node and can not be divided any more, then the fault node was located. Lastly, the type of fault was determined by analyzing the amplitude and phase of the estimated state of the smallest LC containing the fault. The application of HFD method to the IEEE 37 nodes test feeder model proved that the proposed method can detect the fault effectively and rapidly. Moreover, the HFD method can diagnose the different faults at the same time.

Simulation results on the IEEE 37 nodes model demonstrate the validity of the method. Furthermore, since experiments always contain measurement noise, the practicality of method was demonstrated by carrying out simulations that assumed white noise in the measurements (SNR = 30 dB). The results show that our method is effective, and that faults were correctly diagnosed in spite of the noise.

A comparison with conventional methods revealed the following points.

1) To diagnose faults in the IEEE 37 nodes model, an expert system based on knowledge of protection [6-1] requires analysis of the information on 74 protective relays and 74 circuit breakers. In contrast, the EID-based HFD method requires only the voltages of 37 nodes. Furthermore, the EID-based HFD method successively breaks down a large system into smaller and smaller subsystems at lower levels. This reduces the complexity involved in modeling and shortens the computing time needed for fault

diagnosis, while requiring less information.

2) Fault diagnosis based on a Petri net [6-2] requires the construction of at least a 74-dimensional correlation matrix. This involves a large computational expense. The EID-based HFD method diagnoses faults layer by layer, and the dynamic model of a cluster in a layer has only *one* state. Furthermore, the EID-based HFD method only needs to diagnose clusters that might have a fault. Due to the small size of each model and the limited number of clusters that need to be dealt with, the computational complexity is very low. As a result, the computations are very fast.

3) More specifically, for a power system with n states, the computational expense is $O(n^2)$ for a Petri net-based method, but $O(n)$ for the EID-based HFD method. So, the larger the system is, the more apparent the superiority of the EID-based HFD method becomes.

4) For fault diagnosis methods based on a protection principle [6-1] – [6-3], the ease and accuracy of fault diagnosis strongly depend on the completeness and accuracy of the information on protective relays and circuit breakers. In contrast, for the EID-based HFD method the precision of fault diagnosis depends on the accuracy of the local model. In other words, even if a higher-level model is not very accurate, as long as it detects a fault, the models at lower layers can be used to obtain exact information on the fault.

5) Unlike the model-based method in [6-4], the EID-based HFD method not only determines whether or not a fault has occurred, but can also assess the damage caused by a fault at different levels of the system.

6) There are three main differences between the use of a full model and the use of a hierarchical model for fault diagnosis. Assume that the number of states of the system for the full model is n.

   i. Complexity of plant modeling: While a full model takes into account the relationships among the voltages and currents of all the nodes at a given time, the hierarchical model breaks the complexity down into different layers. So, it is much simpler to build a hierarchical model than a full model.

   ii. Complexity of observer design: The complexity of designing an observer is $O(n^3)$ for a full model, but only $O(n)$ for a hierarchical model.

   iii. Cost of implementation: The computational expense is $O(n^2)$ for a full model,

but only $O(n)$ for a hierarchical model

6.2 Further Works

There are several limitations for the EID-based HFD method that could be further improved.

1) It should be pointed out that the EID-based HFD method uses only the voltages of nodes to perform fault diagnosis, and that the smallest unit for fault diagnosis is the load node. To obtain more precise information about a fault (exact location, exact type, etc.), sensor information from the faulty node is needed. So, our method can be used to first find a faulty node; and then local sensor information can be used to determine the exact location and type of the fault in the future. This combination provides a fast, easy way to precisely diagnose faults.

2) As an aid to explaining the EID-based HFD method, this paper considered balanced, linear loads. However, real-world loads may be unbalanced or nonlinear. This method can be directly applied to unbalanced loads, and it can be improved to handle nonlinear loads. These points would be done on in the future.

3) An experiment to test the method would be of great importance as a confirmation of its validity. Other studies have dealt with experimental issues related to fault diagnosis, for example, [6-5] [6-6]. An experimental platform would be constructed to evaluate the method in the near future.

Chapter References

[6-1] **C. Fukui and J. Kawakami.** *An expert system for fault section estimation using information from protective relays and circuit breakers.* IEEE Trans. Power Del., vol. 1, no. 4, pp. 83-90, Nov. 1986.

[6-2] **H. Ren and Z. Mi.** *Power System Fault Diagnosis Modeling Techniques based on Encoded Petri Nets.* present at IEEE Power Engineering Society General Meeting, Montreal, Canada, Oct. 2006.

[6-3] **L. Xu and M. Y. Chow.** *A Classification Approach for Power Distribution Systems Fault Cause Identification.* IEEE Trans. Power Syst., vol. 21, no. 1, pp. 53-60, Feb. 2006.

[6-4] **X. Zhang and P. Pisu.** *Model-based fault diagnosis for a vehicle chassis system.* in Proc. American Control Conference, Jun. 2009, pp. 1116-1121.

[6-5] **C. L. Chuang, Y. C. Wang, C. H. Hung, J. Y. Wang, C. H. Lee, and Y. T. Hsiao.** *A Hybrid Framework for Fault Detection, Classification, and Location--Part I: Concept, Structure, and Methodology.* IEEE Trans. Power Del., vol. 26, no. 3, pp. 1988-1998, Jul. 2011.

[6-6] **J. A. Jiang, C. L. Chuang, Y. C. Wang, C. H. Hung, J. Y. Wang, C. H. Lee, and Y. T. Hsiao.** *A Hybrid Framework for Fault Detection, Classification, and Location--Part II: Implementation and Test Results.* IEEE Trans. Power Del., vol. 26, no. 3, pp. 1999-2008, Jul. 2011.

List of Publications

1. **B. Hu, J.H. She and R. Yokoyama.** *Hierarchical Fault Diagnosis for Power Systems Based on Equivalent Input-Disturbance Approach*, IEEE Trans. Ind. Electron. (Accepted, will publish in 2013).

2. **B. Hu, J.H. She and R. Yokoyama.** *Fault Diagnosis of Power Distribution Feeders with a PV System Using Equivalent-Input-Disturbance Approach*, Journal of Advanced Computational Intelligence and Intelligent Informatics. (Accepted, will publish in Feb. 2013).

3. **B. Hu, J.H. She and R. Yokoyama.** *A New Fault Diagnosis Method for a Power Distribution Feeder with a Grid-Connected PV System Based on Equivalent-Input-Estimation Approach*, International Symposium on Soft Computing sponsored by ASPIRE LEAGUE, Nov. 2012.

4. **B. Hu, R. Yokoyama, J.H. She and Y.C Zhou.** *A Model-based Fault Diagnosis Method for Distribution Networks with Grid-connected PV Systems*, in Proc. ICEE 2012, Jul. 2012.

5. **B. Hu, Y. Nonaka, and R. Yokoyama.** *The Influence of Large-Scale PV Grid-Connected System Installation on Distribution Networks*, Automation of Electric Power Systems**,** vol. 36, no. 3, Feb. 2012.

6. **B. Hu, J.H. She and R. Yokoyama.** *A New Fault Diagnosis Method Based on Hierarchical Model in Power System*, in Proc. ITCA2011, Nov. 2011.

7. **B. Hu, R. Yokoyama, Y. Zhou and M. Wu.** *Performance Evaluation of Combinatorial Optimization Methods Based on Heuristic Algorithms Applied to Power Systems*, International Conference on Electrical Engineering, Jul. 2010.

8. **C. Wu, M. Wu, B. Hu**. *The Optimization and Application of CSP Furnace Burning Process Control System*. Equipment Manufacturing Technology, vol. 6, pp, 74-76, Jun. 2009.

9. **B. Hu, M. Wu, J. Yang and H. Zhu.** *An Optimization Scheduling Method for Coke Oven Pushing Plan in Abnormal Operating Conditions*, in Proc. Chinese Control Conference, Jul. 2008.